ISSN 0915-6348

NATIONAL INSTITUTE FOR FUSION SCIENCE

Symposium on Development and Applications of Intense Pulsed Particle Beams December 6–7, 1990

(Received – May 30, 1991)

NIFS-PROC-8 Jun. 1991

RESEARCH REPORT NIFS-PROC Series

NAGOYA, JAPAN

Symposium on Development and Applications of Intense Pulsed Particle Beams

December 6-7, 1990

Edited by Kiyoshi Yatsui

National Institute for Fusion Science, Nagoya, Japan

Keywords: Pulse-Power Technology, Inertial Confinement Fusion, Intense Charged Particle Beams, Ion-Beam Diodes, Beam-Target Interaction

PREFACE

On December 6 ~ 7, 1990, "Symposium on Development and Applications of Intense Pulsed Particle Beams" was held at National Institute for Fusion Science, Nagoya, as a collaborative research program in the fiscal year of 1990. Approximately thirty five researchers attended the symposium on Dec. 6 and thirty on Dec. 7, who participated from various universities and institutes all over Japan. Totally 15 papers were reported orally. A lot of new achievements were presented at the symposium, which were discussed in detail.

It was recognized by the participator that young scientists or students begin to increase recently in Japan who are interested in pulse-power technology and its applications. In the near future, furthermore, we hope its applications will grow up more widely and practically.

Kiyoshi Yatsui
Symposium Chairman
Nagaoka University of Technology

PROGRAM OF SYMPOSIUM ON DEVELOPMENT AND APPLICATIONS OF INTENSE PULSED PARTICLE BEAMS

December 6 (Thursday), 1990

13:30 ~ 13:35 Preface/Address

K. Yatsui (Nagaoka Univ. of Tech.)

13:35 ~ 14:00 Light Ion Beam Interaction with Target of Indirect Driven ICF

T. Aoki et al. (Tokyo Inst. of Tech.)

14:00 ~ 14:25 Ion-Beam Power Amplification Through X-Ray Conversion

T. Yabe et al. (Gunma Univ.)

14:25 ~ 14:50 Proton Beam Fusion: Beam Propagation and Focusing

K. Niu (Teikyo Univ. of Tech.)

14:50 ~ 15:15 Developments for High Performance Light Ion Beams

S. Miyamoto et al. (Osaka Univ.)

15:15 ~ 15:40 Generation and Focusing of Proton Beam by the Inverse Pinch Ion Diode

Y. Hashimoto et al. (Himeji Inst. of Tech.)

15:40 ~ 16:00 Coffee break

16:00 ~ 16:25 Optimization of Self-Magnetically Insulated "Plasma Focus Diode"

W. Jiang et al. (Nagaoka Univ. of Tech.)

16:25 ~ 16:50 Diagnostics and Evaluation of Anode Plasma in "Point Pinch Diode"

H. Okuda et al. (Nagaoka Univ. of Tech.)

16:50 ~ 17:15 Experimental Study on Spectrum of Microwave Radiation From IREB-Plasma Interactions

R. Ando et al. (Kanazawa Univ.)

December 7 (Friday), 1990

9:00 ~ 9:25	Characteristics of Plasma Injection Type Pulsed Ion Diodes Y. Saito et al. (Tokyo Inst. of Tech.)
9:25 ~ 9:50	Development of Intense Negative Ion Sources K. Horioka et al. (Tokyo Inst. of Tech.)
9:50 ~ 10:15	Production of Pulsed Beams of Negative Light-Heavy Ions S. Shibata et al. (Kobe univ. of Mercantile Marine)
10:15 ~ 10:40	Pulsed Power Generator by an Inductive Energy Storage System N. Shimomura et al. (Tokushima Univ.)
10:40 ~ 11:00	Coffee break
11:00 ~ 11:25	Generation of Relativistic Electron Beams by Pulsed Power Generator Using an Inductive Storage System K. Nagano et al. (Kumamoto Univ.)
11:25 ~ 11:50	Comparison of Tl-, Bi-, and Y-Compound High-Temperature Superconducting Lenses H. Matsuzawa et al. (Yamanashi Univ.)
11:50 ~ 12:15	Intense Beams of Highly-Ionized Metallic Ions Generated in the "Point Pinch Diode" T. Tazima et al. (National Inst. for Fusion Science)
12:15 ~ 12:20	Remarks/Acknowledgements K. Yatsui (Nagaoka Univ. of Tech.)

CONTENTS

Light Ion Beam Interaction with Target for Indirect Driven ICF

Takayuki AOKI
Department of Energy Sciences, the Graduate School at Nagatsuta,
Tokyo Institute of Technology, 4259 Nagatsuta, Midori-ku, Yokohama 227, Japan

Takashi YABE
Department of Electronic Engineering, Gunma University
1-5-1 Tenjin-chou, Kiryu, Gunma 376, Japan

Tomohiro SASAGAWA
Department of Advanced Laser Technology, Central Research Lab., Mitsubishi Electric Co.
8-1-1 Tsukaguchi-honchou, Amagasaki, Hyougo 661, Japan

Keishiro NIU
Plasma Physics Laboratory,
Institute of Physical and Chemical Research, Wako, Saitama 350-01, Japan

Abstract

An intense proton-beam interaction with an aluminum target is investigated by using a one-dimensional simulation. The numerical model is based on hydrodynamics, radiation transport, beam-energy deposition and atomic physics. The NRL-problem (Phys. Rev. A, **31**, (1985)) is checked by this code, and we obtain the same result that more than half of the deposited energy is leaked out from the front-side surface. When the closed geometric target is used, the intensity of the converted X-ray is increased to more than five times that of the open geometric target. In order to examine the smoothing effect in an indirect driven ICF target, a two-dimensional simulation of the radiation transport is carried out. The simulation model is much simplified except the radiation transport, however, it is found that the radiation smoothing layer has much effect

for nonuniform beam irradiation, if the thickness of this layer is more than 1 mm.

Introduction

Light ion ICF has a lot of advantages as compared with the scheme using the other energy drivers.[1] These are the driver efficiency, the beam-target coupling efficiency, the beam total energy, the total system economy, and so on. However, the beam intensity on the target has not been so much improved[2], because of the beam focusability. Moreover, the pulse duration is rather long for the effective target implosion, so that the time-of-flight pulse compression[3] must be considered in a few-meter-radius reactor chamber. A nonuniform irradiation of the beam is also seemed to be critical, because the power balance among the beam modules is unstable at the present pulse-power technology.

In an indirect driven scheme, the deposited beam energy is converted to the X-ray energy. The intensity of the X-ray is uniformized in a radiation smoother layer in which the mean free path of the X-ray radiation is much longer than the target scale. A power amplification of the radiation to the beam is proposed to make use of the fact that the propagation speed of the radiation heat wave is slow in a cold matter.[4,5] Thus far the indirect driven scheme gives a possibility to recover the disadvantages of the conventional direct driven LIB-ICF. In order to study the physics of radiation hydrodynamics, we have developed a one-dimensional (1-D) simulation code, and the preliminary results are obtained. Furthermore, a two-dimensional (2-D) code for the radiation transport has been constructed to examine the effect of the radiation smoothing in the indirect driven ICF target. In the following sections, the detail descriptions will be presented.

1-D Simulation for Proton-Beam Interaction with Al Plane Target

In the 1-D simulation code which we have developed, hydrodynamics,

radiation transport, atomic physics, thermal conduction, beam-energy deposition, equation of state and so no are taken into consideration. In the hydrodynamics, the two temperature model is employed, and a stable and less diffusive algorithm, cubic-interpolated pseudo-particle (CIP[6,7,8]) method is used to solve the equations numerically. The flux limited thermal conduction is included in the equation for the electron internal energy. The realistic equation of state based on the Thomas-Fermi model for the electron is used. In the atomic physics of the target material, the collisional-radiative (CR) model[9] is used, and the rate equation of an ion population has the following form,

$$\begin{aligned}\frac{dN_{z,n}}{dt} = &-\sum_m I_{z,n;z+1,m}N_{z,n}N_e - \sum_k R_{z,n;z-1,k}N_{z,n}N_e \\ &+\sum_{m'} I_{z-1,m';z,n}N_{z-1,m'}N_e + \sum_{k'} R_{z+1,k';z,n}N_{z+1,k'}N_e \\ &-\sum_l E_{z,n;z,l}N_{z,n}N_e - \sum_s D_{z,n;z,s}N_{z,n} \\ &+\sum_s E_{z,s;z,n}N_{z,s}N_e + \sum_l D_{z,l;z,n}N_{z,l} \qquad (1)\end{aligned}$$

where $N_{z,n}$ means the ion population of the charge state z in the nth level. The free electron density is denoted as N_e, and the notations I, R, E, and D indicate the rate coefficients for ionization, recombination, excitation, and de-excitation. The photo-ionization and photo-excitation processes are neglected in this formulation. For the radiation transport, the multi-group diffusion method is used, in which the opacities consist of the free-free transition, the bound-free transition, and the bound-bound transition. In the beam energy deposition, the least-squares fitting formula[10] of the generalized-oscillator-strength[11] is employed for the bound electron contribution. The stopping powers of the free electron and the ion are adapted from the work of Cambell and Mehlhorn[12].

In order to check our simulation code, the NRL-problem is examined, that is, a planar aluminum slab target of 15-μm thickness is irradiated by a 1-MeV monoenergetic proton beam. The beam has a square-shaped pulse with 10 nsec duration and the intensity on the target is 1.6×10^{13} W/cm^2. The simulation result shows the almost same temperature and the density profiles in the time evolution, as that of the NRL group. In Fig.1, the front-side radiation spectra at different time are given. As Rogerson pointed out that more than half of the deposited energy was lost due to the radiation,[10] our result also shows the same tendency. We have carried

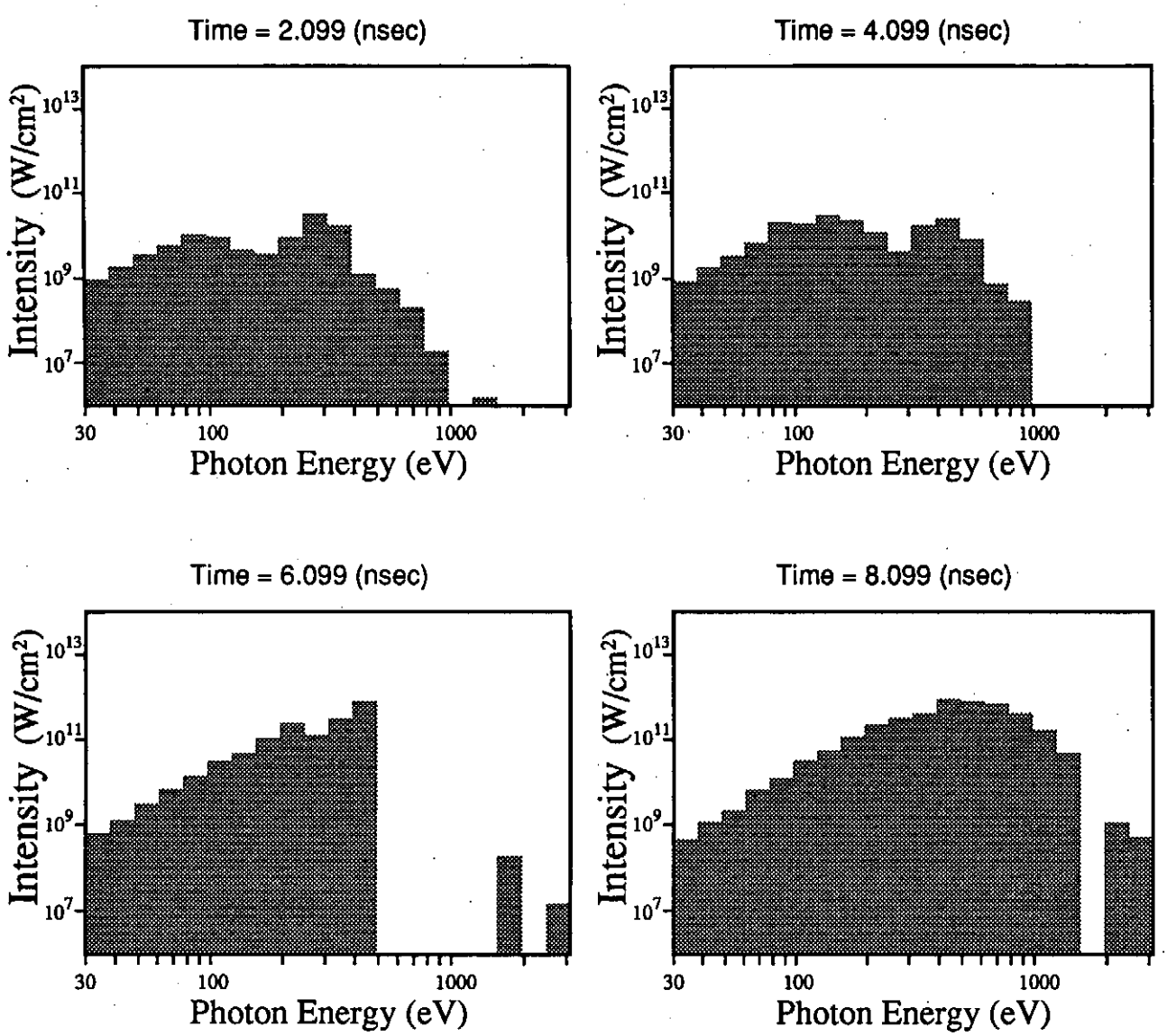

Fig. 1. Front-side radiation spectra of the open geometric target at different times.

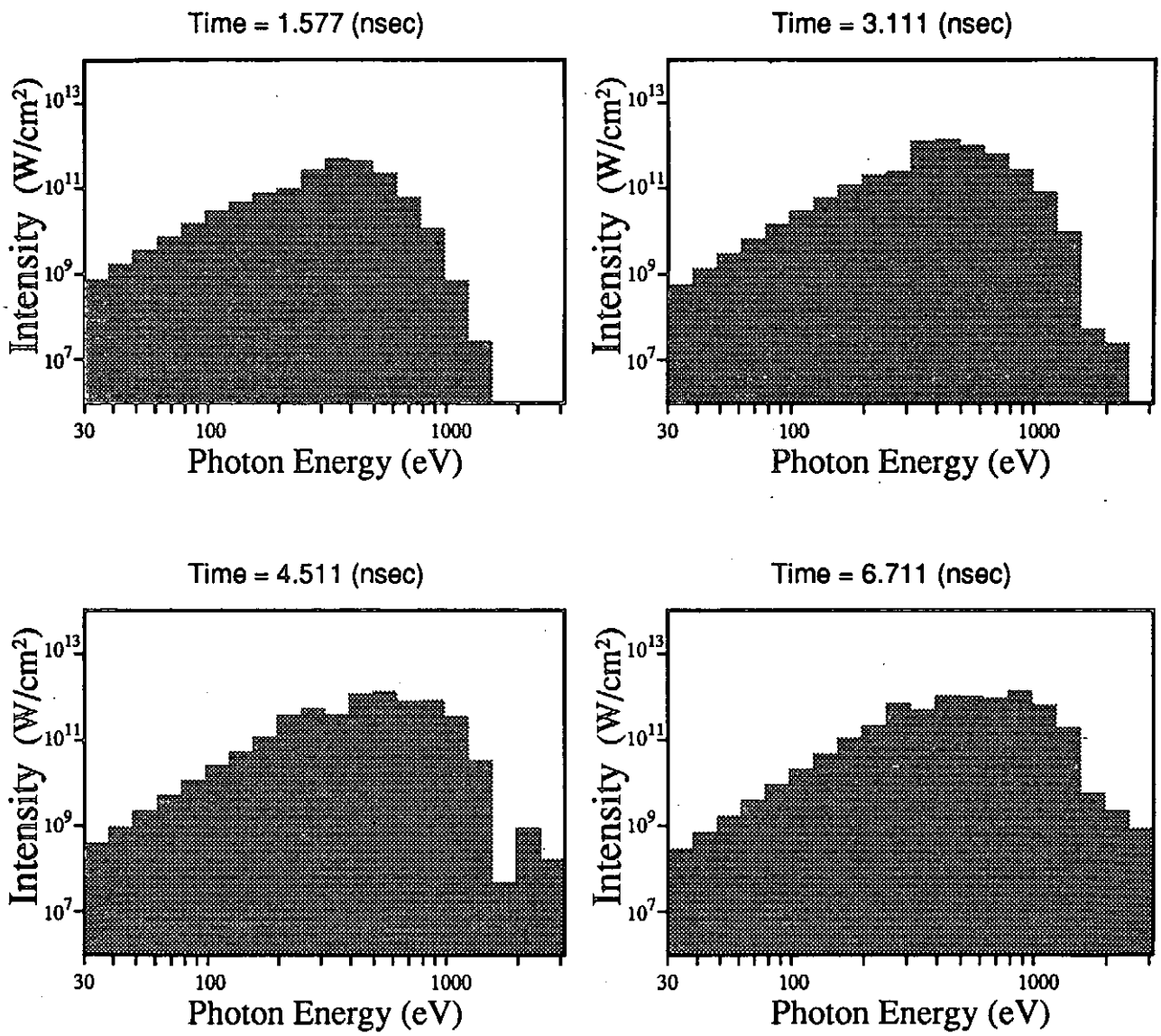

Fig. 2. Front-side radiation spectra of the closed geometric target at different times.

out the simulation using a closed geometric target[13] for the same beam parameters. The beam is assumed to be able to penetrate 3-μm thickness in the target not depositing the beam energy. This cold layer plays a role of the radiation reflector, and the converted X-ray radiation is confined in the inner region of the target. The intensity of radiation increases up to more than five times in comparison with the open geometric target. The radiation spectra in the inner region of the target are shown in Fig.2, and it is understood that the high energy part increases much. It is clear that the closed geometric target is effective for the X-ray conversion scheme. In the radiation reflector, it is necessary that less beam energy is deposited and the material is optical thick for X-ray frequency region.

2-D Simulation for Radiation Transport

The effect of the smoothing layer for the nonuniform beam irradiation is investigated by the 2-D simulation. The simulation model is quit simplified, so that the density is assumed to be constant and no hydrodynamic motion occurs. The thermal conduction is also neglected, because the radiation transport plays a dominant role in the equation of the internal energy. The gray approximation is used with respect to the radiation frequency, and the LTE opacity of SESAME library[14] is used.

The target structure of an indirect driven ICF is shown in Fig.3, and we take the spherical coordinate (r, θ, ϕ), where symmetry is assumed in the ϕ-direction. Initially, the beam energy is assumed to have been deposited in the emitter Al layer. The simulation for one beam irradiation is carried out, representing the most severe case for nonuniformity. The deposited beam energy is converted to the X-ray energy, and the maximum temperature decreases. The radiation is diffused isotropically through the dense and cold material. When the radiation flux is launched into the smoother layer, the diffusion is quit enhanced because this region is optical thin. The intensity of the X-ray is uniformized in this layer, the radiation energy is absorbed uniformly in the surface of the pusher layer. Figure 4 shows the temperature profiles at different times. The gray level indicates the temperature from 0 eV to 200 eV. The temperature differences between the inner surface of the emitter layer and the outer surface of the pusher layer are shown in Fig.5. It is clear that the

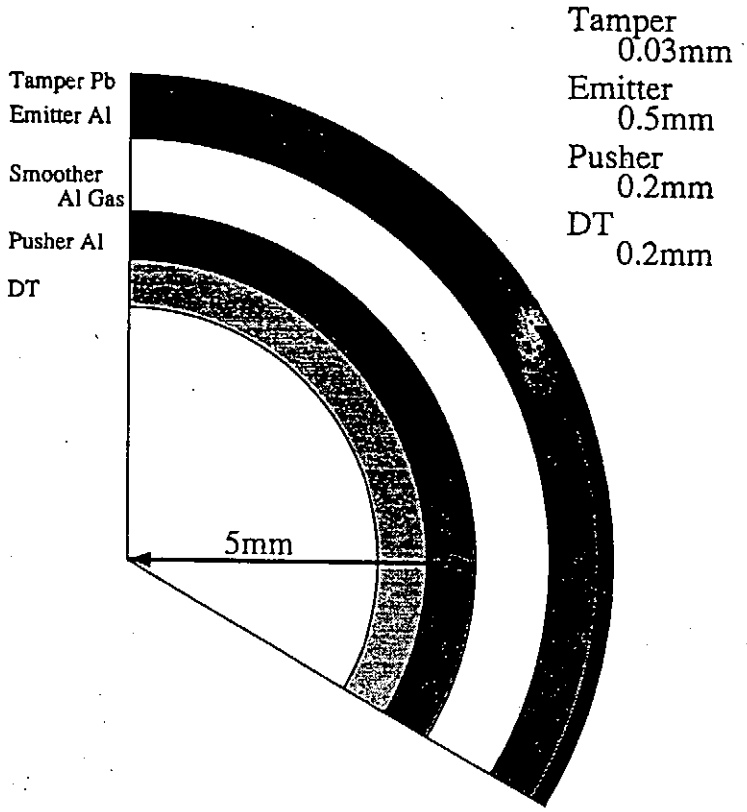

Fig. 3. Target structure for indirect driven ICF.

radiation intensity becomes uniform at 3 nsec, and the radiation energy is absorbed uniformly in the pusher layer.

The effect of the radiation smoother depends strongly on the target structure. The thickness of this layer is the critical parameter. Figure 6 shows the dependency of the thickness on the uniformity of the temperature and the radiation intensity. When the thickness is 0.5 mm, enough uniformity has not been achieved at 3 nsec. For the smoother of 1-mm thickness, the temperature profile becomes uniform at this time. The above results is much optimistic, because a lot of physics are neglected. The thickness of the layer should be determined by the simulation in which the hydrodynamics is included.

Summary

The radiative hydrodynamics of the target irradiated an intense proton beam was investigated by the 1-D simulation in the slab geometry.

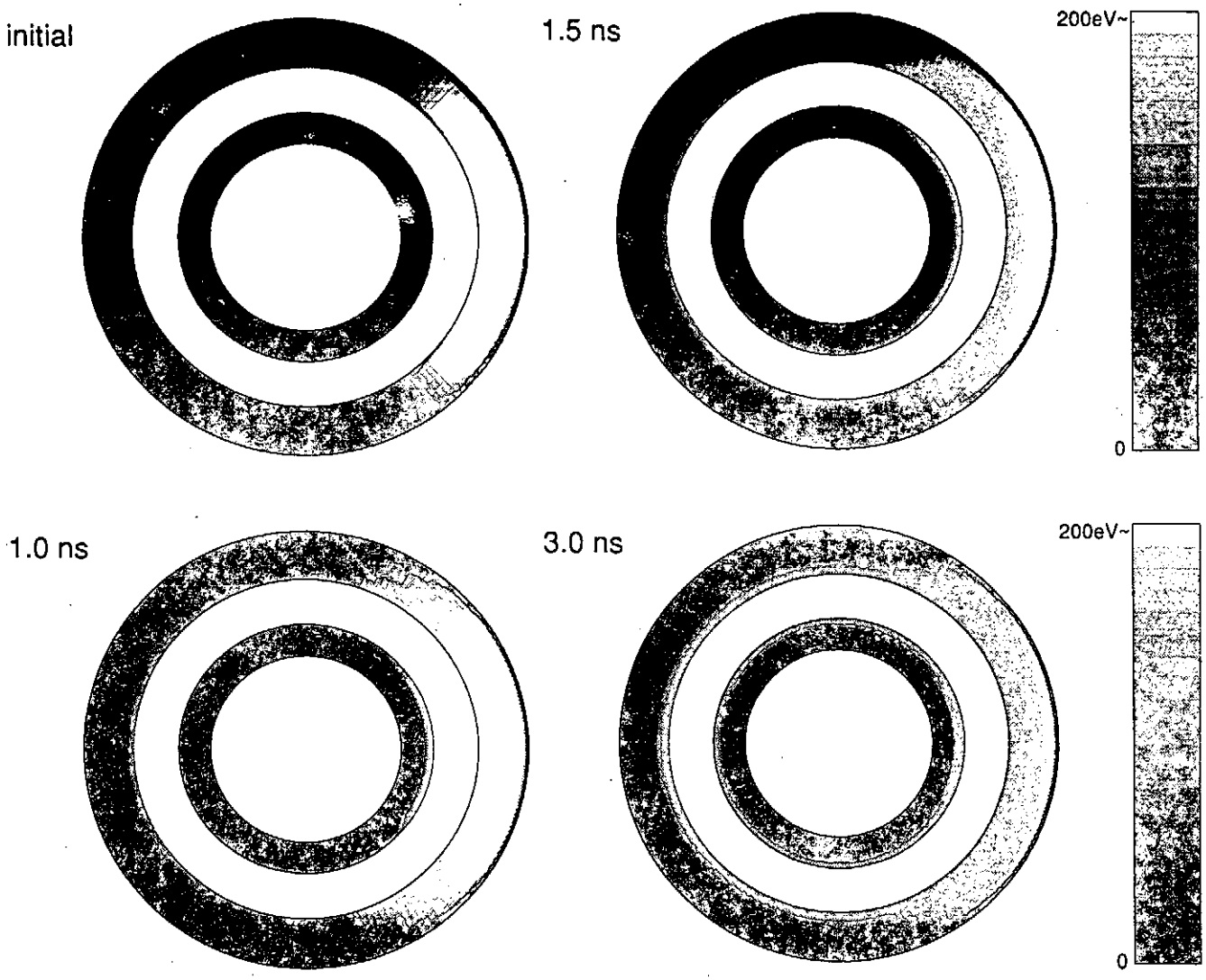

Fig. 4. Temperature profiles of the target at different times. The gray level indicates the temperature from 0 eV to 200 eV.

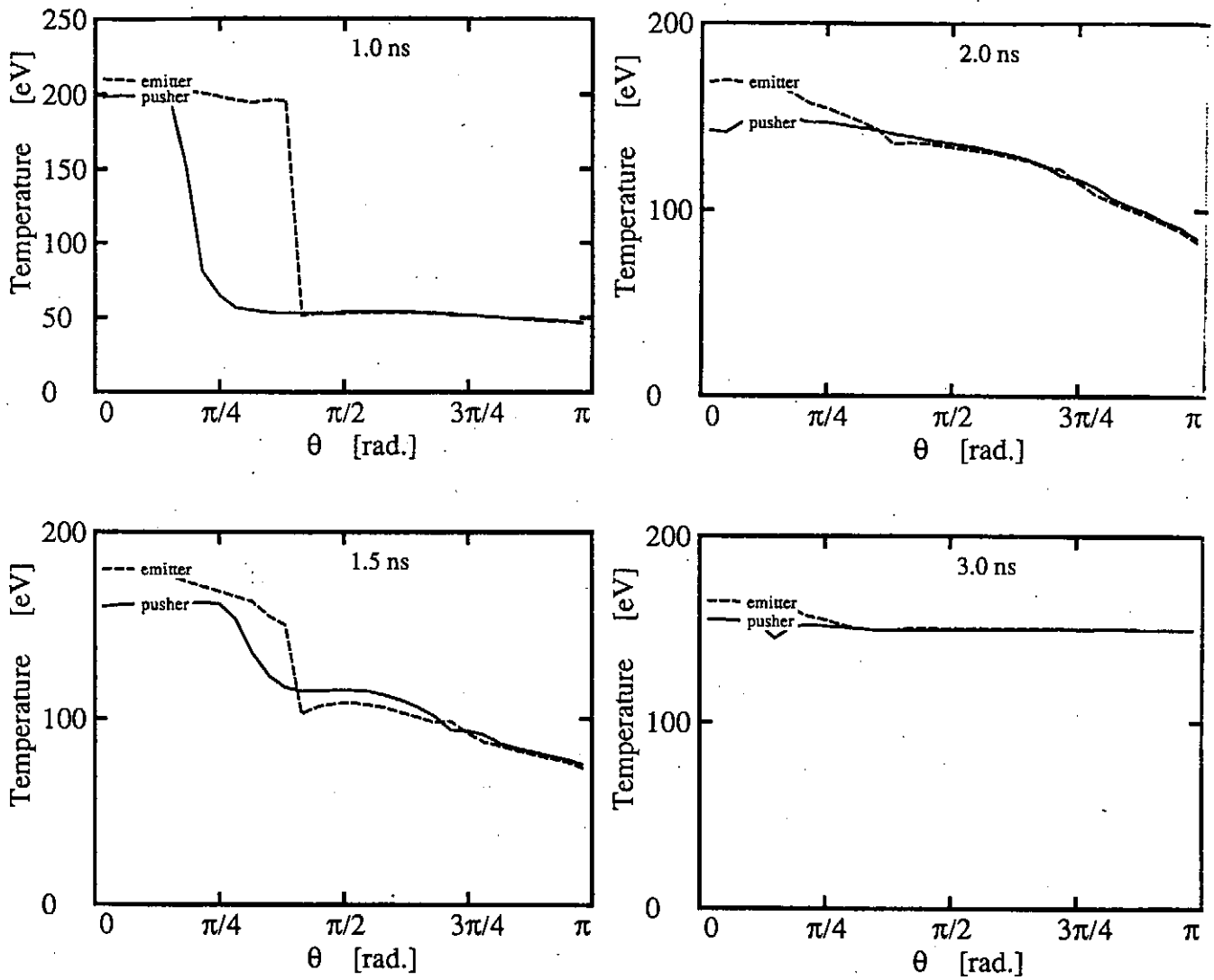

Fig. 5. Temperature differences between the inner surface of the emitter layer and the outer surface of the pusher layer.

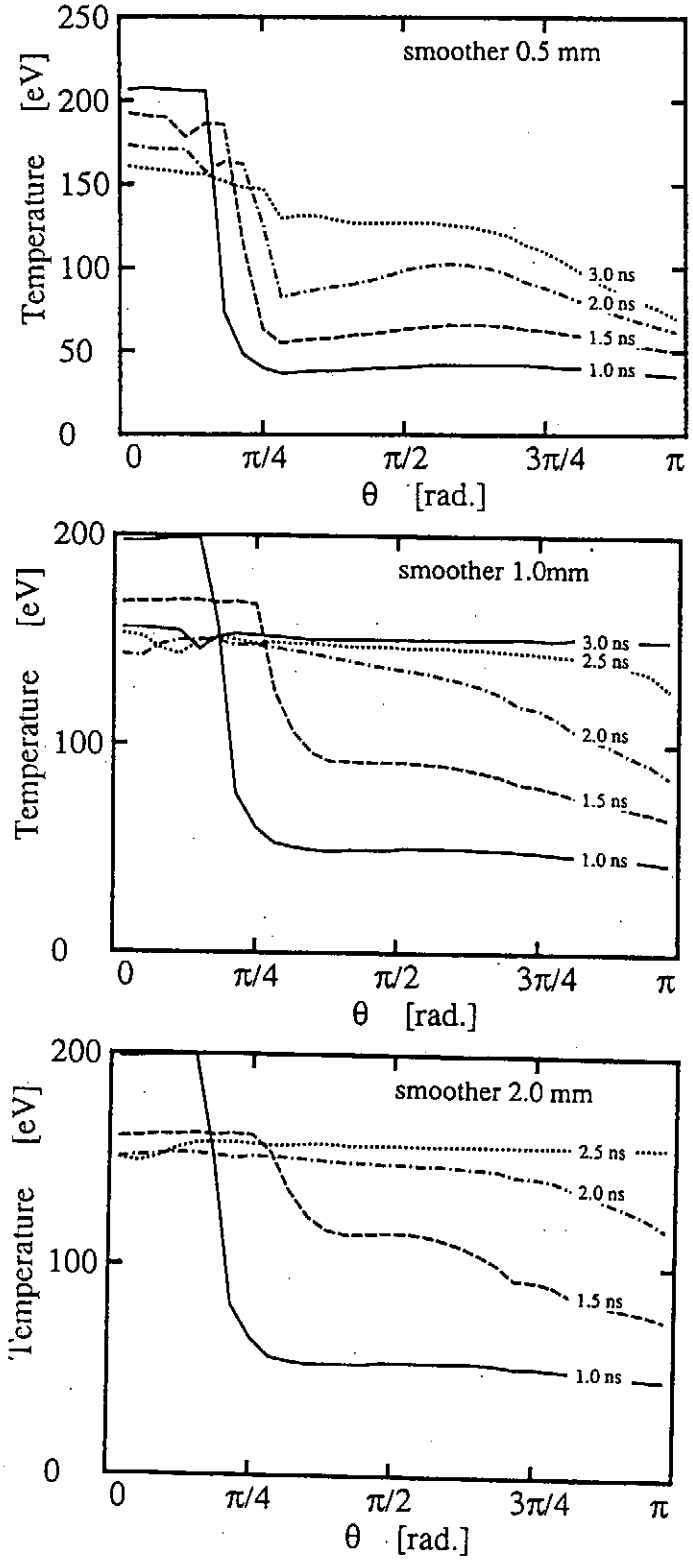

Fig. 6. Dependency of the thickness of the smoother layer on the process of the smoothing.

The collisional-radiative model was used for the atomic kinetics. The non-LTE opacities were calculated and used in the multi-group radiation transport. The X-ray conversion from the beam energy depended on the target structure and the radiation must be confined by the reflector. The reflector is seemed to consist of a high-Z material, however, the CR-model is no longer applicable for the atomic kinetics and a kind of approximations[15] will have to be employed.

The 2-D simulation of the radiation transport in an indirect driven ICF target, was carried out. The simulation results showed that the radiation smoothing layer was effective for the nonuniform beam irradiation. When the thickness of this layer was more than 1 mm, the intensity of the converted X-ray was smoothed out, even for the one-beam irradiation.

References

1) J. P. VanDevender and D. L. Cook, Science, **232**, 831 (1986)
2) D. L. Cook, et. al., in Proceeding of the 7th International Conference on High Power Particle Beams, Karlsruhe, edited by W. Bauer and W. Schmidt., p.35 (1988).
3) P. F. Ottinger, D. Mosher, and J. J. Watrous, Bull. Am. Phys. Soc., **34**, 2142 (1989).
4) T. Yabe, Jpn. J. Appl. Phys., **23**, L57 (1984).
5) T. Yabe, Jpn. J. Appl. Phys., **24**, L104 (1985).
6) H. Takewaki, A. Nishiguchi, and T. Yabe, J. Comp. Phys., **61**, 261 (1985).
7) H. Takewaki and T. Yabe, J. Comp. Phys., **70**, 355 (1987).
8) T. Yabe, et. al., Technical Report of ISSP, Univ. of Tokyo, Ser.A, No.2349 (1990).
9) D. Salzmann and A. Krumbein, J. Appl. Phys. **49**, 3229 (1982).
10) J. E. Rogerson, R. W. Clark, and J. Davis, Phys. Rev. A **31** 3323 (1985).
11) E. J. McGuire, J. M. Peek, and L. C. Pitchford, Phys. Rev. A, **26**, 1318 (1982).
12) T. A. Mehlhorn, J. Appl. Phys. **52**, 6522 (1981).
13) R. F. Schmalz, J. Meyer-ter-Vehn, and R. Ramis, Phys. Rev. A, **34**, 2177 (1986).
14) B. I. Bennet et. al., Los Alamos report LA-7130 (1978).
15) M. Itoh, T. Yabe, and S. Kiyokawa : Phys. Rev. A **35** 233 (1987).

ION-BEAM POWER AMPLIFICATION THROUGH X-RAY CONVERSION

Takashi YABE, Kazuhiko WAKUI, and Takayuki AOKI*
Department of Electronic Engineering, Gunma University
Tenjin-chou 1-5-1, Kiryu, Gunma 376
* *Department of Energy Sciences*
Tokyo Institute of Technology, Nagatsuta, Yokohama

Abstract

An extraction method of the radiation from the high temperature regin heated by ion beam is proposed. This method uses focusing characteristics of radiation waves through nonuniform density profile. A newly developed two-dimensional code is used to design this system. The ion beam of 3 TW/cm^2 is converted into the soft X-ray of 10 TW/cm^2 at the surface of the radiation emitter.

1. Introduction

We have proposed a scheme to compress and amplify an ion beam pulse[1] through soft X-ray conversion. This is so because a slowly propagating radiation wave acts as an accumulator of ion beam energy. Since the propagation speed of radiation heat wave is relatively slow, the energy flux from incident ion beam can be temporally stored within heat wave and hence the radiation power is amplified owing to this effect.

Recently, Honrubia[2] presented a calculation with a multi-group radiation transport. Although he observed a moderate power amplification, it is still not sufficient for fusion application. This paper shows that we can expect more effective amplification when a special configuration is used. We have performed two-dimensional hydrodynamic simulations in order to find an efficient amplification mechanism.

In section 2, a new hydrodynamic simulation code with radiative transfer is introduced. By using this code, ion beam amplification is examined in sections 3-4.

2. Two-Dimensional Hydrodynamic Code

Numerical methods for multi-dimensional hyperbolic equations are still a topic of considerable interest. Although many modern schemes based on an approximate Riemann solution have been proposed, they are sometimes cumbersome in including various terms other than hydrodynamic processes. Adding to this, since

they use a limiter function or switching function, real physical phenomena such as oscillations of high wave number are sometimes suppressed.

We have developed a new numerical method CIP (Cubic Interpolated Pseudoparticle) as a general solver for hyperbolic equations coulpled with source, sink, diffusion, or any other terms. This scheme has been tested with cylindrically converging shock waves, two-dimensional shock tube problem, the Rayleigh-Taylor instability, soliton formation in the KdV equation and so on. Since details are available in open literature,[3-5] we will not discuss it here. Some of the results are shown in Figs.1 and 2. Figure 1 shows the density contour of a Mach 3 flow[5] in a two-dimensional shock tube with a step. The top figure shows the result with a coarse mesh and its result is quite similar to the bottom figure with a fine mesh. This result is similar to or better than the best result with other modern schemes.[6]

Figures 2a and 2b show the two- and three-dimensional R-T instabilities. This comparison indicates that the mushroom structure in the three dimensions is much smaller than that in two dimensions. This difference may cast a shadow on two-dimensional simulations frequently used, since the R-T instability is widely recognized as a source of mixing in implosion processes. The details appear in Ref.7)

In simulating the ion beam amplification, we need to solve the diffusion equation :

$$\rho c_v \frac{\partial T}{\partial t} = \nabla(D \nabla T) + Q, \tag{1}$$

for radiation, where Q is the source term and/or hydrodynamic terms. In most of simulation codes, a matrix solver such as ICCG has been used. However, the speed of ICCG in vector computers may not increase in proportion to the vector length. We have proposed to use the SSI (Symmetrical Semi-Implicit) method for this solution,[8] since the SSI need not use matrix solver but is explicitly solved with a large time step. Although it is stable for infinite Δt, comparison with analytical solutions recommends the time step which satisfies $D\Delta t/\rho c_v \Delta x^2 < 10 \sim 50$.

Since the original SSI is given only for one-dimensional case, it is of use to show its two-dimensional version here.

$$T^{n+1}_{i,j} = (Q^n_{i,j} + \rho c_v T^n_{i,j}/\Delta t + B1 + B2 + B3 + B4)/B5$$

where $B1 - B5$ are defined as

$$B1 = [D^n_{i+1/2,j} T^n_{i+1,j} + D^n_{i-1/2,j} T^n_{i-1,j} + D^{n-1}_{i+1/2,j} T^n_{i+1,j} + D^{n-1}_{i-1/2,j} T^n_{i-1,j}]/\Delta x^2$$

$$B2 = -[D^{n-1}_{i+1/2,j} T^{n-1}_{i+1,j} + D^{n-1}_{i-1/2,j} T^{n-1}_{i-1,j}]/\Delta x^2$$

$$B3 = [D^n_{i,j+1/2} T^n_{i,j+1} + D^n_{i,j-1/2} T^n_{i,j-1} + D^{n-1}_{i,j+1/2} T^n_{i,j+1} + D^{n-1}_{i,j-1/2} T^n_{i,j-1}]/\Delta y^2$$

$$B4 = -[D^{n-1}_{i,j+1/2} T^{n-1}_{i,j+1} + D^{n-1}_{i,j-1/2} T^{n-1}_{i,j-1}]/\Delta y^2$$

$$B5 = \rho c_v/\Delta t + (D^n_{i+1/2,j} + D^n_{i-1/2,j})/\Delta x^2 + (D^n_{i,j+1/2} + D^n_{i,j-1/2})/\Delta y^2$$

where $D_{i+1/2,j} = (D_{i+1,j} + D_{i,j})/2$, and similar definition is used for f and the subscript j.

3. Analysis of Ion Beam Amplification

If the ion beam is incident on high-Z material that is optically thick, the energy propagates through it like a diffusion wave. In the diffusion process, the size of a heated region expands in proportion to $t^{1/2}$, while the ion beam energy is injected in proportion to t. Thus, the energy is accumulated in this region causing high temperature. Since the radiation power is proportional to σT^4, small increase of temperature largely enhances the radiation power.

The equation for the propagation of radiation is

$$\rho c_v \frac{\partial T}{\partial t} = \nabla(\frac{16\sigma\lambda_R T^3}{3} \nabla T), \tag{1}$$

for nearly equilibrium situation. If we estimate the propagation length L of the radiation wave within a time t such as $\partial T/\partial t \sim T/t$ and $\nabla T \sim T/L$, then we have $L = [(16\sigma\lambda_R T^3 t)/(\rho c_v)]^{1/2}$ from Eq.(1). The thermal energy accumulated in this region L is $\epsilon = \rho c_v T L$ and this energy must be supplied from the ion beam It. This balance determines the evolution of temperature. The black body radiation flux σT^4 from this plasma is given by[9)]

$$\frac{\sigma T^4}{I} = \frac{3L}{16\lambda_R}. \tag{2}$$

This means that the radiation intensity can be larger than the incident ion beam intensity if the length of amplifier is sufficiently longer than the radiation mean free path. This also raise another problem on how to extract the radiation energy from such an optically thick plasma. In some case, the amplifier and the target may be the same or fused shutter[2)] may be neccesary. In the next section, we will discuss this point more clearly.

Before going into detail, we make a scaling law for the power amplification. In doing this , we use xenon gas as an amplifier, because the opacity data for xenon is available from SESAME data table as a high-Z material. The SESAME data are fitted to give ;

$$\lambda_R = 1.36 \times 10^{-8} T_{eV}^{2.16}/\rho^{1.18} \quad cm, \tag{3}$$

The density is in g/cm^3. With this value we obtain

$$T_{eV} = 176.6(I_{13}^2 t_{ns}\rho^{0.18}/Z\beta)^{0.14}, \tag{4}$$

$$\sigma T^4 = 99.9(I_{13}^2 t_{ns}\rho^{0.18}/Z\beta)^{0.56}, \quad TW/cm^2 \tag{5}$$

$$L = 0.052 I_{13}^{0.722}(t_{ns}/Z\beta)^{0.86}/\rho, \quad cm \tag{6}$$

where β is defined as $c_v = 3Zk_B\beta/2m_i$. In the simulations shown in the next section, β is set to 1.5 in comparison with the Thomas-Fermi equation of state fitted by A.Bell.[10,11]

To obtain the maximum amplification a further limitation is required; most of the energy is expected to go to the thermal energy. This is achieved by using a low density layer[9] or high-intensity beam which satisfies

$$L > C_s t, \tag{7}$$

where C_s is the sound velocity. If C_s is estimated by $(Zk_BT/m_i)^{1/2}$, Eqs.(4) and (6) now yield ;

$$\rho < \frac{45.8 I_{13}^{0.58}}{t_{ns}^{0.21} Z^{1.29} \beta^{0.79}}, \tag{8}$$

These scaling have been investigated in detail[1] using the one-dimensional hydrocode HIMICO coupled with average ion model and multi-group radiation transport as well as the ion beam stopping calculation similar to that given by Mehlhorn.[12] In the next section, we will show two-dimensional simulations but with a simplified physics included.

4. Simulation of Ion Beam Amplification

The important point in this process is how to use the radiation from the region of the highest temperature. When the ion beam is injected from the righthand side and the radiation wave propagates leftward, the temperature decreases to the left. This decrease is not much for the radiation because of large nonlinearity of the diffusion coefficient. However, since the radiation power is proportional to σT^4, it is sensitive to this decrease. Therefore, it is important to find a way to extract the radiation from high temperature region. In this section, we propose a possibility to do this. This method uses the collision of two thermal waves.

Figure 3 shows the time evolution of the temperature when the proton beam of 1.5 MeV, 3 TW, 60 ns FWHM in a triangular pulse shape is incident on the xenon gas of 0.01 g/cm^2 from the righthand side. In this calculation, we have used the CIP for hydrodynamics, the one-temperature approximation for fluid and radiation, $\beta = 1.5$, and with the ion beam stopping.[12] For the solution of the radiative diffusion, we have used SSI, where the matrix equation need not be solved and the calculation speed is quite high suitable for multi-dimensional simulations. Surprisingly, this simulation is quite similar to the more elaborate one by HIMICO.

In another simulation, the two ion beams are incident from both sides. The length of the amplifier is doubled. The time evolution of the temperature for this case is shown in Fig.4. As is easily understood, the temperature at the center is the same as the maximum temperature. However, how can we use the radiation from this region. One possibility is to use a configuration shown in Fig.5. The

radiation waves propagate through the tube and collide in the middle of the tube, where the radiation is extracted in a perpendicular direction through a hole on the wall of the tube.

Another method is to use the focusing of the radiation. Since the propagation speed of the radiation is inversely proportional to the density, the radiation wave directs towards the high-density region. By properly changing the xenon gas density, the two radiation waves can collide at any place we like. Figure 6 shows the configuration used in the simulation, whose results are shown in Fig.7. Here, the increment of the contour is 5 eV. A very low density region ~ 0.001 g/cm^2 of 1 cm radius is located at the center. The xenon density linearly varies from 0.005 g/cm^3 (top or bottom) to 0.015 g/cm^3 (center). Since the ion beam stopping length is also inversely proportional to the density, the radiation wave is driven obliquely from the begining.

The radiation wave should be designed to collide at the inner surface of the amplifier which is the outer surface of the low density region(0.001 g/cm^3 and 1 cm radius) at the center. Although the calculation shown in Fig.7 is not yet optimized, the temperature of 100 eV at this surface is already attained. It should be noticed that this temperature is almost the peak temperature obtained in Figs.3 and 4. In the final figure, the contour corresponding to 100 eV is indicated by an arrow. The radiation from plasmas of 100 eV is about 10 TW/cm^2. Therefore, the intensity of incident ion beam is amplified by 3 times even in this low intensity beam of 3 TW/cm^2. This result does not change seriously even if the fluid motion is suppressed.

5. Summary

We have developed a new two-dimensional hydrodynamic code including radiation transport which is solved with the SSI method with high efficiency. Implementatin of this code is quite easy compared with the preceding schemes. This code is applied to the ion beam amplification. A new extraction method of the radiation from the region of the highest temperature has been proposed and 3 times amplification has been demonstrated even in the case of 3 TW/cm^2 ion beam, which is available at present and is a parameter close to PBFA II at SNL. The amplification will increase in proportion to the incident power.

The important point in this paper is that the amplification of the power is of no doubt but the radiation power which can be effectively used depends on the extraction method. For the latter, there may be a variety of schemes. We have proposed only two schemes. In such a design, two and three dimensional code is quite effective. More effective schemes are under consideration.

One of the authors (T.Y.) would like to thank Professor Dr. F. Winterberg for indicating a possibility of focusing radiation heat waves through variable density.

References

1) T.Yabe, Jpn.J.Appl.Phys. **23**(1984)L57, **24**(1985)L104, **26** (1987)L296.
2) J.J.Honrubia, Laser and Particle Beams **8** (1990)117.
3) T.Yabe and E.Takei, J.Phys.Soc.Japan **57** (1988) 2598.
4) T.Yabe, T.Ishikawa, Y.Kadota and F.Ikeda **59** (1990)2301.
5) T.Yabe *et al.*, Technical Report of ISSP (The Institute for Solid State Physics, The University of Tokyo), Ser.A, No.2349 (1990) ; accepted for publication in Comput. Phys. Comm. (1991).
6) P.Woodward and P.Colella, J.Comput.Phys. **54** (1984) 115.
7) T.Yabe and H.Hoshino, NIFS-61 (National Institute for Fusion Study) (1990); submitted to Phys.Rev.A.
8) T.Ishikawa and T.Yabe, The Fourth IEEE Conference on Electromagnetic Field Computation, Tronto, Ontario, October (1990).
9) K.Unterseer and J.Meyer-ter-Vehn, Jpn.J. Appl. Phys. **23** (1984) L728.
10) R.Latter, Phys. Rev. **99** (1955) 1854.
11) A.R.Bell, *New Equation of State for MEDUSA*, Rutherford Laboratory Report, RL-80-091 (1981).
12) T.A.Mehlforn, J. Appl. Phys. **52** (1981) 6522.

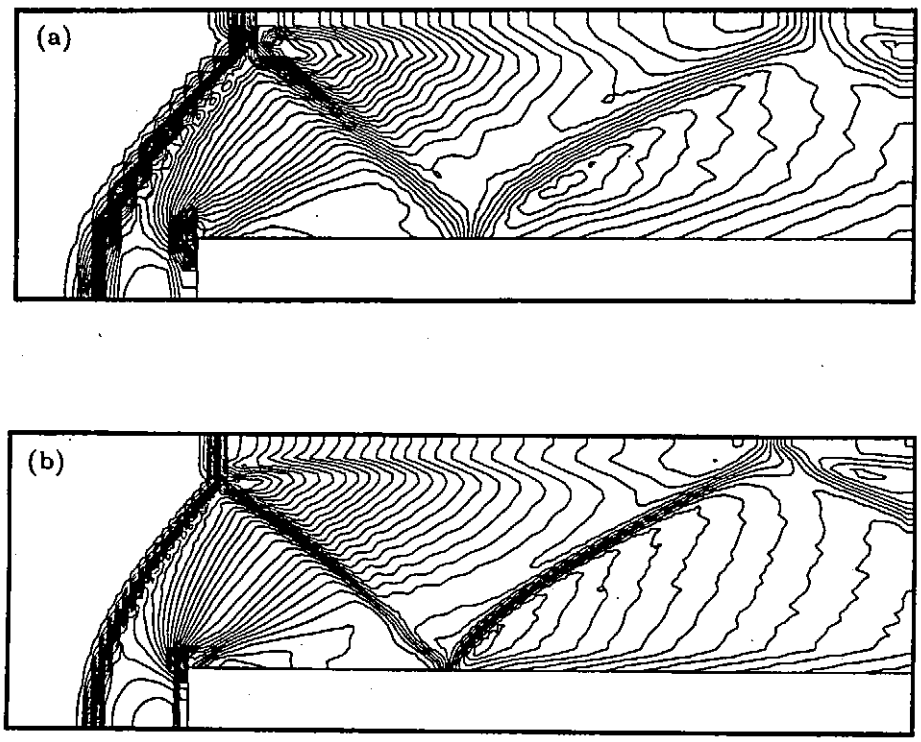

Fig.1 Density contour of a Mach 3 flow in a tube with a step in 60×20(Top) and 120×40 (Bottom) mesh system.

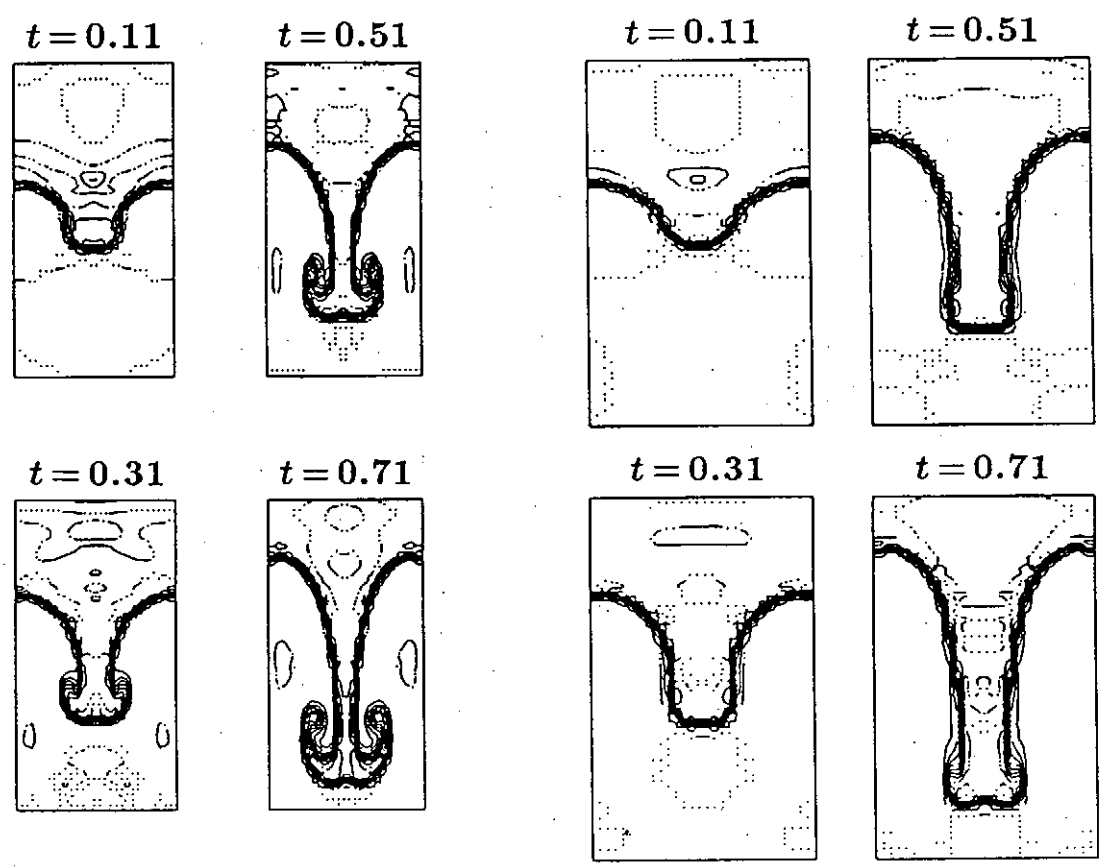

Fig.2 Time evolution of the Rayleigh-Taylor instability in (a) two- and (b) three-dimensions.

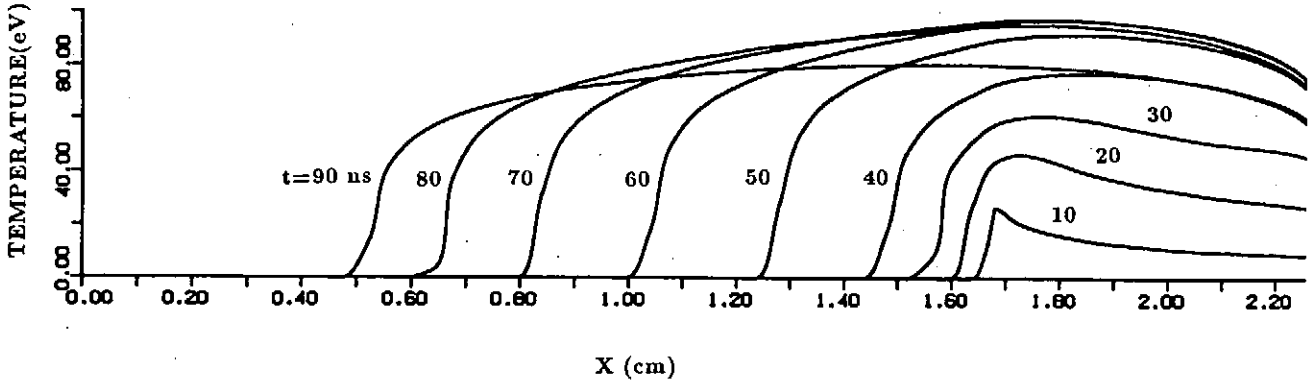

Fig.3 Time evolution of the temperature when the ion beam is injected from the righthand side.

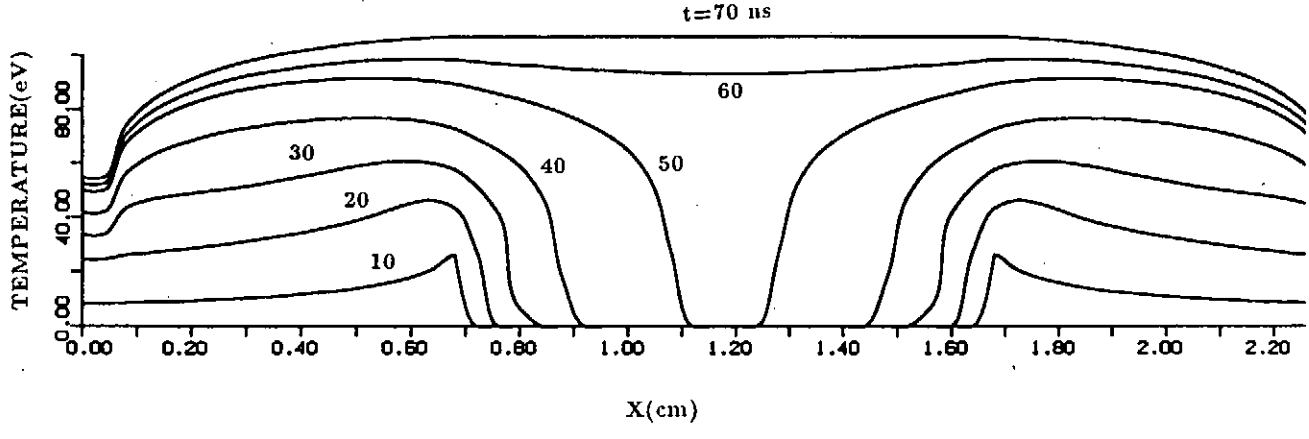

Fig.4 Time evolution of the temperature when two ion beams are injected from both sides.

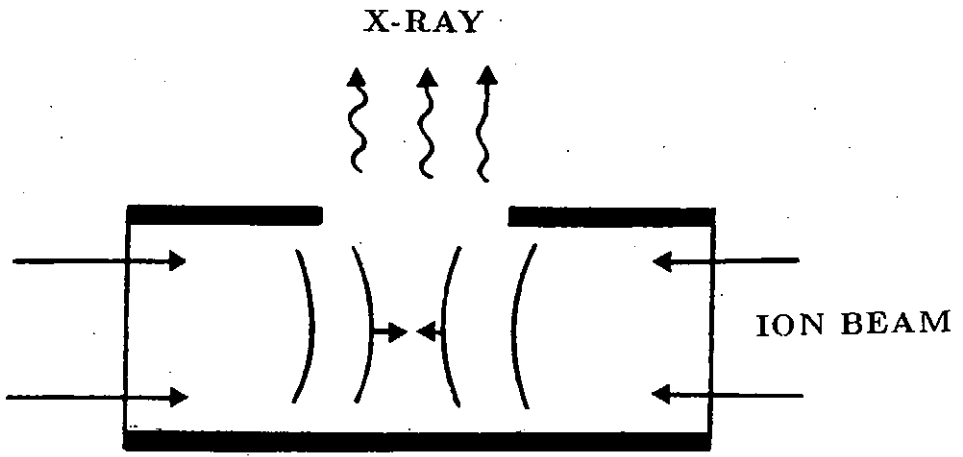

Fig.5 If the tube has a hole in the middle, radiation from the colliding thermal waves can be extracted.

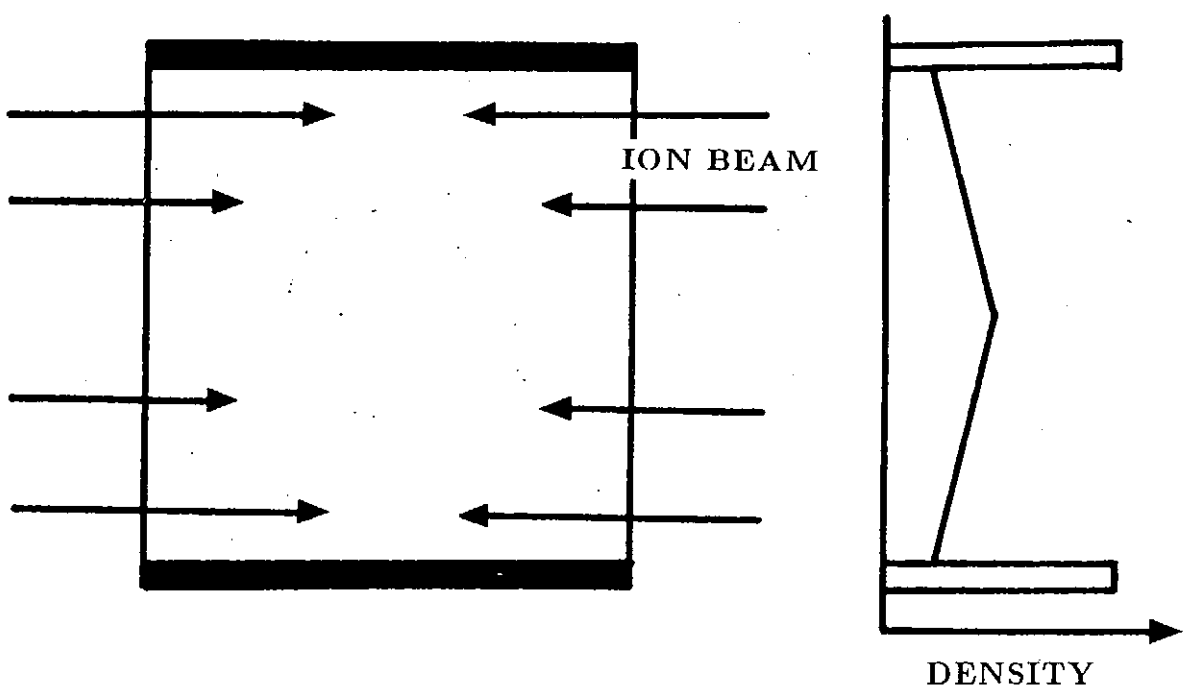

Fig.6 Alternative scheme which uses the focusing of thermal waves. Density changes vertically but not horizontally.

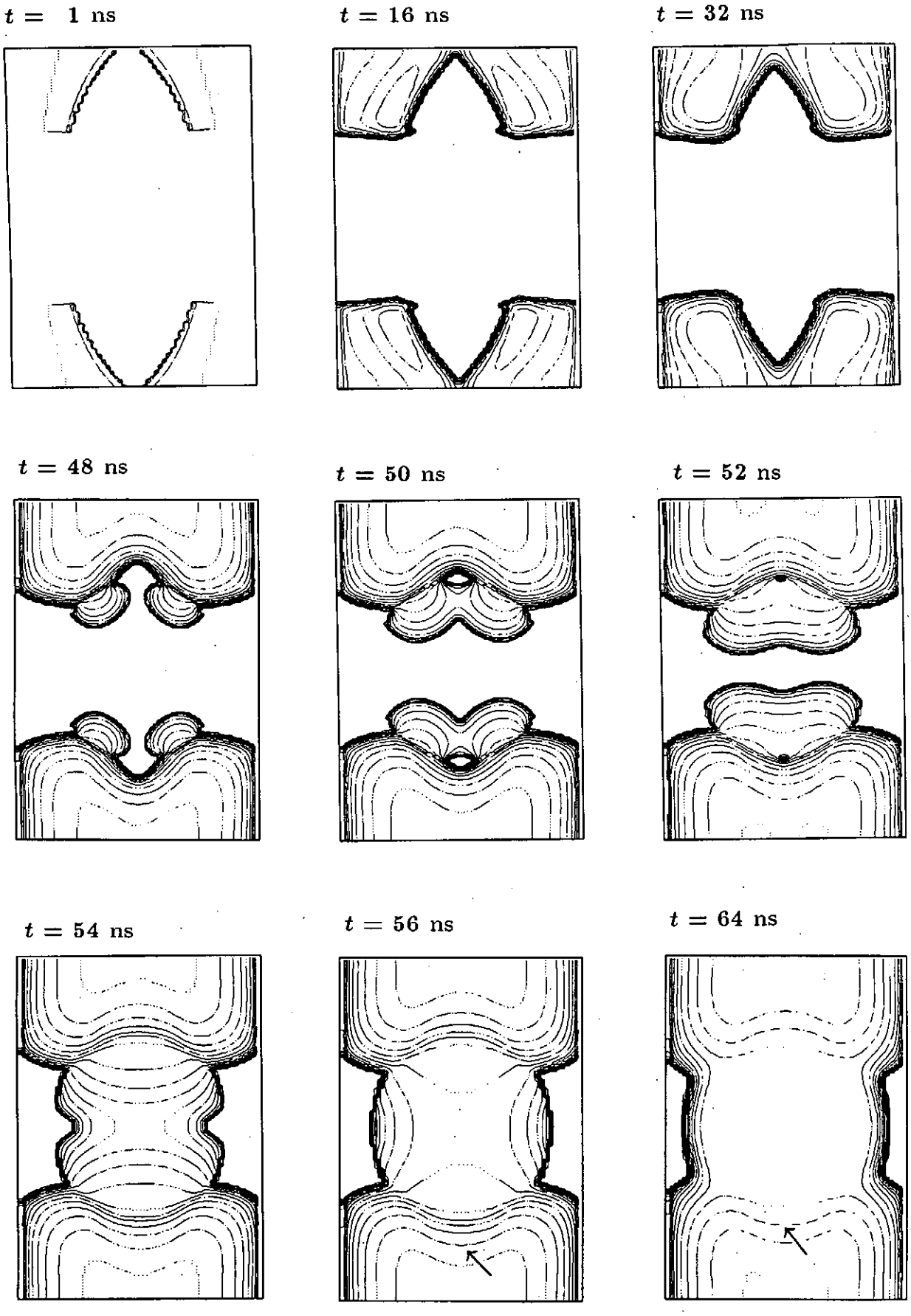

Fig.7 Time evolution of the temperature in the amplifier proposed in Fig.6. The increment of the contour is 5 eV and the contour for 100 eV is indicated by an arrow in the last figure.

PROTON BEAM FUSION —BEAM PROPAGATION AND FOCUSING—

Keishiro Niu
Physics Laboratory
Teikyo University of Technology
Uruido, Ichihara, Chiba 290-01, Japan

ABSTRACT A fusion power plant of 1GW electric output is proposed here by using proton beam of 12MJ per shot for energy driver. Technical difficulties appear in beam propagation and focusing. In order to delete the unneutralized charge at the leading edge of the propagating proton beam, simultaneous launching of electron beam is proposed here. If the electron beam current exceeds the proton beam current by 50kA, cooling of proton beam will be achieved in the region of beam convergence. An indirect driven target can release enough fusion output energy in spite of nonuniform beam irradiation. The flibe for coolant in the reactor cavity with thickness of 50cm thermalizes the neutrons which are produced by fusion reactions, and the flibe protects the solid wall from being damaged. Tritium breeding ratio can exceed unity.

1. INTRODUCTION

It seems that the goal of nuclear fusion is in a far way from the present stage of technology. Much partial advancements have been achieved in many types of experimental machines for fusion. Even one shortage of technology, however, leads us to the vital failure. If one machine breaks through all technologies for fusion including energy conversion from kinetic energy of neutrons to electricity, it plays no use when energy pay rate=(total amount of energy generated from the machine during operational life)/(total energy consumed in constructing and operating the machine) cannot exceed unity.

Proton beam has many advantages for energy driver of inertial confinement fusion (ICF). The large amount of proton beam energy can be extracted economically[1,2]. Since proton is the lightest ion, proton beam can be extracted from the anode plasma ahead of other ions. The conversion ratio from the electric energy to the kinetic energy of proton beam is high. The target interaction with the proton beam is simple and efficient. The essential two points for proton beam fusion are the beam propagation and the target structure. Especially with respect to the beam propagation and focusing, simultaneous launching of electron beam is proposed to delete the charge at the leading edge of the beam and to cool the beam.

The indirect driven target is proposed to be used for spherically symmetric implosion of the fuel in spite of nonuniform beam irradiation[3].

Although a proposal of power plant by light ion beam (LIB) fusion has been given[4], another plant of proton beam by inertial confinement fusion (ICF) is given here as a reasonable one from technical and economical points of views. The paper includes the analysis for thermalization of neutrons which are generated by fusion reactions and for tritium breeding in the coolant—flibe. These points are investigated in section 5.

2. PULSED POWER SUPPLY SYSTEM

The power supply system is similar to those proposed before[5]. Here proton beam is extracted from the diode with the particle energy of 4MeV. In order to extract the proton beam from a diode with the particle energy of 4MeV, the output voltage of Marx generator is 8MeV. This value seems to be reasonable for the ordinary Marx generator. For proton beam impinging on a spherical target, a spherically symmetric irradiation of proton beam on a target may be difficult to be realized. Therefore, an indirect driven target is proposed to be used[3]. In this case, the beam energy, required to realize the fusion output energy of 3GJ from a target, is 12MJ per shot. Here, 12 power supply systems are prepared. Each two of them are combined together to extract one proton beam, whose energy is 2MJ per shot. The power supply system is as follows:

Marx Generator 12 modules

1 charging voltage 200kV
2 capacitance of a bank 5.0μF
3 number of capacitor banks 40
4 stored energy 4MJ
5 output voltage 8MV

Cylindrical Intermediate Storage Capacitor 12 modules
1 insulator water
2 inner (anode) radius 3m
3 outer (cathode) radius 4m
4 length 7m
5 charging time 310ns

Pulse Forming Line 12 modules
1 input voltage 8MV
2 output voltage 4MV
3 length 0.67m
4 pulse width τ_b=30ns

Once the power in a Marx generator is shifted into an intermediate storage capacitor, which is a coaxial cylinder filled with water for dielectric material. The inner (anode) radius is 3m, the outer (cathode) radius is 4m, and the length is 7m. The charging time is estimated to be 310ns. The pulse forming line has the length of 0.67m for the pulse width of 30ns. The input voltage is 8MV and the output voltage is 4MV.

Here the electron beam is proposed to be launched to the target simultaneously with the launching of ion beam. The power supply system for electron beam is as follows:

Power Supply System for Electron Beams 6 modules
1 output voltage −6.20kV
2 stored energy 3.93×10^2J

Bank for Grid
1 capacitance 354pF
2 charging voltage 168kV
3 stored energy 5kJ

The electron beam is launched from a triode to the target at the same time with the launching of proton beam in order to neutralize the charge of the proton beam during propagation in the reactor cavity. To let the electron beam have the same velocity with that of proton beam which has the propagation energy of 4MeV, the cathode voltage of triode to accelerate the electron is −6.20kV. This voltage is supplied by a kind of Marx generator, whose stored energy is 3.93×10^2J. The total energy stored in the Marx generators of 6 modules to extract six electron beams is only 2.38kJ. To the grid of triode, the voltage of 168kV is supplied through a capacitor bank of 3.55μF, where 50kJ is initially stored. Thus the total stored energy for six capacitor banks of grid circuits is only 300kJ. Required energy to extract six electron beams is negligible in comparison with that for proton beams.

To construct the total power supply systems, the cost is estimated to be \$120M, which is less than 10% of the construction cost of light water reactor of 1GW. Economically and technically, proton beam fusion system seems to be reasonable.

3. BEAM-EXTRACTION AND BEAM-PROPAGATION

For intense proton beam, beam focusing is difficult to be achieved[6]. One of the reasons for this uncomfortable poor focusing of proton beam seems to come from the unneutralized proton charge at the leading edge of beam[7,8]. In order to delete the unneutralized proton charge, the simultaneous launching of electron beam is proposed. The diode to extract proton beam and the triode to extract electron beam are shown in Fig. 1.

The parameters of diode and triode are as follows.

diode

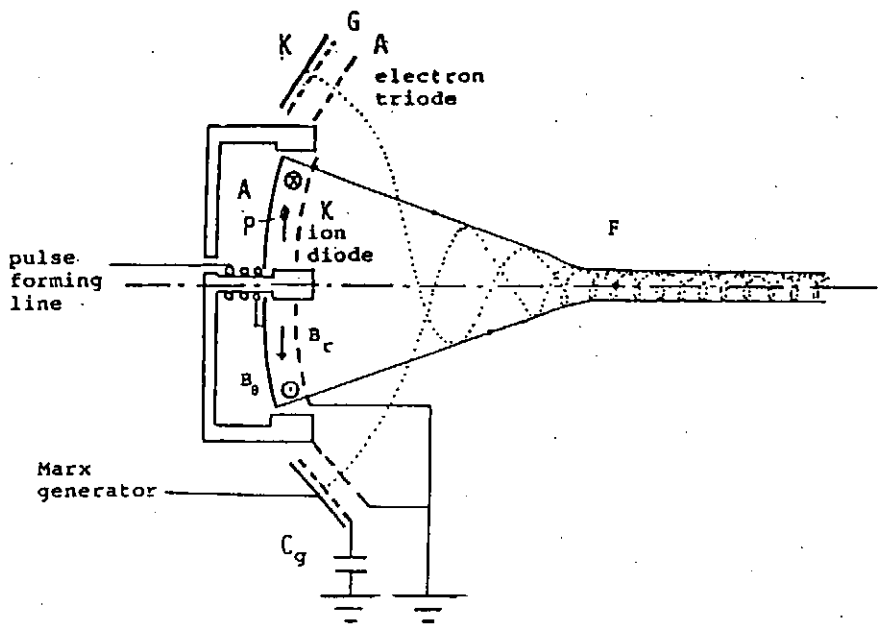

Fig. 1. Diode for proton beam and triode for electron beam.

1 anode inner radius $r_i = 1$cm
2 anode outer radius $r_o = 32.5$cm
3 anode area $S_A = 3.32 \times 10^3 \mathrm{cm}^2$
4 AK gap distance $d_{AK} = 9.51$mm
5 azimuthal field $B_\theta = 4.55$T
6 radial field $B_r = 4.54 \times 10^{-4}$T for $v_\theta = 2.77 \times 10^4$m/s
7 anode voltage $V_A = 4$MV
8 proton current density $j_p = 5\mathrm{kA/cm}^2$
9 proton total current $I_p = j_p S_A = 16.60$MA

triode
1 cathode inner radius $r_{in} = 35$cm
2 cathode outer radius $r_{out} = 43.4$cm
3 cathode area $S_K = 2.08 \times 10^3 \mathrm{cm}^2$
4 KA gap distance $d_{KA} = 1$cm
5 cathode voltage $V_K = -6.20$kV
6 KG gap distance $d_{KG} = 2.0$mm
7 grid voltage $V_G = -168$kV
8 electron current density $j_e = -8\mathrm{kA/cm}^2$
9 electron total current $I_e = j_e S_A = -16.65$MA

The anode of diode is too wide. Really, the diode is divided into, for example, 6 pieces. Between the connecting two pieces, the coil to supply B_θ is inserted. (See Fig. 2.)

The number densities and the velocities of the proton and electron beams are comparable. During the order of 10^{-13}s after the electron beam leaves the anode, the electron beam neutralises the charge of proton beam. The pulse duration is set to be 30 ns. The proton energy of one beam is 2 MJ, while the electron energy of one beam is only 1.09 kJ. If 10 % of the electron beam current flows into the grid surface, 0.52 J/cm^2 of electron beam energy is deposited on the grid. This amount of electron beam energy will not damage the grid mesh. The cathode of diode and the anode of triode are hollow rings. By controlling V_K and V_G, the electron total current I_e should be adjusted to exceed the proton total current I_p by 50 kA. That is, $I_{eff} = I_p + I_e = -50$kA. Thus the electron beam completely neutralises the charge of proton beam at the leading edge, and

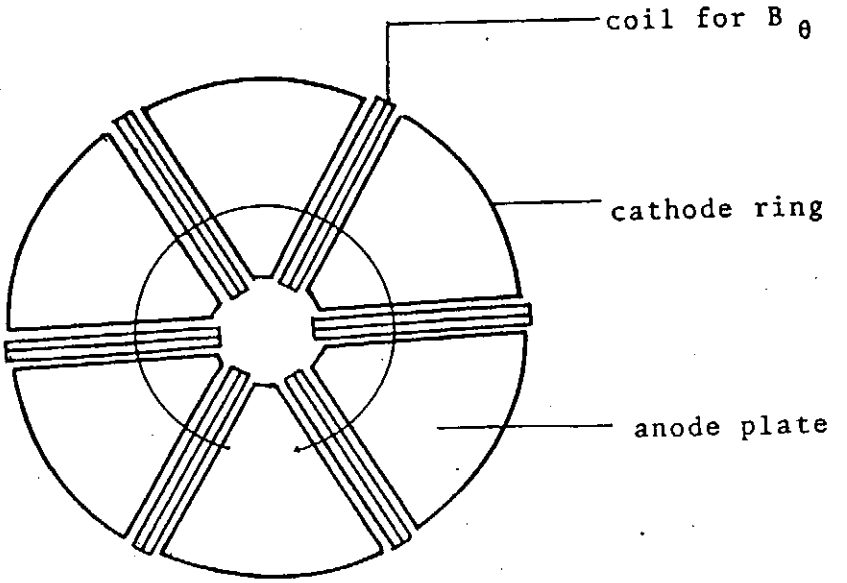

Fig. 2. Front view of diode and coils for B_θ.

suppresses the proton beam from electrostatic divergence. This is the most important point of the proposal of simultaneous electron beam launching to converge the proton beam.

The gap between the anode and cathode of diode is highly evacuated. There are only proton particles. The equation of motion of a proton in the gap is,

$$m_p \frac{d\mathbf{v}}{dt} = e(\mathbf{E}_o + \mathbf{E}_s + \mathbf{E}_m + \mathbf{v}\times\mathbf{B}) \tag{1}$$

where m_p is the proton mass, $\mathbf{v}$ the velocity, e the charge, $\mathbf{E}_o$ the electric field given by the anode voltage, $\mathbf{E}_s$ the electrostatic field by proton charges, $\mathbf{E}_m$ the electric field by the proton motions and $\mathbf{B}$ the magnetic field by the coils for electron insulation. In the cylindrical coordinate system $\mathbf{r}(r, \theta, z)$, the proton motion is observed. When the radius of anode curvature has 57.2 cm, $E_{or} = -10^8$V/m at the central point P in the diode in Fig. 1. Here suffix r refers to the radial component. $\mathbf{E}_m$ is smaller than $\mathbf{E}_s$. It is estimated that $E_{sr} = 10^8$V/m and E_{sr} almost cancels out E_{or}. The term $v_z B_\theta$ is estimated to be 6×10^7V/m. If the curvature of the anode is modified as a function of r, the velocity of proton, which leaves the cathode surface, can be controlled[9,10]. The r-component of proton velocity at the cathode surface (at the central part near P) is estimated to be 8×10^6m/s, which corresponds to 1.2MeV. Proton particles are focused at the neighborhood of focal point F by the r-component of proton velocity. After the focal point F, if the proton particles reserve the r-components of their velocities, the proton beam has a high temperature of 1.2MeV. With this high temperature, the proton beam has difficulty to be confined in a small radius during propagation.

The effective beam current $I_{eff} = I_p + I_e = -50$kA induces the negative azimuthal magnetic field in the region of beam-convergence. At $r = 15.75$cm near P on the cathode of diode, $B_\theta = 0.0657$T. At $r = 1$cm near the focal point F, $B_\theta = 0.212$T. Thus the electron gyro radii are smaller than 1mm everywhere in the region of beam convergence. In the region of beam-convergence, electrons do drift motions. Proton particles experiences this magnetic field, too. But proton paths have such large radii as 70cm. Proton particles fly ballistically toward F. If the magnetic field is of this order of magnitude, all proton particles loose almost all the r-components of velocities at F because of the Lorentz force $v_z B_\theta$. (See Fig. 3.)

In other words, the effective beam current $I_{eff} = -50$kA cools the beam temperature. This is the second important point of our proposal. The proton particles have local divergence-angles of order of one degree at the cathode surface of diode. The radius of propagating beam at the focal point F cannot be reduced to less than 5mm.

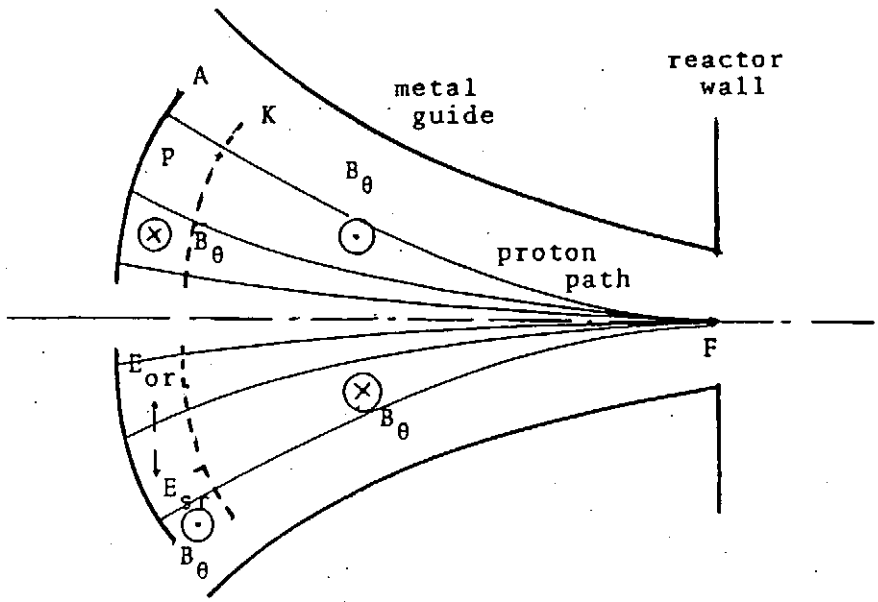

Fig. 3. Ideal paths of proton particles in convergence region.

So far, the self-induced magnetic field by beam current itself has been proposed[11,12]. The simultaneous electron launching, however, cancels out the proton beam current. Therefore, the revival of plasma channel is proposed. After the focal point F, plasma channel is formed in the reactor to propagate proton beam[13-15]. When the discharge current is 100kA in the plasma channel, the Lorentz force confines the proton beam with the temperature of 1.67keV in the radius of 5mm. Thus the cool proton beam can propagate in the plasma channel. In the gap between the anode and cathode of diode, a weak radial magnetic field B_r is applied. This weak field produces the θ-component of proton velocity. In this way, the slow rotation of proton beam during propagation induces a weak axial field B_z, which stabilizes the beam propagation.

4. INDIRECT-DRIVEN-TARGET

In order to simplify reactor structure, number of proton beams in the reactor cavity cannot increase. Six beam irradiation has been already proposed [1,16]. With such a small number of beams, beam irradiation is not uniform on target surface. For such nonuniform beam irradiation, to use indirect driven target has been proposed[3,17]. For intense proton beam with beam energy of 12MJ and the pulse width of 30ns, the indirect driven target with a large radius has been proposed to be used[18,19]. The structure of target is schematically shown in Fig. 4.

The parameters of target, whose outer radius is 8.7mm, is written down as follows.

lead tamper
1 density $\rho_{Pb} = 11.3\text{g/cm}^3$
2 thickness $\delta_{Pb} = 23.4\mu\text{m}$
3 mass $M_{Pb} = 120\text{mg}$
4 rate of beam energy deposition $C_{Pb} = 20\%$

lead radiator
1 density $\rho_{ra} = 2.13\text{mg/cm}^3$
2 thickness $\delta_{ra} = 690\mu\text{m}$
3 mass $M_{ra} = 1.49\text{g}$
4 rate of beam energy deposition $C_{ra} = 80\%$
5 temperature T_{ra}=8K$\rightarrow$ 1.7keV$\rightarrow$600eV
6 expansion velocity v_{ra}=1.61×10^5m/s
7 inward radiation intensity $I_{ra} = 4.06\times10^3\text{W/cm}^2$

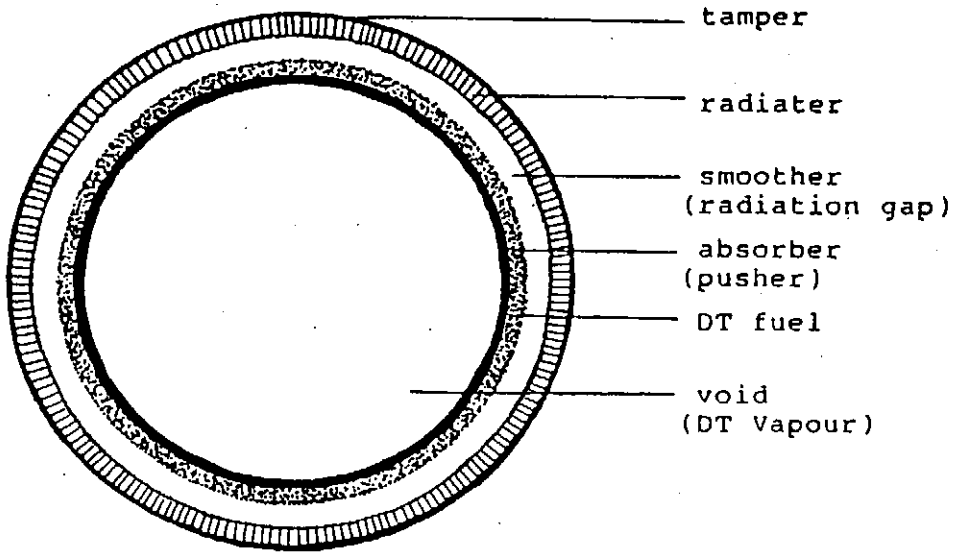

Fig. 4. Structure of indirect driven target.

radiation gap (smoother, vacuum)
1 thickness $\delta_{sm} = 2$mm
2 closing time $\tau_{sm} = \delta_{sm}/v_{ra} = 12.4$ns<20ns
aluminum absorber (pusher)
1 density $\rho_{Al} = 2.7$g/cm^3
2 thickness $\delta_{Al} = 217\mu$m
3 mass $M_{Al} = 264$mg
4 temperature $T_Al = 8K \rightarrow 200$eV
5 pressure $p_{Al} = 0 \rightarrow 10^{12}$Pa
6 propagation velocity of hot region $v_{Al} = 5.42\times10^3$m/s
7 transparent time $\tau_{Al} = \delta_{Al}/v_{Al} = 40$ns
solid fuel
1 density $\rho_{DT} = 0.19$g/cm^3
2 thickness $\delta_{DT} = 286\mu$m
3 mass $M_{DT} = 23$mg
inside void
1 radius $r_v = 5.5$mm
2 saturated vapor pressure p_v=7×10^{7}Pa

It is shown that radiation mixing in the smoother layer smooths out the nonuniformity of pressure on the surface of pusher-layer[19]. Fuel implosion occurs in a spherically symmetric way. The target is expected to obtain the pellet gain of 250 and to release fusion energy of 3GJ per shot.

5. NEUTRON THERMALIZATION AND TRITIUM BREEDING IN FLIBE

The reactor to be used is just the same with that proposed by Niu and Kawata[1]. The flibe is proposed to be used as coolant in the rotating reactor. The flibe is chemically stable and the neutron with energy of 14.6MeV is thermalized in the flibe layer with the thickness of 50cm. No damage is expected to be accepted on the structual reactor wall by the spattering, blistering and swelling.

Figure 5 shows the accumulated neutron numbers which are counted at the outer surface of flibe layer with thickness of 50cm or 75cm in the spherical reactor cavity of radius of 5m. On

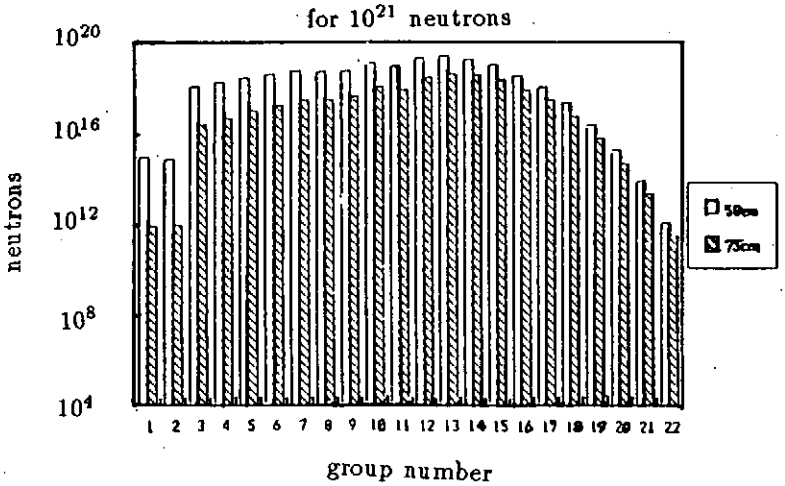

Fig. 5. Numbers of neutrons which leak out from the outer surface of flibe.

the inner surface of the flibe layer, 10^{21} neutrons with the particle energy of 14.6MeV impinges in a moment. The group number corresponds to the energy range of neutrons: 1, 14-12MeV; 2, 12-10MeV; 3, 10-8MeV; 4, 8-6MeV; 5, 6-5MeV; 6, 5-4MeV; 7, 4-3MeV; 8, 3-1.4MeV; 9, 1.4MeV-900keV; 10, 900-400keV; 11, 400-100keV; 12, 100-17keV; 13, 17-3keV; 14, 3keV-550eV; 15, 550-100eV; 16, 100-30eV; 17, 30-10eV; 18, 10-3eV; 19, 3-0.1eV; 20, 0.1-0.04eV; 21, 0.04-0.01eV; 22, 0.01-0.0025eV.

From fig. 5, number of neutrons, which leak out from outer surface of flibe with the particle energies more than 10keV, is counted to be 10^{18}. Among the damages in the solid wall, that by swelling is the most severe. If one neutron is assumed to knock on 10 lattice atoms on the average in the solid wall outside the flibe, it takes 420 years (life time of wall) until the solid wall with the thickness of 1/4 inch accepts the damage of 20% by impinging neutrons.

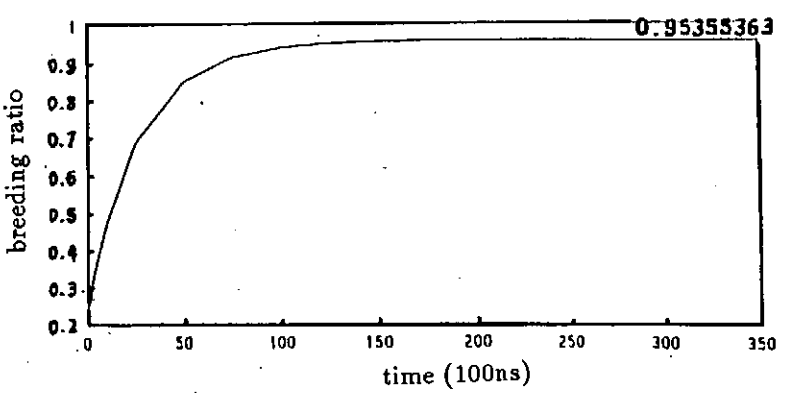

Fig. 6. Tritium breeding ratio.

The volume of flibe per fusion reactor is required to be $300m^3$, when the thickness of flibe layer is 50cm. The corresponding mass of flibe is 660t, in which the lithium mass is 200t. The total lithium mass on the earth is estimated to be 1.8×10^{10}t. Enough number of fusion power plants with flibe-wall can be constructed. One of difficulties to operate fusion power plant is diminished by using the liquid wall of flibe and the cost to construct the plant decreases much.

Figure 7 shows the accumulated tritium breeding ratio versus time for the flibe with thickness of 50cm. At t=150ns, breeding ratio is saturated. But the ratio is less than unity. Figure 8 indicates breeding ratios in the flibe with thickness of 1m for ^{7}Li by high energy neutrons, ^{6}Li

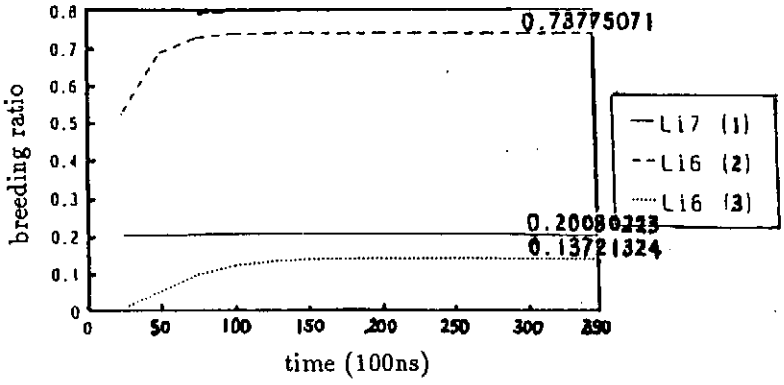

Fig. 7. Tritium breeding ratio due to ^{7}Li by high energy neutrons, ^{6}Li by intermediate energy neutrons and ^{6}Li by low energy neutrons.

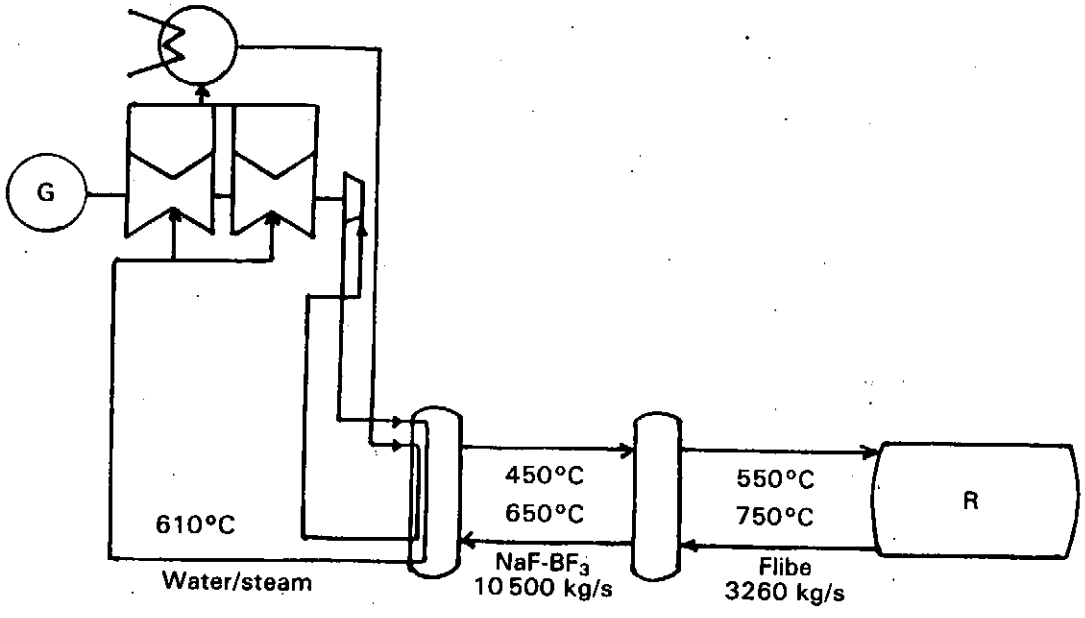

Fig. 8. Heat exchange system of plant.

by intermediate energy neutrons and ^{6}Li by thermalized neutrons. The natural lithium in flibe includes 97.5% of ^{7}Li and 2.5% of ^{6}Li. Figure 8 shows that ^{6}Li plays an important role on tritium breeding. If the mixing ratio of ^{6}Li increases to 5% in the lithium in flibe, tritium breeding ratio will exceed unity in flibe with thickness of 50cm.

Figure 9 shows heat exchange system outside the fusion reactor.

6. SUMMARY

Power supply system for proton beam of 12MJ with pulse-width of 30ns can be constructed with a reasonable cost. The first wall of a molten salt can protect structural materials of reactor from damage[20]. The most sever problem for proton beam fusion is the beam focusing and the beam propagation. To delete unneutralized proton charge, which causes the beam divergence at the leading edge, electron beam is launched simultaneously. The excess of electron beam current plays a role on cooling of proton beam. The usage of indirect driven target with a large radius is complementary to the poor focus of beam for proton beam fusion.

REFERENCES

1) Niu K. and Kawata S., Fusion Tech. **11**, 365 (1987).
2) Cook D. L. et al., Proc. Beams'88 (Karlsruhe) 35 (1988).
3) Niu K., Laser and Particle Beams **7** 505 (1989).
4) Niu K.,Aoki T. and Naramoto H., Laser Interaction and Related Plasma Phys. **8**, 605 (1989).
5) Niu K. and Aoki T., Laser Interaction and Related Plasma Phys. **9** (1990) (in printing).
6) Bailey J. et al., Book of Abstract of 5th Atomic Physics for Ion Driven Fusion (Schliersee) 4.3 (1990).
7) Kaneda T. and Niu K., Jpn. J. Appl. Phys. **28**, 903 (1989).
8) Kaneda T. and Niu K., Laser and Particle Beams **7**, 207 (1989).
9) VanDevender J. P. et al., Proc. on ICF Research by High-Power Particle Beams (Nagaoka) 25 (1986).
10) Miyamoto S. et al., Proc. Beams'86 (Kobe) 111 (1986).
11) Aoki T. and Niu K., Laser and Particle Beams **6**, 737 (1988).
12) Aoki T. and Niu K., Laser and Particle Beams **8**, 111 (1990).
13) Cooperstein G. et al., Proc. on ICF Research by Light-Ion beam (Nagaoka) 1 (1982).
14) VanDevender J. P. et al., Laser and Particle Beams **5**, 439 (1987).
15) Kawata S., Niu K. and Murakami H., Jpn J. Apply Phys. bf 22 302 (1983).
16) Niu K., Aoki T. and Takeda H., Laser Interaction and Related Plasma Phenomena (Monterey) **8**, 613 (1989).
17) Meyer-ter-Vehn J., Proc. on Heavy Ion Inertial Fusion (Darmstadt) 25 (1988).
18) Velarde G. et al., Book of Abstract of 20th ECLIM (Schliersee) 5-1 (1990).
19) Niu K., Aoki T., Sasagawa T. and Tanaka Y., Laser and Particle Beams (submitted).
20) Naramot H. and Niu K., Symp. on Target Interaction of Particle Beam (Nagoya) IPPJ-900, 12 (1989).

Developments for High Performance Light Ion Beams[1]

S.Miyamoto, A.Zakou, S.Yasumura, K.Takitani,
Y.Yasuda, T.Akiba, K.Imasaki*, C.Yamanaka* and S.Nakai

Institute of Laser Engineering, Osaka University
Institute for Laser Technology*, 2-6 Yamada-oka, Suita, Osaka 565

Abstract

We are pursuing to develop an energy driver for inertial confinements fusion using two-stage diode on induction adder pulse power system. Two-stage ion diode has promising advantage for this purpose. The main advantages are 1) the easiness to generate the high voltage required for heavier ion acceleration, 2) the controllability of diode impedance in the ion beam injected diode, and 3) the efficient acceleration of high energy ions by the charge stripping acceleration. The experiments have been performed on an induction adder accelerator "Reiden-SHVS". The second stage diode was operated in an ion beam injected mode. The limiting current is increases over the space charge limiting value of the single diode, without anomalous current enhancements. The experimentally observed behavior of oscillation in a B-dot signals shows the transition of diode operation from a stable virtual anode formation mode to the unstable space charge instability mode.

1. INTRODUCTION

In recent years, ion diode have been the key subject of considerable experimental and theoretical research for use as an inertial confinement fusion (ICF) driver. Ion diodes convert the pulsed power energy into a uniform ion beam suitable for pellet implosion. In magnetically insulated ion diode, the flow of electrons across the diode gap was inhibited by applied magnetic field.[1,2] Recent experimental and theoretical work on the ion diode [3,4] implies the existence of a limiting voltage V* at which the ion current diverges and diode impedance collapse. This is the problem of non-controlling ion source. To avoid this phenomena, the ion source limiting operation is considered. One method is to use an externally injected ion source plasma.[5,6] Ion current density is limited by the ion flux. Plasma injection ion source shows an improvements on turn-on delay of ion beam generation and lower the early time impedance.[6] Another method to control the diode impedance is to use an ion beam injected diode. Ion beams generated in a

[1] Presented at the conference on "Nuclear Fusion Application of "High Bright Pulsed Particle Beams" December 6, 1990, Nagoya, Japan.

separate ion diode (first stage) injected into the main acceleration diode (second stage).

In this paper, we show a two stage charge stripping ion diode system for the light ion fusion driver. And we report the studies of the two stage ion diode experiments in which the plasma injected diode was used as a first stage diode and the second stage diode was operated as the ion beam injected diode.

2. CONCEPT OF TWO-STAGE DIODE

A conventional single stage ion diode has a difficulties in accelerating the high energy heavier ion. It requires a higher diode voltage and then, a higher insulation magnetic field. The space charge limiting current is proportional to $V^{3/2} * d^{-2}$. In other hand, the critical magnetic insulation field B_c is proportional to V/d in high voltage region. Then the space charge limiting current is

$$J_i \propto B_c^{\,2} V^{-1/2}$$

For given applied field, the limited current is proportional to the square root of voltage. High current density beam generation in high voltage diode requires highly enhanced current operation at which the diode impedance control is difficult.

Two stage diode avoids high voltage diode operation and then lower the required current density. Table I shows the comparison between the single diode and the two-stage diode for ICF applica tion.

Table I. Comparison between the single and the two-stage diode for ICF application.

	Advantage	Disadvantage
Single diode	Simple Many experiments	High voltage diode High insulation B Highly enhanced current
Two-stage diode	Low voltage diode Low insulation B Low enhace operation Separate ion source and accelerator Charge stripping	Beam trajectory between two diodes

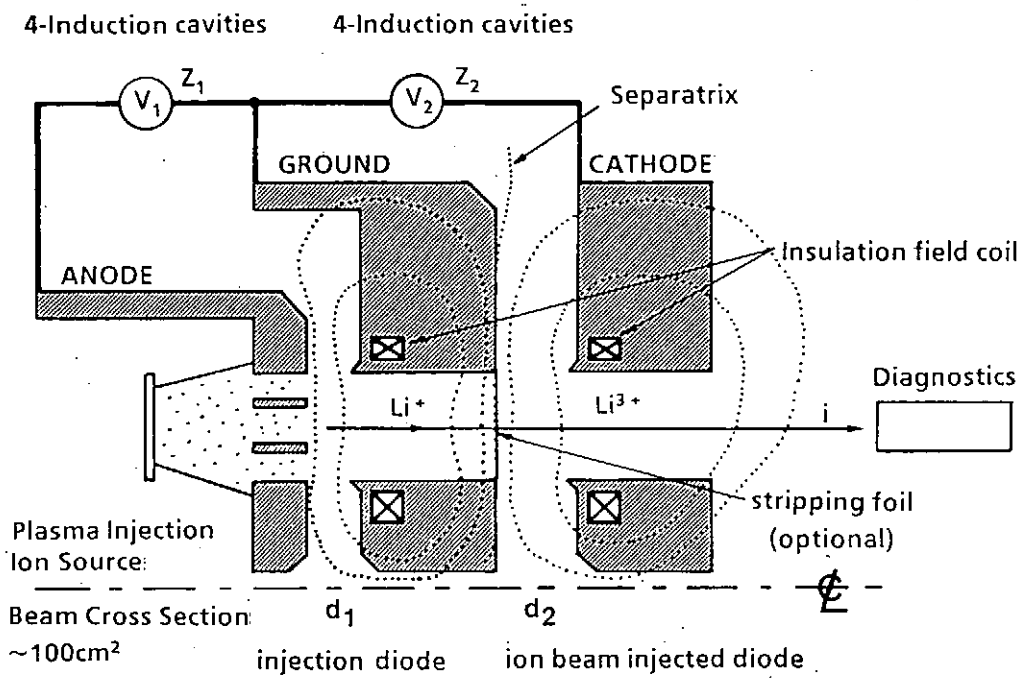

Fig.1 Schematic of two-stage charge striping ion diode installed on a induction adder accelerator for light ion beam fusion. A singly charged ions are stripped after acceleration at first stage diode. The stripped ions are accelerated by second diode.

Figure 1 shows a schematic of two stage charge stripping ion diode.[7] The energetic ions accelerated at the first diode are injected into the second diode through a charge stripping thin foil. The injected ions are stripped to higher charge state at the foil and accelerated in the second diode efficiently. Table II shows example of design parameters of a module for light ion fusion driver. First stage diode of voltage 6MV generates Li^+ ion beam which is stripped to fully ionize state of Li^{3+} by the stripping foil. Ions are assumed 24 MeV acceleration energy at the second stage diode of voltage 8MV.

Table II. Designed parameter for a module of two-stage charge stripping light ion fusion driver.

	First stage	Second stage
Ion Species	Li^+	Li^{3+}
Voltage	6 MV	8 MV
AK Gap	1.1 cm	1.4 cm
Insulating Field	4 T	4 T
Critical Voltage	12.5 MV	16.3 MV
Operating Ion	1.3 kA/cm^2	3.9 kA/cm^2
Current Density Anode active area	250 cm^2 (Rout = 12 cm, Rin = 8 cm)	
Total Ion Beam Power	9.8 TW	

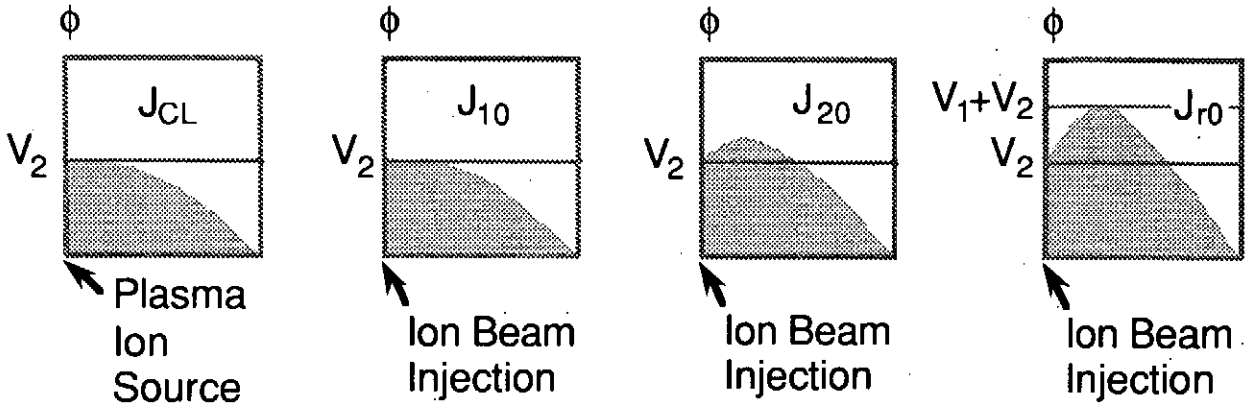

Fig.2 Schematic configuration of the potential profiles in the ion beam injected diode.

The potential distribution in the ion beam injected diode is different from the conventional diode with a stationary anode plasma ion source. Figure 2 shows schematic potential profiles in the ion beam injected diode. Energetic ion beams are injected from left side. Figure 2 (a) shows a potential profile for simple Chiled-Langmuir space charge limited current.

The analogy of the electron tube analyses shows the existence of two specific current densities, J_{10}, J_{20} and J_{r0}, for a gap with a potential deference V_2, fixed width d_2, and an injected beam energy ZeV_1.[8]

J_{10} is the current density at which the beam space charge is just sufficient to form an electric field in the accelerating gap that opposes the beam. (Fig.2 (b))

J_{20} is the maximum steady-state current that can be transmitted through the second diode gap. However, the height of the potential bump (the virtual anode) is smaller than a maximum virtual anode potential (potential Max = $V_1 + V_2$).(Fig.2 (c))Jr0 is the transmittable current density through the second diode with the maximum virtual anode potential.(Fig.2 (d)) These critical currents are calculated by a monopolar steady-state analyses as

$$\frac{J_{10}}{J_{CL}} = \left(\sqrt{1+\frac{V_1}{V_2}} + 2\sqrt{\frac{V_1}{V_2}}\right)^2 \left(\sqrt{1+\frac{V_1}{V_2}} - \sqrt{\frac{V_1}{V_2}}\right)$$

$$\frac{J_{20}}{J_{CL}} = \left(\frac{V_1}{V_2}\right)^{9/2} \left(\sqrt{1+\frac{V_2}{V_1}} - 1\right)^3 \left(\left(4+\frac{V_2}{V_1}\right)\sqrt{1+\frac{V_2}{V_1}} + \frac{3V_2}{V_1} + 4\right)^2$$

$$\frac{J_{r0}}{J_{CL}} = \left(\left(\frac{V_1}{V_2} \right)^{3/4} + \left(1 + \frac{V_1}{V_2} \right)^{3/4} \right)^2$$

where $J_{CL} = \frac{4}{9}\varepsilon_0 \left(\frac{2q}{M} \right)^{1/2} V_2^{3/2} d_2^{-2}$ is the Child-Langmuir space charge limited current.

Operation at $J < J_{10}$ results in an electric field that tends to extract beam from the injection side of the diode. Unless this surface is nonemitter, a significant portion of the accelerated beam will be extracted from this surface. this suggest that it is desirable to operate with $J > J_{10}$ to avoid accelerating the unwanted ions generated from the anode electrode of second diode. Operation at $J > J_{20}$ results in a space charge instability[9]. The virtual anode potential and its position change oscillativelly. Partial ions are reflected back to the injection side. Sluz and Desjarlais [8] applied the electron sheath development theory to multi-stage ion beam injection diode. This analyses shows that the critical currents increase due to the diamagnetic electron sheath developments (in bipolar case the critical currents J_{10}, J_{20}, and J_{r0} are denote as J_1, J_2, and J_r).

In LIB-ICF application, the second diode should be operated with small virtual anode to avoid the unstable operation and also avoid the unwanted ion acceleration from stripping foil. Then the desirable operation regime is $J_1 < J < J_2$.

3. EXPERIMENTAL APPARATUS

Experiments were performed on Reiden-SHVS [10] induction adder accelerator. Figure 3 shows a configuration of the induction adder section of Reiden-SHVS. It consists of eight stages induction adder cavities. Reiden-SHVS has a capability to generate 4 MV, 40 kA, 100 ns pulse into a single diode or to divide the voltage into two diodes. Positive and negative center electrodes are extended from both side. The diodes are located at the center of the machine. Figure 4 shows experimental setup of the two-stage ion diodes. The ground electrode is combined a cathode of first diode and an anode of second diode. Each diodes are powered by four induction cavities.

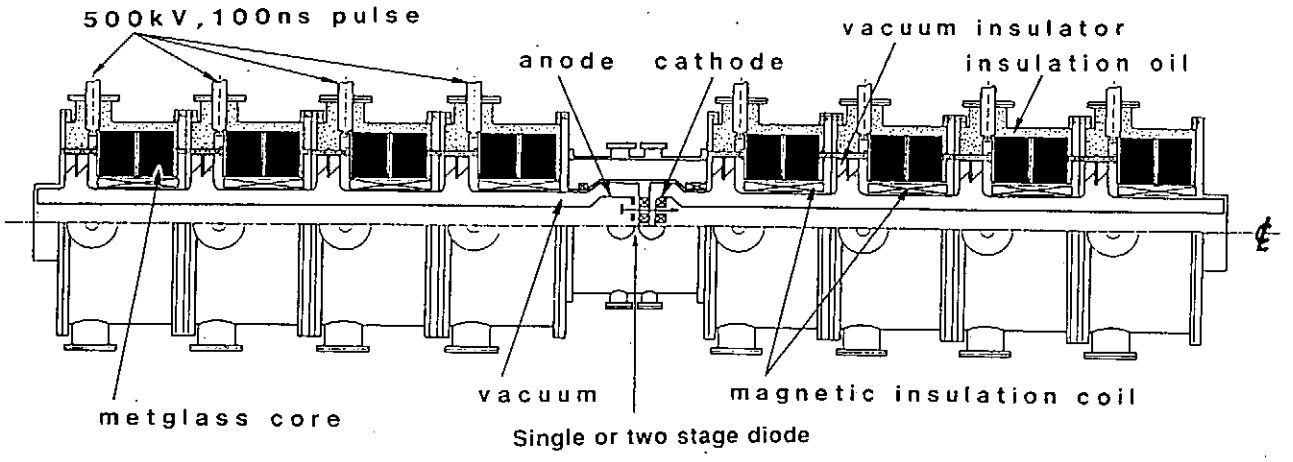

Fig.3 Configuration of the induction adder section of Reiden-SHVS.

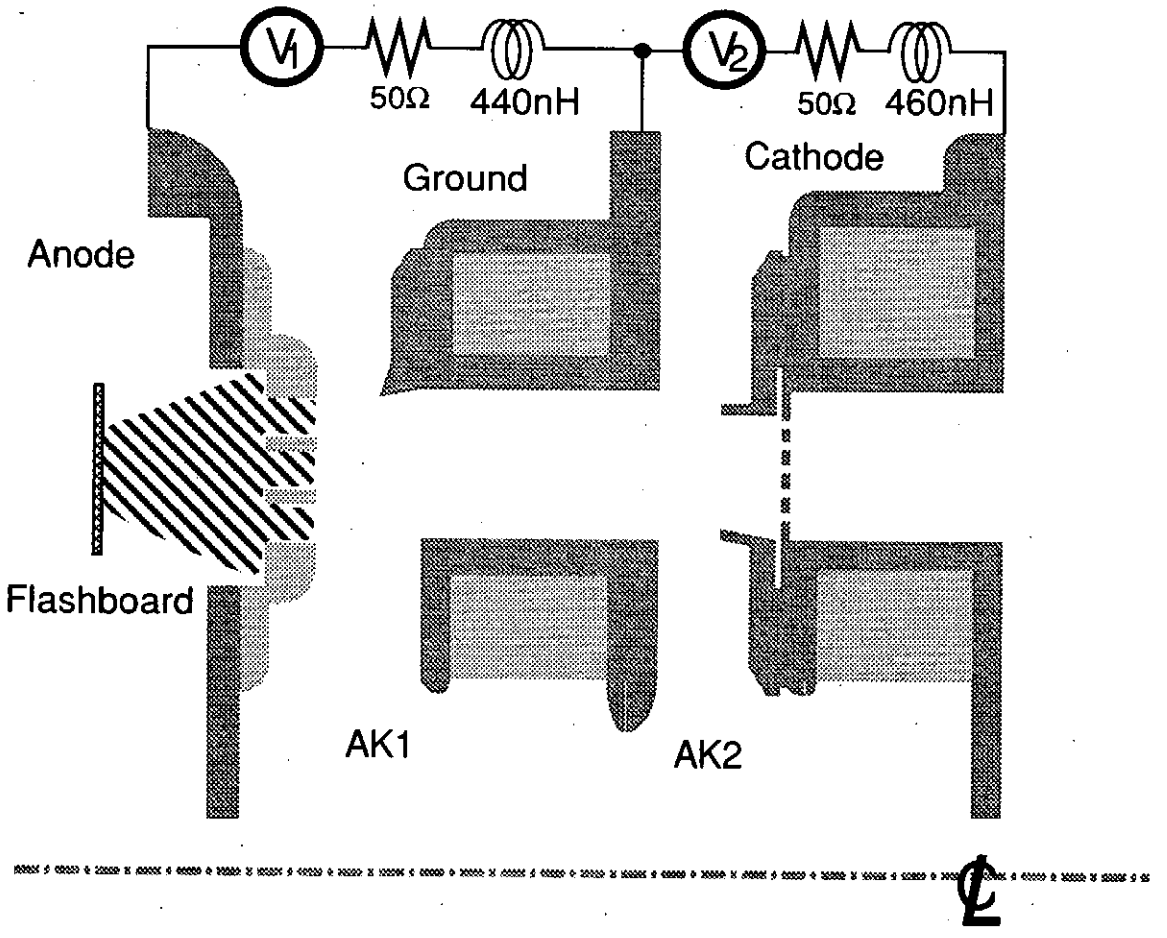

Fig.4 Experimental setup of the two-stage magnetically insulated diode. First stage (left) is an applid-Br ion diode with a plasma injection ion source in the anode electrode. Second stage (right) is operated as an ion beam injected diode.

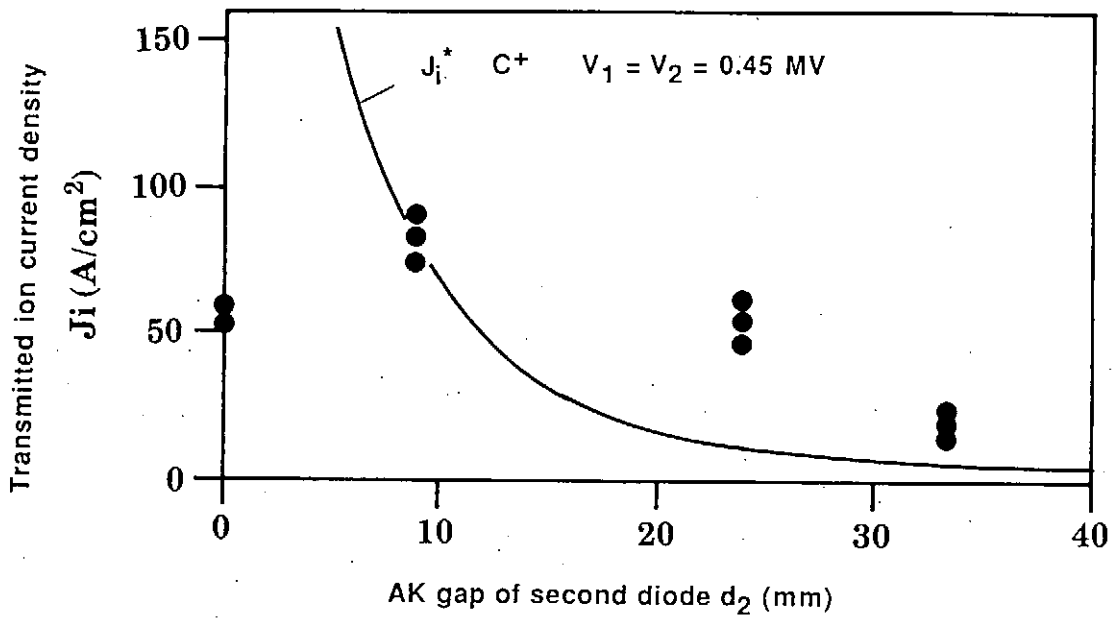

Fig.5 The measured ion current density at 12 cm behind the second diode as a function of AK gap of second diode.

The anode electrode of first stage diode is made from aluminum to exclude the insulation magnetic field. Two types of ion sources, a pallafin grooves anode and a carbon flashboard plasma injection source located behind the anode, are used. The flashboard is driven by a 25 kV, 1.2 μF capacitor bank. The outer and inner radius of active anode area was 8 cm and 5.7 cm, respectively, then the active anode area was 100 cm^2. The diode gap and insulation field were d_1 = 9.2 mm and B_1 = 7 kG in first diode. In second diode, d_2 (B_2) was varied from 0.83 cm (9 kG) to 3.33 cm (6kG). Diode currents were measured by B-dot probes. The ion current density is measured by the biased charge collectors behind the second stage diode.

4. EXPERIMENTAL RESULTS

Figure 5 shows the transmitted ion current density as a function of AK gap of second diode. The solid line in Fig.5 is calculated steady state limiting current J_{20} (Eq. (1)) for C^+ ions assuming the first and second diode voltage were 0.45 MV. With increasing the second diode gap

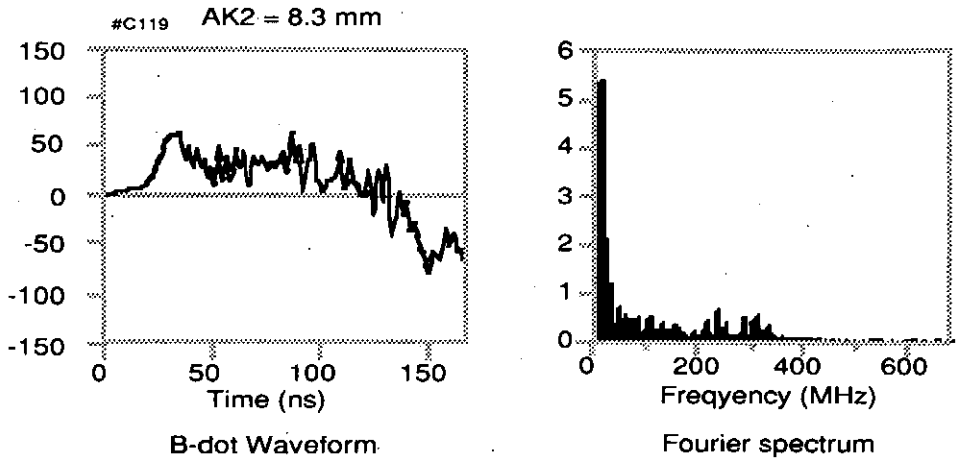

(a) d_2 = 0.83 cm

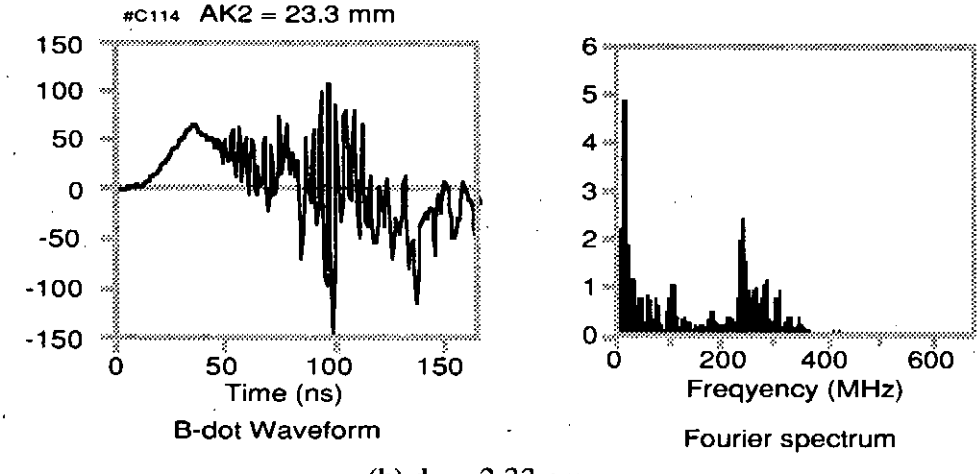

(b) d_2 = 2.33 cm

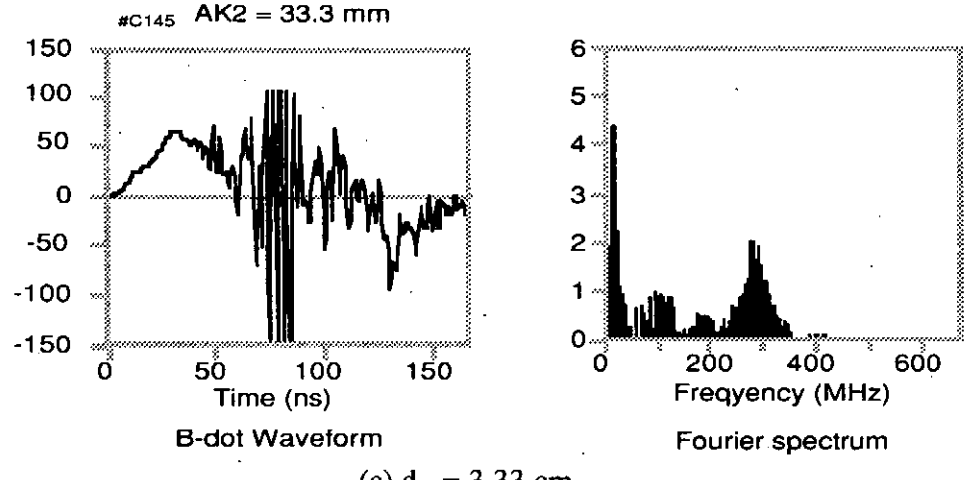

(c) d_2 = 3.33 cm

Fig.6 B-dot signals and its Fourier spectrum for various AK gaps and diode conditions. (a) d_2 = 0.83 cm , (b) d_2 = 2.33 cm, (c) d_2 = 3.33 cm, (d) ion source off and (e) applied-B field off.

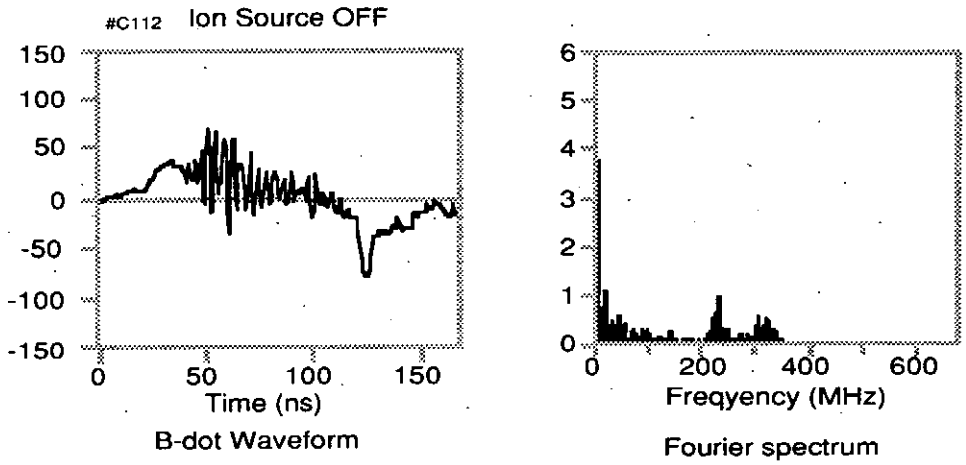

(d) ion source off

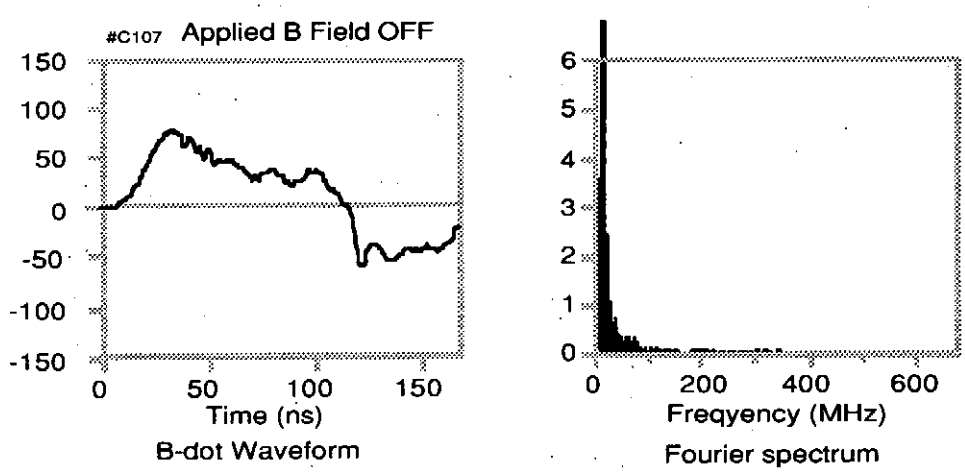

(e) applied-B field off

Fig.6 B-dot signals and its Fourier spectrum for various AK gaps and diode conditions. (a) d_2 = 0.83 cm , (b) d_2 = 2.33 cm, (c) d_2 = 3.33 cm, (d) ion source off and (e) applied-B field off.

increases, the ion current density in the second diode change from source limited value to the space charge limited value. In the case of AK gap larger than 20 mm, monopolar theory predict that the ion flow is unstable [9]. Because of the transmittable current in the second diode decreases with increasing the virtual anode potential at high virtual anode potential region.

In this condition, the oscillations was observed on the B-dot signals of first stage diode. Figure 6 shows B-dot prove waveform and its Fourier spectrum for various AK gaps and diode conditions. This oscillation was also observed in the case of paraffin groove anode ion source. The amplitude of oscillation was suppressed or quenched by turning off the ion source plasma (Fig.6 (d)) or by turning off the applied-B field (Fig.6(e)). The source of this oscillation should

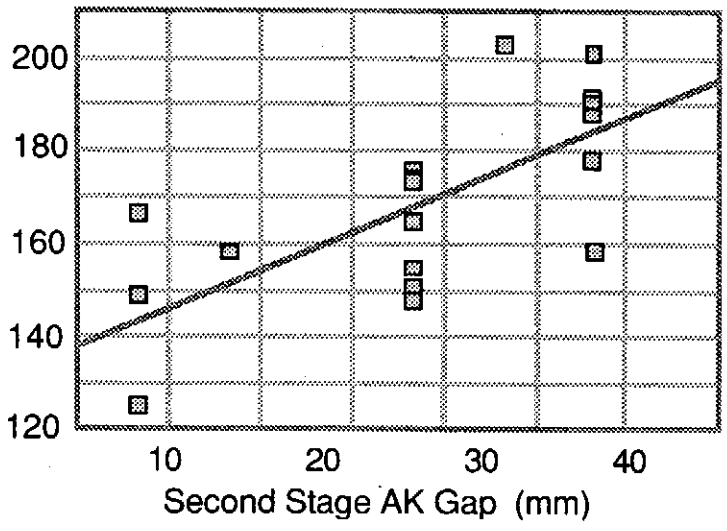

Fig.7 Average frequency of oscillation as a function of AK gap.

be the reflected ions from second stage diode due to the excessiveness of ion injection.

Figure 7 shows average frequency of oscillation as a function of AK gap. Oscillation frequency in B-dot signals tend to increase with AK gap of second diode. The computer simulations of the space charge instability [9] show that the normalized oscillation frequency increased with a normalized current density $\alpha = J/J_{CL}$ as

$$\frac{\omega_{osc} t_0}{2\pi} \propto \alpha^{\kappa}$$

$$\kappa = 0.5 - 1$$

where ω_{osc} is the frequency of oscillation, $t_0 = d_2/v_0$ is the transit time of the injected ion in the second diode gap without a space charge effect. (arufa) is proportional to the square of d_2 and t_0 is proportional to d_2. Then ω_{osc} is proportional to $d_2^{(2(kai)-1)} = d_2^{(0-1)}$. The experimental dependence of the oscillation frequency is qualitatively agree with the simulation of space charge instability.

This results indicates that appropriate ion beam injection can form the stable virtual anode and we can use virtual anode as a ion filter to reduce the ions from the injection side. Diode operation should keep at stable regime for the ICF energy driver application.

5. CONCLUSION

Two-stage ion diode experiments are performed on Reiden-SHVS induction adder accelerator. Second stage diode was operated as ion beam injection diode. The space charge limited ion current density increases by the energetic beam injection. The experimentally observed behavior of oscillation in a B-dot signals shows the transition of diode operation from a stable virtual anode formation mode to the unstable space charge instability mode.

REFERENCES

[1] R.N.Sudan and R.V.Lovelace, Phys. Rev. Lett. **31**, 1174(1973).
[2] T.M.Antonsen, Jr. and E.Ott, Phys. Fluids **19**, 52 (1976).
[3] P.A.Miller, J. Appl. Phys. **57**, 1473 (1985).
[4] M.P.Desjarlais, Phys. Rev. Lett. **59**, 2295 (1987).
[5] J.B.Greenly et al. J. Appl. Phys. **63**, 1872 (1988).
[6] S.Miyamoto et al. Proc. 7th Int'l Conf. on High Power Particle Beams, Karlsruhe, 1988, p.47 (Kernforshungszentrum Karlsruhe, Federal Republic of Germany, 1988), paper **AI2**.
[7] S.Miyamoto et al. Proc. 8th Int'l Conf. on High Power Particle beams, Novosibirsk, USSR, July 2-5, 1990, **C.A07** pp.190-198.
[8] S.A.Slutz and M.P.Desjarlais, J. Appl. Phys., **67**,6705(1990).
[9] C.K.Birdsal and W.B.Bridges, J. Appl. Phys., **32**, 2611(1961).
W.B.Bridges and C.K.Birdsal, J. Appl. Phys., **34**, 2946(1963).
[10] T.Akiba et al. Nuclear Instrum. and Methods in Phys. Rev, **A259**, 115(1987).

GENERATION AND FOCUSING OF PROTON BEAM BY THE INVERSE PINCH ION DIODE

Y.Hashimoto, M.Sato, M.Yatsuzuka, S.Nobuhara

Department of Electrical Engineering,
Faculty of Engineering, Himeji Institute of Technology,
Shosha, Himeji, Hyogo 671-22, Japan

Abstract

We performed generation and focusing of ion beams by the "Inverse Pinch Ion Diode" which has a flat anode. The ion beams were extracted from a radial position of 10~15 mm on the anode and the ion beams were focused on the diode axis at 120 mm from the anode. At this point, an ion current density of 0.4 kA/cm^2 and a power density of 0.1 GW/cm^2 were obtained. A focal angle was estimated to be 7° .

§ 1.Introduction

In recent years, it has been interested that intense ion beams generated with a pulse power machine are applied to material development[1-3]. For applications of the ion beams to the heat source, such as sputtering and annealing, it is necessary that the ion beams have a high power density. However, in a small scale pulse power machine, the ion beams are not able to obtain a high power density without focusing of the ion beams.

Focusing of the ion beams with the "Inverse Pinch Ion Diode"(IPD)[4-5] which has a flat anode has been performed. The schematic drawing of IPD is shown in Fig.1. The diode consists of a circular cathode with a ring projection and a ring anode. The cathode is connected to a ground plate with a metal rod which is located at the axis of the ring anode. When a pulse high voltage is applied to the diode, the electrons emitted from the cathode are accelerated to the

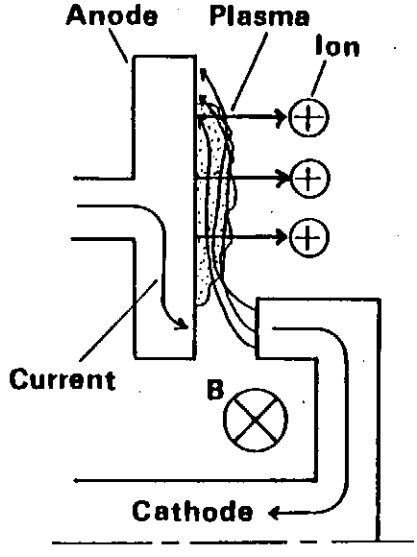

Fig.1 Schematic drawing of the "Inverse Pinch Ion Diode".

anode. At the same time, the current flowing along the metal rod generates a strong azimuthal magnetic field. The electrons are insulated by this magnetic field and effective ion beam generation is expected.

In this paper, experimental results for ion beam focusing with IPD are presented. Particularly, characteristics of focusing, such as focal distance, focal angle etc., are reported.

§ 2. Experimental Setup

The experimental setup of IPD is shown in Fig.2. This diode was set at the end of the pulse power generator "HARIMA-II"(400kV,3 Ω ,50ns)[8]. The diameters of the ring cathode and the anode are 18 mm and 50 mm, respectively. A 2 mm thick acrylic plate is attached on the anode surface as an ion source. The anode-cathode gap spacing was 3 mm.

A diode voltage is measured at an anode rod with a resistive voltage divider and a diode current is measured by using a Rogowski coil. A biased ion collector (BIC) is employed to measure an ion current density. The BIC has a small aperture (0.3mm in diameter) and the collector is biased with a voltage of -450V in order to avoid accompanying electrons, and the BIC is movable to radial and axial direction in the diode. The focal angle of the ion beams is estimated by using a shadow box. The shadow box consists of a grounded plate which has pinholes (0.5 mm in diameter) and a CR-39 film as a damage plate.

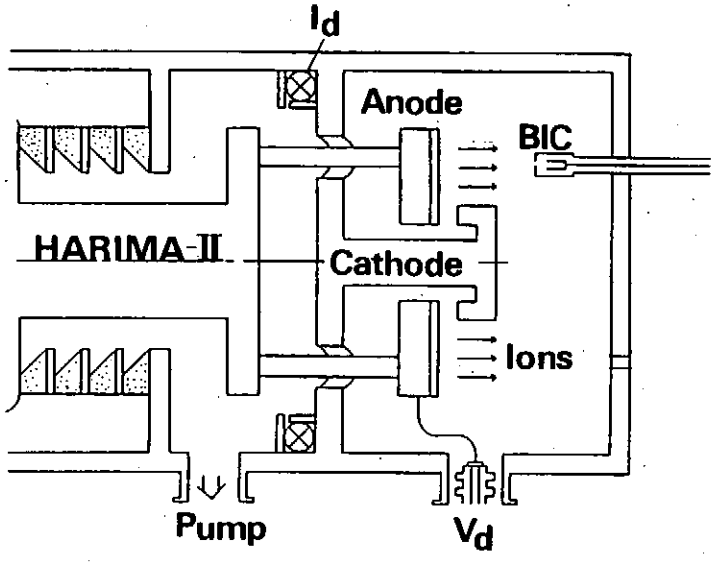

Fig.2 Schematic drawing of the experimental setup.

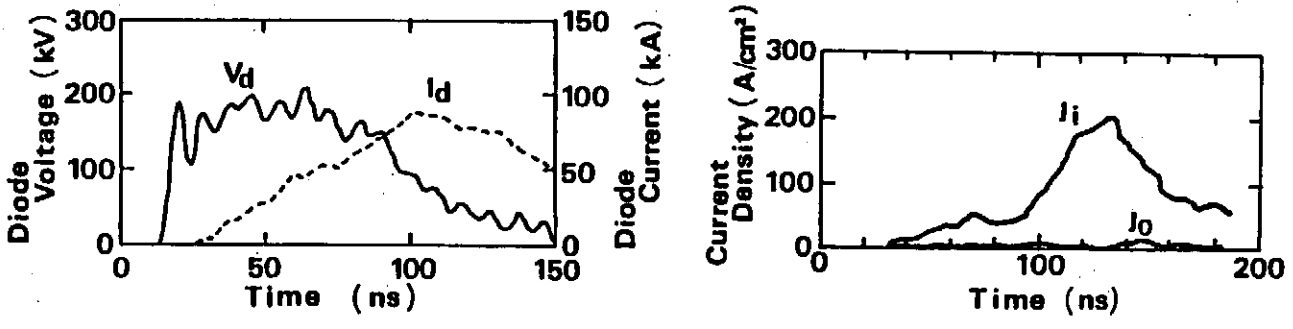

(a) The waveforms of the diode voltage(Vd) and the diode current(Id).

(b) The ion current density measured with the BIC.

Fig.3 Diode characteristics

§ 3.Experimental Results

3.1 Diode characteristics

Figure 3(a) shows the typical waveforms of the diode voltage(Vd) and the diode current(Id). The diode voltage reaches to the peak value of 180 kV in about 10 ns and its pulse width is 70 ns (FWHM). The diode current rises up at about 10 ns after Vd is started to rise, and reaches its peak

value of 95 kA by 75 ns. Figure 3(b) shows the ion current density measured by the BIC with the bias voltage to the collector(Ji) and with no bias voltage(Jo). In Fig.3(b), Ji has a peak value of 0.2 kA/cm^2, and there is a little signal (Jo) with no bias voltage, because of neutralization for the ion beams due to accompanying electrons. A neutralization ratio is calculated to be 98%.

3.2 Damaged anode by electron bombardment

A photograph of the acrylic plate attached to the anode surface after several operations is shown in Fig.4. The damage by electron bombardment is the most large at a slight outside of the cathode. It is expected that a lot of ions are extracted at this place. At an outer edge of the anode the damage is large too, the electrons are removed to outside of the anode by the self magnetic field.

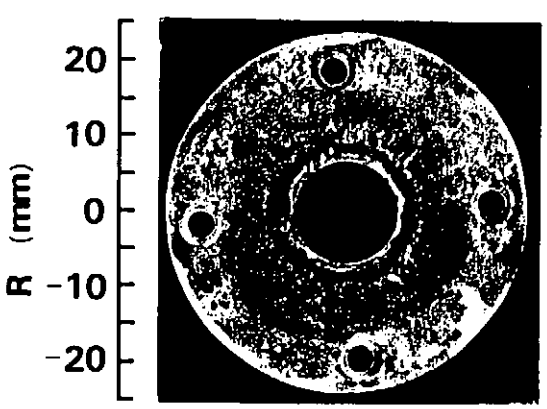

Fig.4 The photograph of the acrylic plate attached on the anode after several operations

3.3 Ion beam focusing

Figure 5 shows radial profiles of the ion current density measured with the BIC located at different axial positions. These results indicate the space distribution of the ion beams. At L=60 mm, a radial profile of the ion current density has a maximum value at 10-15 mm from the diode axis, where L is a distance from the anode. However, at L ≧ 90 mm, a radial profile of the ion current density has a maximum value on the diode axis. Therefore, it is found that the ion beams are focused.

Figure 6 shows an axial profile of the ion current density measured with the BIC on the diode axis. The ion current density increases gradually and has a maximum value of 0.4 kA/cm^2 at L=120 mm. The focal distance is estimated to be 120 mm. At this place a focal radius (r^*) of the ion beams is 10 mm (FWHM of a radial profile at L=120mm in Fig.5) and a power density of the ion beams ($Pj=Vd \times Ji$) is estimated to be 0.1 GW/cm^2. A total current of the ion beams (Ii) estimated from the radial profile at L=120 mm is 5.6 kA. An ion production efficiency ($\eta i=Ii/Id$) is calculated to be 8%.

Figure 7 shows a photograph of the CR-39 film with the shadow box which was located at 120 mm from the anode. From Fig.7, the focal angle of the ion beams of <7° is obtained. If the ions are accelerated with an angle of 7°, it is calculated that the ion beams are extracted from a slight outside of the cathode on the anode. This results is agree with the result of the anode damage (Fig.4) and a radial profile of the ion beams at L=60 mm.

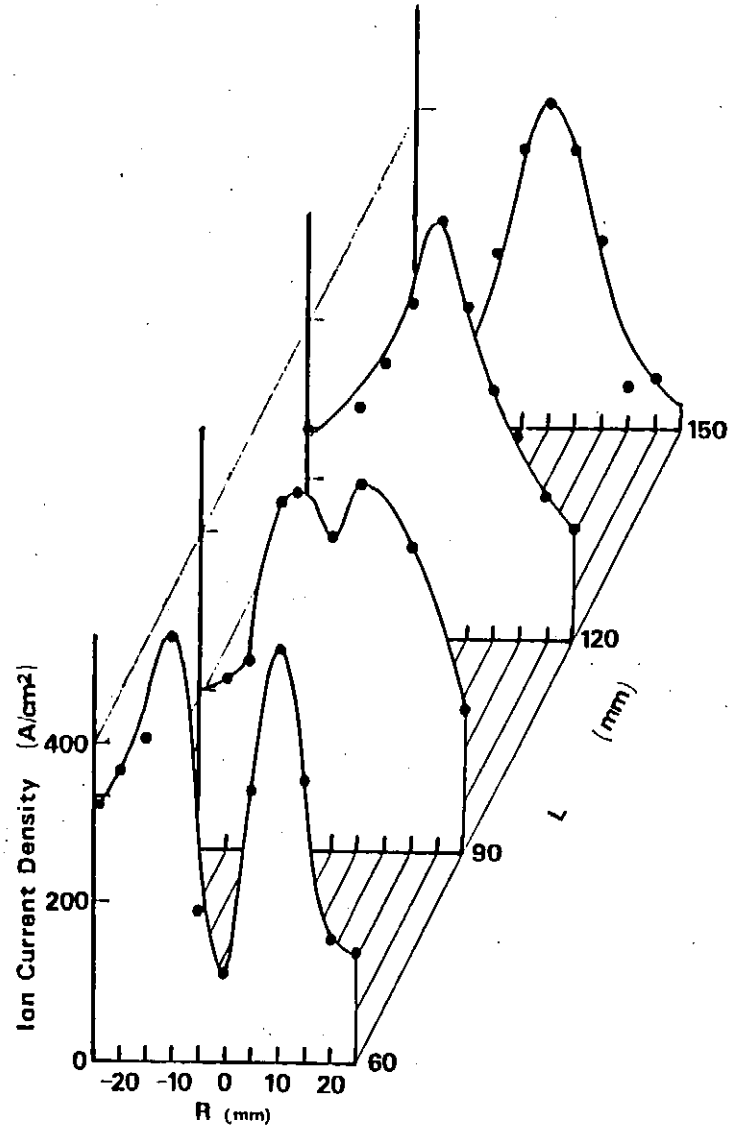

Fig.5 The space distribution of the ion beams, where R is a distance from the diode axis and L is a distance from the anode.

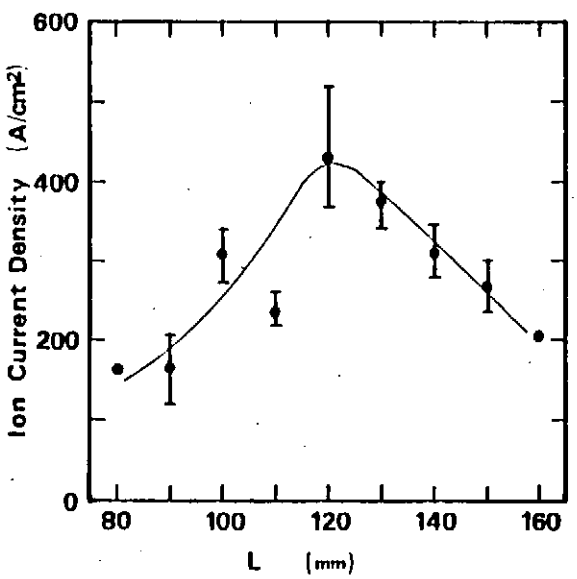

Fig.6 The axial profiles of the ion beams.

Fig.7 The photograph of CR-39 film with the shadow box.

§ 4.Summary

We tried generation and focusing of the ion beams with the "Inverse Pinch Ion Diode" which has a flat anode. The main results are followings;

1. The ion beams were extracted from a slight outside of the cathode on the anode (r=10~15 mm), and the ion beams were focused on the diode axis at 120 mm from the anode.

2. The ion current density of 0.4 kA/cm^2 and the power density of 0.1 GW/cm^2 were obtained at the focal point.

3. The focal angle was estimated to be 7° by using the shadow box.

In this experiment, it is considered that electrostatic field is dominant for focusing of the ion beams. Therefore it is expected that the focal distance of the ion beams is able to be varied due to changing the diode size.

REFERENCES

1) Y. Nakagawa, T. Ariyoshi, M. Itami, and Y. Fujii: Jpn. J. Appl.Phys. **27** (1988) L719.

2) K. Yatsui: Laser and Particle Beams **7** (1989) 733.

3) R. T. Hodgson, J. E. E. Baglin, R. Pal, J. M. Neri, and D. A. Hammer: Appl. Phys. Lett. **37** (1980) 187.

4) S. Miyamoto, K. Imasaki, A. Yoshinouchi, T. Ozaki, S. Higaki, H. Fujita, M. Saito, R. Ozaki, S. Nakai, and C. Yamanaka: Proc. 4th IEEE Int. Conf. Pulsed Power Conf., Albuquerque, (1983) 482.

5) S. Miyamoto, A. Yoshinouchi, T. Ozaki, S. Higaki, H. Fujita, K. Imasaki, S. Nakai, and C. Yamanaka: Jpn. J. Appl. Phys. **22** (1983) L703.

6) M. Sato, M, Yatsuzuka, Y. Hashimoto, K. Azuma, and S. Nobuhara: IPPJ-900, Inst. Plasma Phys., Nagoya, (1989) 49.

Optimization of Self-Magnetically Insulated "Plasma Focus Diode"

Weihua Jiang, Katsumi Masugata and Kiyoshi Yatsui
Laboratory of Beam Technology,
Nagaoka University of Technology, Nagaoka, Niigata 940-21

Abstract

The behavior of coaxial type, self-magnetically insulated "Plasma Focus Diode" (PFD) is analyzed with a one-dimensional calculation model. The calculated results concerning the stability of the electron sheath are used in design of the spherical PFD. Furthermore, the focusability of the spherical PFD is estimated with the calculated results and the experimental results of cylindrical PFD.

I. Introduction

Intense light-ion beam (LIB) is considered to be one of the promising candidates of the energy driver for inertial confinement fusion (ICF). In order to ignite the fusion fuel contained in the target pellet, it is necessary to generate an ion beam with enough high power density and good focusability.

The "Plasma Focus Diode" (PFD)[1-3] is a self-magnetically insulated ion-beam diode. It is capable of generating an intense ion beam with two-dimensionally, very tight line

focusing.

The structure of PFD is shown in Fig. 1. It consists of two coaxial cylindrical electrodes: the anode (the outer cylinder) and the cathode (the inner cylinder). Figure 2 shows the basic priciple of PFD operation. Ions accelerated from the anode tend to focus toward the center line while the electrons are insulated by the self-magnetic field produced by the diode current.

The characteristics of PFD have been investigated both experimentally and theoretically[4-9]. Experimental results have shown that the focusing radius of the ion beam in PFD is 0.18 ~ 0.25 mm, varing along the axial direction, and that the ion-beam power density at the focusing region is ~ 0.1 TW/cm^2. Calculated results have given a theoretical model of PFD and have shown that the stability of PFD operation can be controlled by the geometry of the electrodes.

It is clear that the ion beam power density in PFD can be increased by focusing the ion beam three-dimensionally which needs the electrodes to shape spherically. Since the electrons in the gap of PFD drift in the axial direction, it is possible that the variation of geometry in the axial direction affects the electron movement and then stability of PFD operation. In this paper, using the calculated model reported previously, we have investigated the operational characteristics of spherical PFD. Furthermore, the focusability of the shperical PFD is estimated with the experimental data of cylindrical PFD and the magnetic field of maximum diode current.

II. Analytical Model of PFD

We have developed a one-dimensionally analytical model to give steady-state description of PFD. In this model, the

electrons are moving non-laminarly and the axial velocity of electrons is determined by the magnetic flux and is always smaller than or equal to the kinetic energy given by the electric potential. The electron density is supposed to be constant in the radial direction.

The conceptual structure of the one dimensional model is shown in Fig. 3. The gap is divided into two regions, A ($r_c \leqq r \leqq r_s$) and B ($r_s \leqq r \leqq r_a$). From the Poisson's equation, we have:

$$\text{(in region A)} \qquad d(rE(r)) = e(n_e(r) - n_i(r))rdr/\varepsilon_0 \quad , \qquad (1)$$

$$\text{(in region B)} \qquad d(rE(r)) = -en_i(r)rdr/\varepsilon_0 \quad , \qquad (2)$$

where

$$J_i(r)r = ev_i(r)n_i(r)r = \text{Const.} \quad , \qquad (3)$$

$$v_i(r) = [2e(V_d - \phi(r))/m_i]^{1/2} \quad , \qquad (4)$$

where E is the electric field, n_e the electron density, n_i the ion density, J_i the ion-current density, V_d the diode voltage between the gap, and ϕ the electric potential. For these equations, the boundary conditions are: $\phi(r_c) = 0$, $\phi(r_a) = V_d$, $E(r_c) = 0$, and the continuity of E and ϕ at r_s, namely the radius of the surface of the electron sheath. Equations (1) ~ (4) were integrated numerically to give the potential profile in the gap. Amoung the three parameters of $J_i(r)r$, n_e and r_s, any prescribed one can be used to calculate the other two.

The relations of the magnetic field and the axial velocity of electrons are given by:

$$d(rB(r)) = \mu_0 en_e(r)v_z(r)rdr \quad , \qquad (5)$$

$$d(v_z(r)m) = eB(r)dr \quad , \qquad (6)$$

where B is the magnetic field, v_z the axial velocity of electrons, and m the mass of electron. The boundary conditions are $B(r_c) = \mu_0 I_c/(2\pi r_c)$, and $v_z(r_c) = 0$.

In order to determine the variation in axial direction, we involed the following boundary conditions. At the upstream, the axial velocity of electrons at the surface of the electron sheath equals to that determined by electric potential, i.e., they move only in axial direction. At the downstream, the surface of the electron sheath reaches the anode.

Figure 4 shows the calculated results of (a) position of the surface of electron sheath and (b) ion-current density on anode surface. We see from Fig. 4 that electrons occupies most part of the gap of PFD. The total diode current is calculated for voltage ranging from 1.0 to 1.9 MV, and the results are shown in Fig. 5 together with experimental data obtained at the peak power of seven shots of PFD. The calculated results are found to be in considerable agreement with the experimental results.

III. Design of Spherical PFD

Since the calculated results given by the above model agree with experimental results very well, we use it to analyze the electron movement in spherical PFD.

Figure 6 shows the calculated results of the distribution of the ratio of the electric force ($F_E = eE_r$) to the magnetic force ($F_B = ev_z B_\theta$) applied on electrons obtained from the above model, where V_d = 1.5 MV, r_a = 1.75 cm, r_c = 1.1 cm, I_e = 100 kA, and I_c varies as a parameter. Since the electric force directs toward the anode and the magnetic force directs toward the cathode, the electron sheath will be stable if the

ratio shown in Fig. 6 are close to 1. The difference of the cathode current (I_c) between the upstream and downtream sides is equal to the total ion current. From Fig. 6, we see that, at the upstream side, the magnetic force is stronger than the electric force for some of the electrons. On the other hand, at the downstream side, the electric force is stronger than the magnetic force for all electrons. Hence, the state given by the model is principly unstable and decay in time until the balance is reached for electrons.

Figure 7 shows the same ratio with Fig. 6, where V_d = 1.5 MV, I_e = 100 kA, I_c = 20 kA, r_c = 1.1 cm and the anode radius (r_a) varies as a parameter. We see from Fig. 7 that the ratio of F_E/F_B varies with the gap length. Therefore, in order to cancel the influence caused by the variation of I_c, the gap length should change along the axial direction. It has been shown experimentally that the operation of tapered PFD is more stable than that of normal PFD.[10]

Figure 8 shows the variation of the ratio of F_E/F_B against the cathode radius where the gap length is constant d = 0.7 cm and V_d = 1.5 MV, I_e = 100 kA and I_c = 20 kA. With smaller r_c, the magnetic field is stronger and then the ratio of F_E/F_B is smaller. For spherical PFD, r_c varies along the axial direction. Hence, by comparing Fig. 8 with Fig. 6, we see that the cathode radius at the upstream side should be larger than that at the downstream side. Therefore, the shape of spherical PFD is basically that shown in Fig. 9, which shows the primarily designed structure of spherical PFD.

The size selection of spherical PFD is a compromise between the anode area and the focusability. Supposing the azimuthal divergence does not differ from that of cylindrical PFD, we have estimated the focusing radius to be ~ 0.4 mm for anode radius of 2.5 cm. In addition, the ions are deflected

by the azimuthal magnetic field caused by the diode current. The range of deflection at the center is calculated and the results are shown in Fig. 10, where V_d = 1.5 MV, r_c = 20 mm, and r_a = 25 mm. It is found that, with I_d = 250 kA, the deflected range is ~ 1.5 mm. Hence we suppose that the focusing region is a small cylinder with 0.4 mm in diameter and 2 mm in length. If the anode area is 30 cm^2 and the ion current density at the anode surface is 1.0 kA/cm^2, the average ion current density at the focusing region will be ~ 240 kA/cm^2 and the power density will be ~ 0.36 TW/cm^2 where V_d = 1.5 MV and the 40 % transparency of the cathode has been utilized.

IV. Conclusions

We summerize our conclusions as follows:

(1) The calculated results have shown that the electron sheath in the gap of PFD is basically unstable.

(2) Analysis of electron movement in the sheath have shown that the stability can be controlled by the geometry of the electrodes.

(3) Initial estimation of focusability of the three-dimensionally focusing, spherical PFD gives the ion beam power density of ~ 0.36 TW/cm^2.

References

1. K. Yatsui, Y. Shimotori, Y. Araki, K. Masugata, S. Kawata, and M. Murayama: Proc. 11th Int'l Conf. on Plasma Phys. and Controlled Nuclear Fusion Research, Kyoto, IAEA-CN-47/B-Ⅲ-9 (1986).
2. K. Yatsui, K. Masugata and S. Kawata: Laser Interaction and Related Plasma Phenomena (Plenum Press, New York & London), 8, 653 (1988).
3. K. Yatsui, K. Masugata, Y. Shimotori, K. Imanari, M. Murayama, M. Yokoyama and T. Takaai: Proc. 7th Int'l Conf. on High-Power Particle Beams, Karlsruhe, West Germany, I, 522 (1988).
4. K. Yatsui, Y. Shimotori, H. Isobe, W. Jiang, and K. Masugata: Proc. 12th Int'l Conf. on Plasma Phys. and Controlled Nuclear Fusion Research, Nice, France, IAEA, 3, 153 (1988).
5. K. Masugata, H. Isobe, K. Aga, M. Matsumoto, S. Kawata, W. Jiang, and K. Yatsui: Laser and Particle Beams, 7, 287 (1989).
6. K. Yatsui, K. Masugata, Y. Sekimoto, W. Jiang, H. U. Karow, H. Bluhm, D. Rusch, W. Bauer, and G. Kessler: Proc. 8th Int'l Conf. on High-Power Particle Beams, Novosibirsk, USSR, 1, 535 (1990).
7. W. Jiang, K. Masugata, and K. Yatsui: Proc. 8th Int'l Conf. on High-Power Particle Beams, Novosibirsk, USSR, 2, 733 (1990).
8. W. Jiang, K. Masugata, and K. Yatsui: Proc. Symp. on Development of Intense Pulsed Particle Beams and Its Applications, NIFS-PROC-5, 45 (1990).
9. W. Jiang, K. Masugata, and K. Yatsui: Laser and Particle Beams, 8, #3 (in press) (1991).
10. W. Jiang: Doctoral Thesis (Nagaoka University of Technology, 1991).

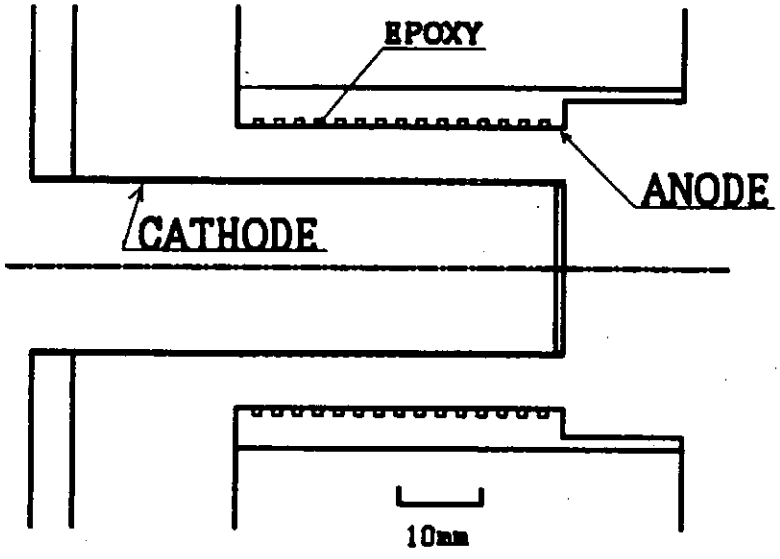

Fig. 1 Structure of " Plasma Focus Diode".

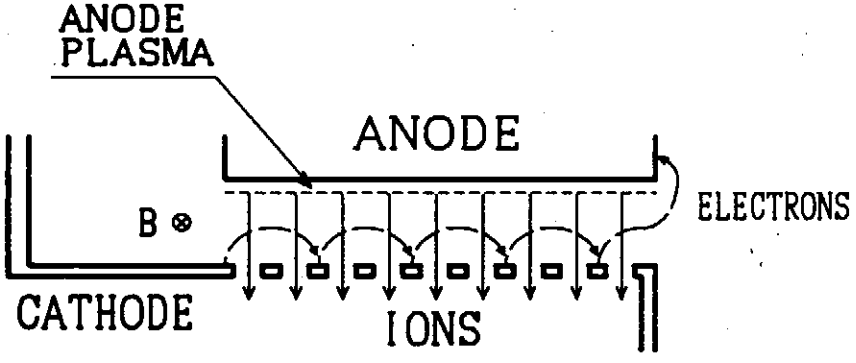

Fig. 2 Basic principle of PFD

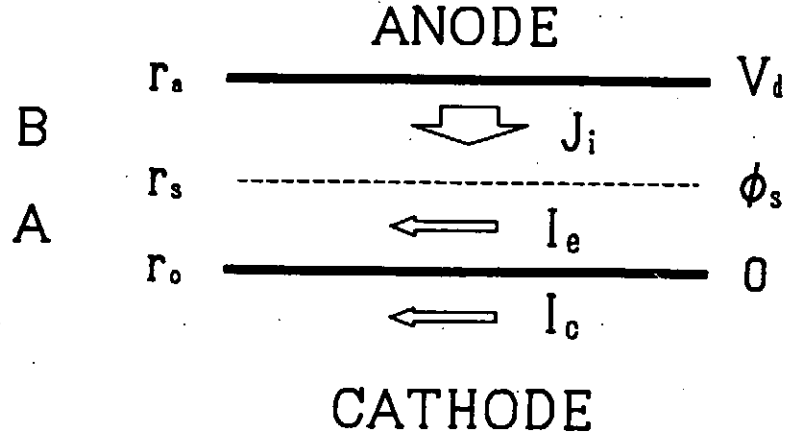

Fig. 3 Conceptual structure of calculation model of PFD.

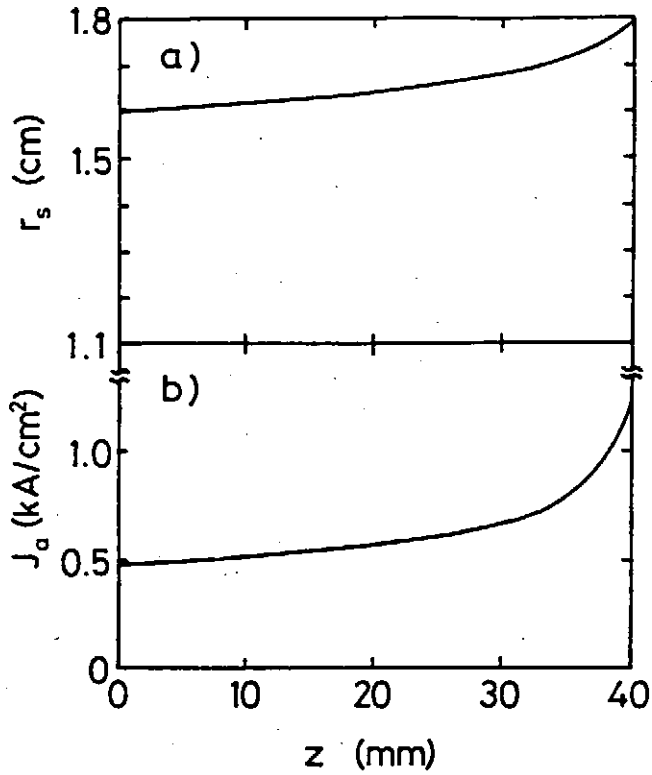

Fig. 4 Calculated results of axial variation of (a) position of electron-sheath surface (r_s) and (b) ion-current density on anode surface (J_a), with V_d = 1.5 MV.

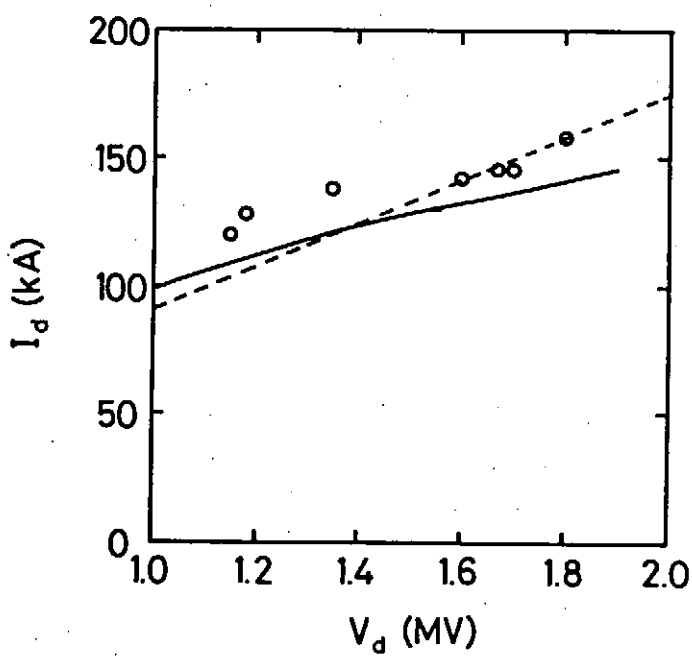

Fig. 5 Calculated results of total current (I_d) as a function of diode voltage (V_d) (solid line), together with the experimental data obtained at peak power of seven shots (circles).

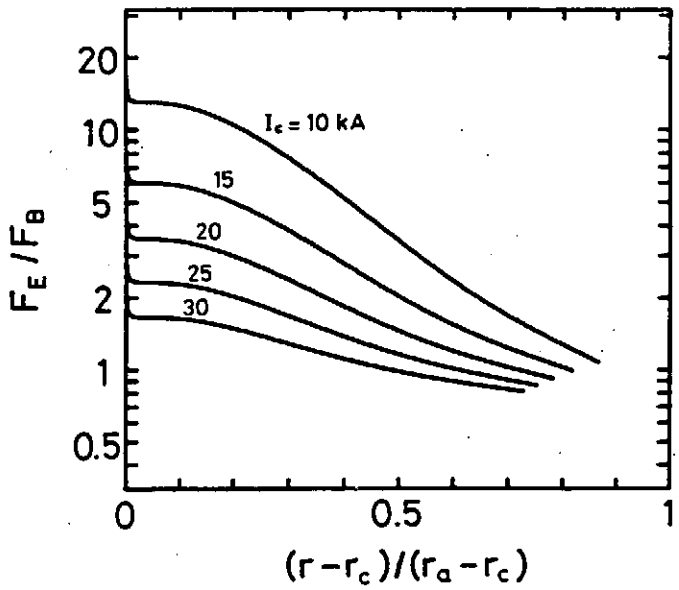

Fig. 6 Calculated results of the distribution of the ratio of electric force to magnetic force applied on electrons, with I_c as a parameter.

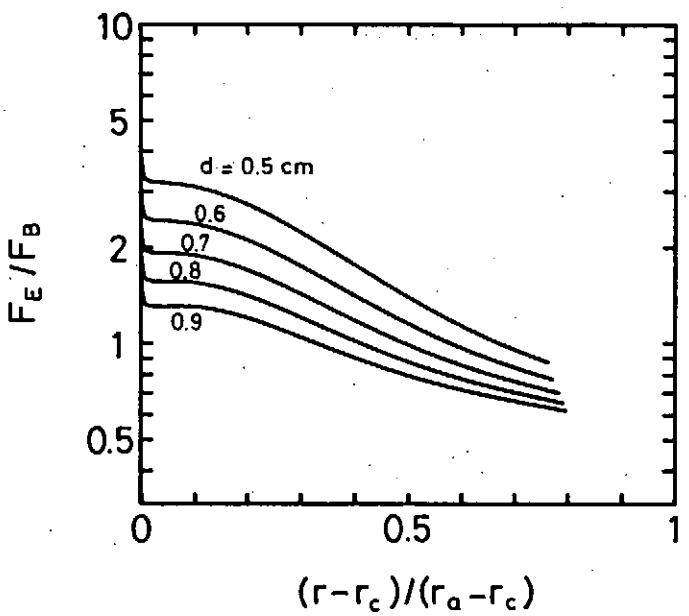

Fig. 7 Calculated results of distribution of F_E/F_B of electrons, with d as a parameter.

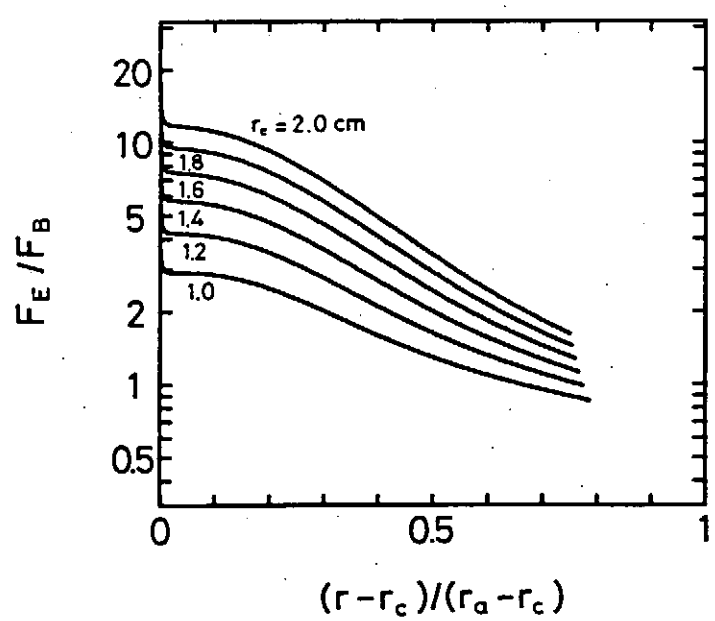

Fig. 8 Calculated results of distribution of F_E/F_B of electrons, with r_c as a parameter.

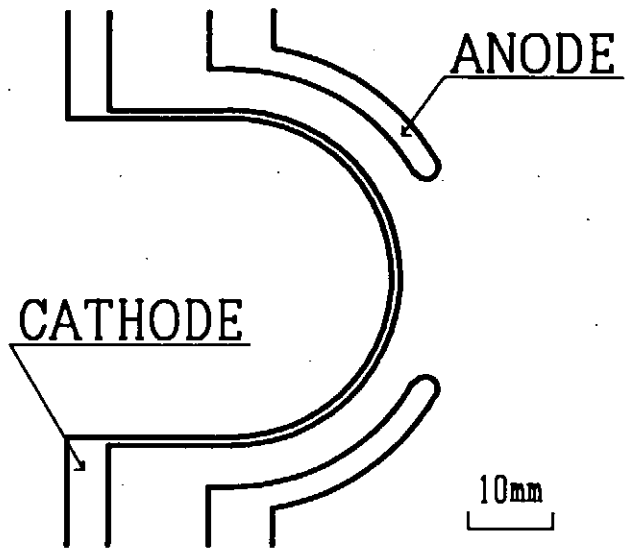

Fig. 9 Structure of the primarily designed spherical PFD.

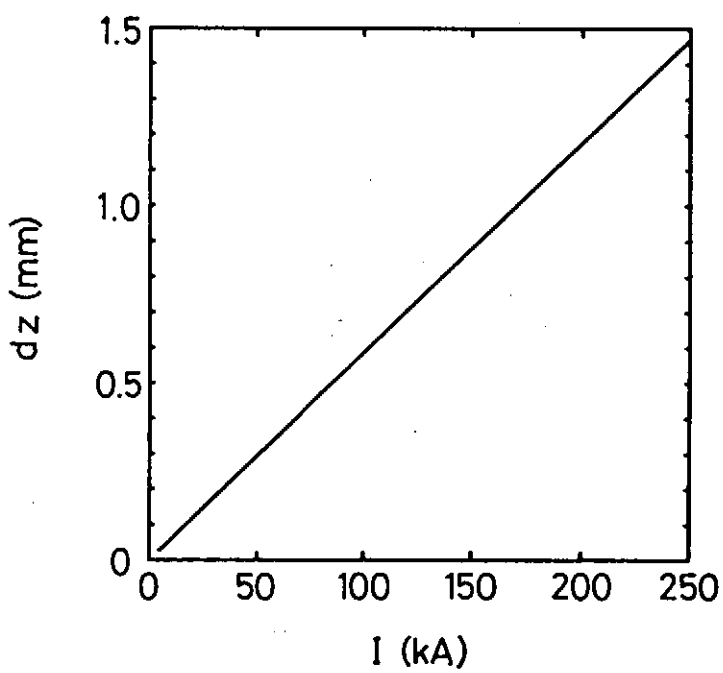

Fig. 10 Calculated results of the relation of ion deflection at the center with the diode current.

Diagnostics and Evaluation of Anode Plasma in "Point Pinch Diode"

Hisato Okuda, Hajime Sugimura, Masamitsu Seki, Yuji Sekimoto, Katsumi Masugata, Kiyoshi Yatsui, and Teruhiko Tazima*

Nagaoka Uinversity of Technology, Nagaoka, Niigata 940-21
*National Institute for Fusion Science, Nagoya 464

Abstract

Diagnostics and evaluation have been carried out on anode plasma in "Point Pinch Diode" produced by the irradiation of pinched relativistic electron beam. Mass spectra of ions extracted from the plasma measured by Thomson-parabola spectrometer have shown that the main component of the ions accelerated in the diode are ⓐ proton and H_2^+, ⓑ highly ionized carbon and oxygen, and ⓒ singly ionized carbon, oxygen, and moleculars such as CO_2^+, OH^+, H_2O^+. Time-integrated X-ray and particle pinhole images have shown the macroscopic spot size of the electron beam on the plasma to be less than ~ 0.5 mm in diameter, in which fine structures are found with size less than 0.05 mm. A K_α satellite line of Al-Ⅴ is observed with crystal spectrograph, which indicates the existence of Al^{4+} in the plasma.

§ 1. Introduction

In a pinched relativistic electron beam (REB) diode[1], electron beam is tightly pinched in an acceleration gap, which is irradiated onto a metalic anode. The high current-density irradia-

tion with current density more than MA/cm^2 produces high-energy density target plasma. Such a plasma can be applied to bright soft X-ray or neutron source. On the other hand, ions of the target plasma are accelerated in the gap with high current density due to that the density of the plasma is high and the space charge of ion beam is neutralized by the high density electron beam.

In "Point Pinch Diode", a kind of pinch REB diode, which consists of a spherical cathode and a flat anode, high bright ion-beam production has been observed[2]. The ion beam contains highly ionized carbons and oxygens. However, clear understanding of the mechanism of such a high bright, highly ionized ion beam production has not been obtaind. To clarify the mechanism, it is important to evaluate properties of the anode plasma.

In this paper, we will show the experimental results of the evaluation of the properties of the anode plasma. Highly-resolved Thomson parabora spectrometer (TPS), X-ray and particle pinhole camera, crystal X-ray spectrograph were used for the measurements.

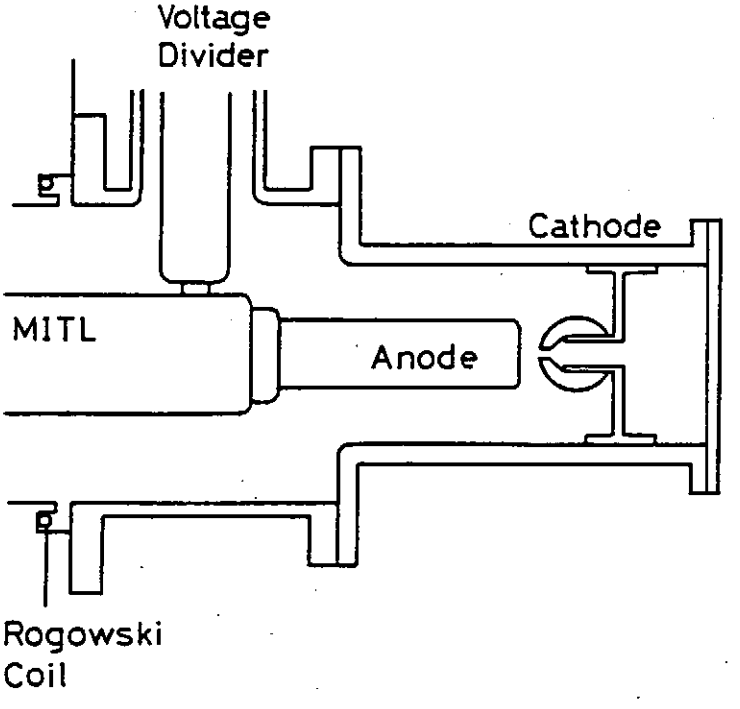

Fig. 1. Schematic drawing of the experimental setup.

§ 2. Experiment

2-1 Diode geometries and characteristics

Figure 1 shows experimental setup of "point pinch diode". Pulse power generator "LIMAY-I"[2] (3Ω, 50 ns) in the National Institute for Fusion Science was used in the experiment. The cathode is made of a spherical stainless-steel of diameter ~ 10 mm with a hole of diameter ~ 2 mm on the axis. The anode is a metal (aluminium, aluminium coated carbon or copper, 15 mm × 15 mm × 2mm^t) attached on the end of magnetically insulated transmission line (MITL). The gap length is ajusted to be ~ 3.2 mm. The chamber is evacuated to ~ 1×10^{-4} Torr. The diode voltage (V_d) is measured by a resistive voltage divider connected to the end of MITL. The diode current (I_d) is measured by a Rogowsky coil.

Figure 2 shows typical wave forms of V_d and I_d. We see V_d rises in ~ 10 ns and has a plateau of ~ 500 kV with the pulse width ~ 60 ns. I_d is almost linearly increases in time in the duration of V_d. The peak value of I_d is observed to be ~ 70 kA after the fall of V_d.

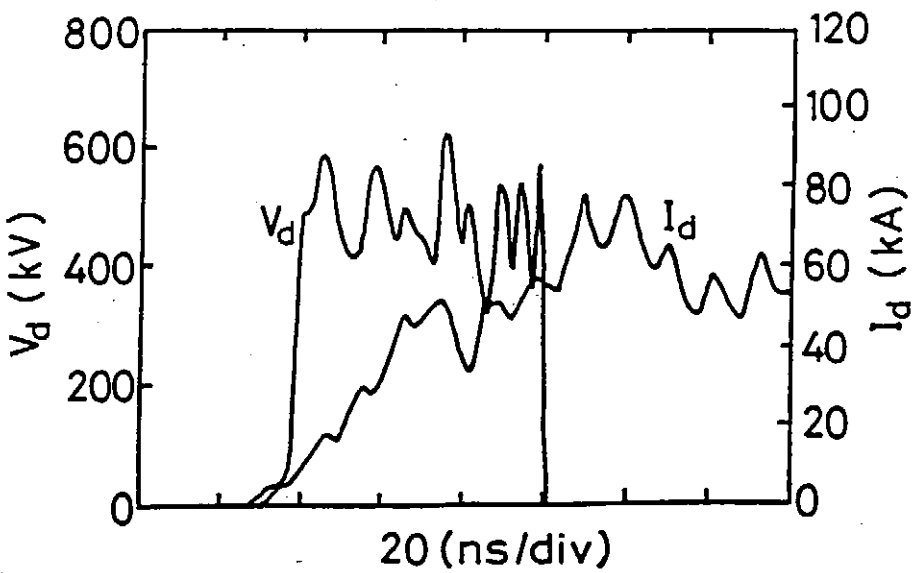

Fig. 2. Typical wave forms of V_d and I_d.

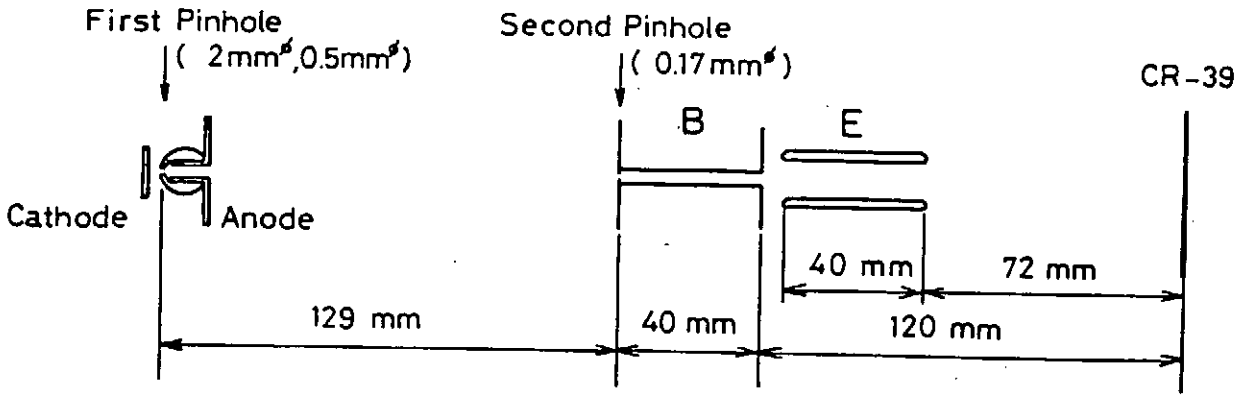

Fig. 3. The experimental setup with a Thomson-parabola spectrometer.

2-2 Analysis of ion species

Figure 3 shows the experimental arrangement of TPS[3]. Ions accelerated in the gap are collimated by a cathode hole (1st pinhole, 2mm$^{\phi}$ or 0.5 mm$^{\phi}$) and 2nd pinhole (0.17 mm$^{\phi}$), and injected into TPS. The ions injected are deflected by magnetic and electric fields applied in the same direction and recorded on the track recording film(CR-39).

Figure 4 shows typical traces obtained with Cu anode. Figure 4(a) and (b) are obtained by using the 1st pinhole of 2 mm$^{\phi}$ and 0.5 mm$^{\phi}$, respectively. Diode voltage was ~ 450 kV for (a) and ~ 300 kV for (b). From these figures, we can see that many kinds of ions are detected. These traces of ions can be divided into 5 groups as follows:

① H^+ and H_2^+ with maximum energy in agreement with V_d,

② C^+~ C^{5+}, and O^+~ O^{6+} with wide energy spread,

③ ions of mass number(A) to charge state(Z) ratio (A/Z) ~ (12~57), with narrow energy spread,

④ neutrals,

⑤ negative ions.

From Fig.4(b), we see that high energy ends of each traces in group ② are on a straight line passing through the origin. Furthermore, high energy end of the traces of C^{4+} and O^{5+} in Fig.3

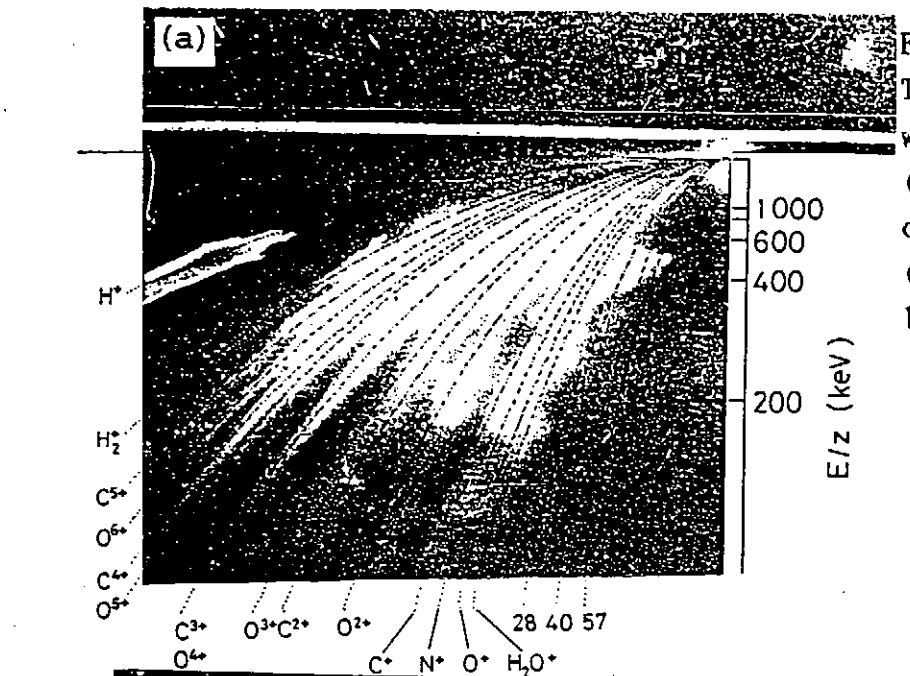

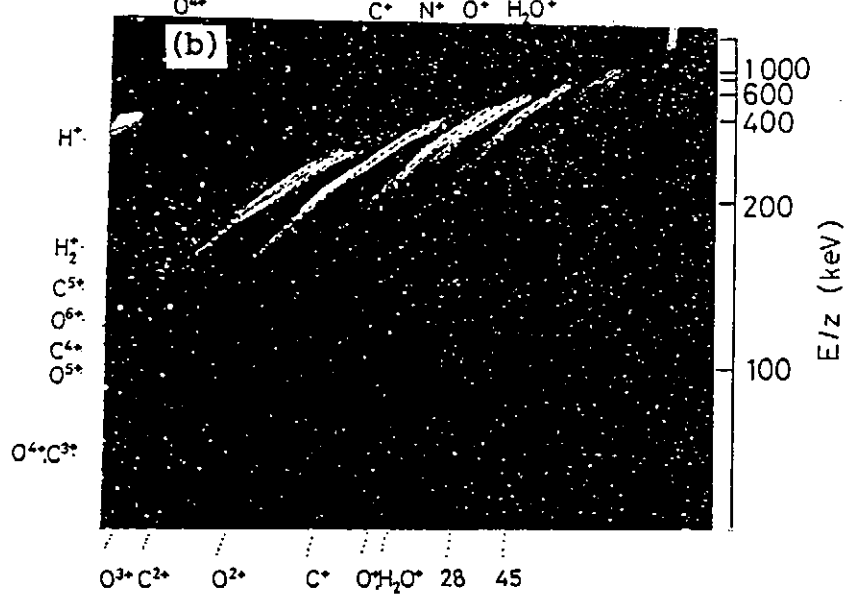

Fig. 4.
Typical TPS traces obtained with Cu anode.
(a) V_d ~ 450 kV, diameter of 1st pinhole ~ 2 mm.
(b) V_d ~ 300 kV, diameter of 1st pinhole ~ 0.5 mm.

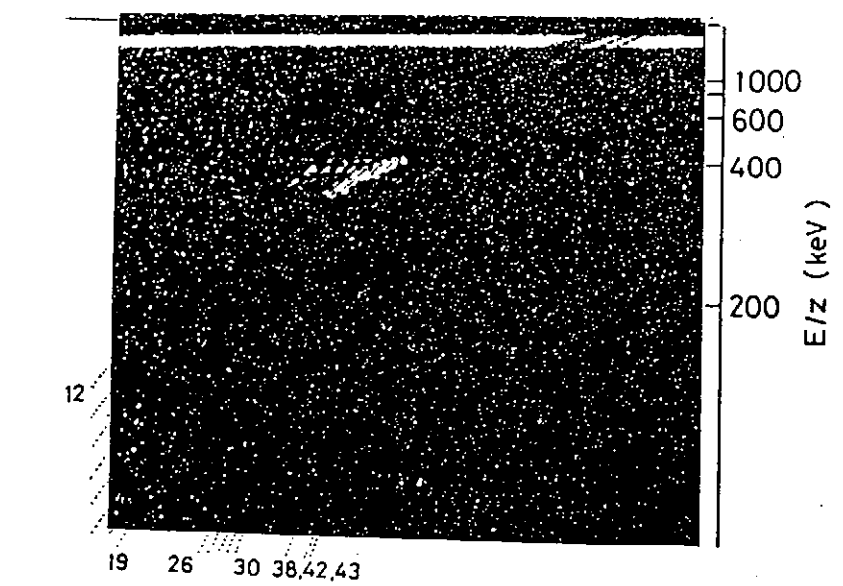

Fig. 5.
High resolution TPS trace obtained with Al coated carbon anode. V_d ~ 400 kV, 1st pinhole ~ 0.5 mm$^{\phi}$, 2nd pinhole ~ 0.175 mm$^{\phi}$.

(b) ~ 300 keV, which consists with V_d. Hence, we can find that ions of group ② are originally accelerated at the states of C^{4+} or O^{5+} and charge-exchanged in the drift region.

The negative ions (group ⑤) are considered to be produced from ③ by charge-exchange because the absolute value of A/Z and E/Z are same as those of group ③. Neutrals are also considered to be produced from positive ions by charge-exchange.

Ions in group ③ is considered to be singly ionized because no traces are observed in the area between group ③ and the origin (neutral point). If $Z \geq 2$, tracks should be exist in the area due to the charge-exchange. These ions have a wide spread of A/Z, which suggests that many kind of ions are included. However, exact values of A/Z were not obtained in this measurement due to the poor resolution of the TPS. To analyze these ions, we have improved the resolusion.

To increase the magnetic deflection, additonal magnet with magnetic field ~ 0.75 T is attached in front of the TPS. Applied elecric field for the electric deflector is also increased. The size of 1st and 2nd pinholes used were 0.5 mm' and 0.175 mm', respectively.

Figure 5 shows the typical traces obtained in the shot of V_d ~ 400 kV with Al anode coated on carbon. We see that the spot size of the beam is less than the width of $\Delta(A/z) = 1$ at the point of E/Z ~ 400 keV and A/Z ~ 19. That is, the resolution (ΔA) is less than 1 at that point.

From Fig. 5 we see that ions of A = 12 ~ 19 and 26 ~ 30, are observed. In addition, tracks are observed around A = 40, for which we couldn't obtain the exact value of A due to the poor resolution. The mass spectrum obtained is found to be quite similar to the typical spectrum of residual gas in a vacuum

chamber[4]. Possible candidate of ions with A = 12 ~ 19 are listed in Table I.

Table I. Possible ions with A/z of 12 to 19

A/z	12	13	14	15	16	17	18	19
ion	C^+	CH^+	N^+ CH_2^+	CH_3^+	O^+ CH_4^+	OH^+	H_2O^+	F^+ [a] H_3O^+

[a] Fron is used for the cleaning of the electrode.

As the residual gas is mainly applied from the surface of the chamber, the main source of the ions are considered to be the atoms or molecules adhered on the anode.

From the experiment above, we summarize that the ions accelerated in the diode are ⓐ proton and H_2^+, ⓑ highly ionized carbon and oxygen, and ⓒ singly ionized ions of carbon, oxygen and simple molecules such as CO_2^+, OH^+, H_2O^+. These ions are originated from the atoms or molecules adhered on the anode surface. In spite of using metallic anode, metallic ions are not observed clerly. The reason is considered to be as follows; The surface of the target plasma is covered by the ions produced by adhered moleculer, which disturbs the extraction of metallic ions.

2-3 Evaluation of the size of pinched REB

To evaluate the pinch diameter of the REB, time integrated X-ray pinhole camera[5] and particle pinhole camera were used. The pinhole used for the X-ray camera was the combination of thick, tapered Pb pinhole (thickness 6 mm^t ~ 10 mm^t, hole diameter ~ 1 mm$^\phi$) with thin Cu pinhole (thickness 0.1 mm^t, hole diameter 0.2 mm$^\phi$ or 0.15 mm$^\phi$). The former was used for eliminating hard X-

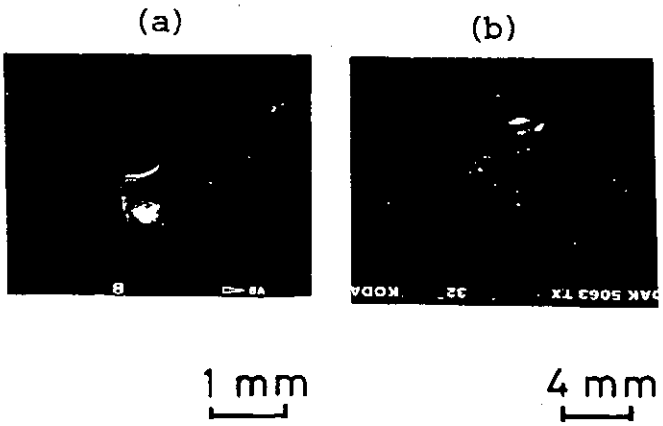

Fig. 6. X-ray pinhole images.
(a) front view (b) side view.

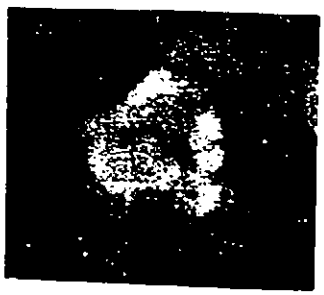

Fig. 7.
Particle pinhole image.

ray background and the latter was to obtain space-resolution[5]. Al and Be foil were used as a filter for eliminating light and ions, and for attenuating the intensity of X-ray. X-ray pinhole image was recorded on Kodak Tri-X Film.

Figure 6 shows the typical X-ray pinhole images of front view (a) and side view (b) of the diode with Cu anode. The pinhole diameter, the system magnification, and the space resolution were 0.15 mm', 9.8, and 0.22 mm for (a), and 0.20 mm, 2.25, and 0.22 mm for (b), respectively. The filter is 30-μm thick Al for (a), and 45-μm thick Al with 20-μm thick Be for (b). From Figs.6(a) and (b), pinch diameter of electron beam is evaluated to be ~ 0.4 mm and ~ 0.5 mm, respectively.

Figure 7 shows the particle pinhole image obtained on CR-39 for Al anode. Pinhole of 0.03 mm' was placed just behind the cathode on the diode axis. We see the macroscopic diameter of ~ 0.4 mm, which agrees with the X-ray images shown in Fig. 6. A microscopic spots of diameter ~ 0.05 mm was also obtained in the image, which indicates micro-structures in the electron beam or in the plasma.

2-4 Observation of Al-K_α X-ray satellites from a target plasma

K_α satellite lines are produced when thermal ionization due to beam heating is accompanied by inner shell ionization[6]. The satellite lines are blue-shifted with respect to the normal K_α line. In our diode, heating of metallic anode (target) and impact K-shell ionization occur simultaneously by the irradiation of pinched electron beam, while satellite lines are expected to be observed.

To evaluate the ionization state of target plasma produced on the Al anode, we have observed Al-K_α satellites by using flat crystal X-ray spectrograph. The spectrograph was carefully shielded against hard X-ray by using Pb board and installed inside the vacuum chamber. PET crystal[7] was mounted in the spectrograph with an angle of 67.5 degree. Be foil of thickness ~ 20 μm was used as a window. The spectra were recorded on Kodak DEF-392 film.

Figure 8 shows a spectrogram of the target plasma produced on the Al anode. Satellite line of Al-V was clearly observed, which indicates ions of Al^{4+} exists in the plasma.

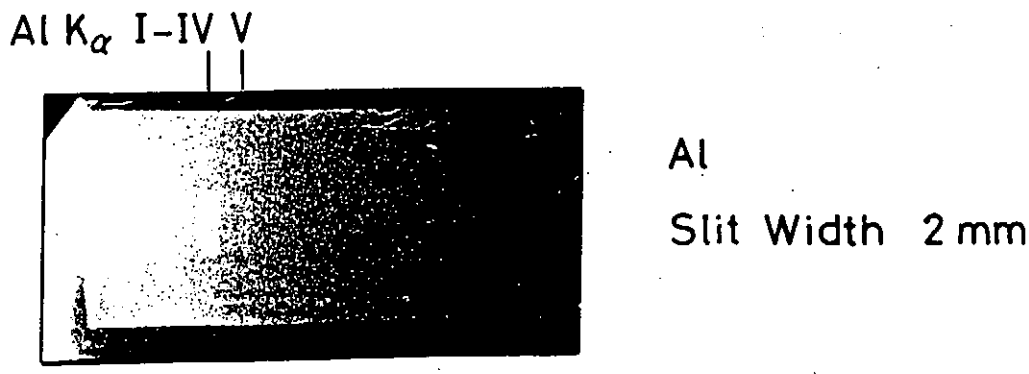

Fig.8. Typical X-ray spectrogram of the plasma on the Al anode.

§ 3. Summary

Highly-resolved mass spectrum of the ion beam indicates that the ions exracted from the anode plasma is mainly consists of ⓐ protons and H_2^+, ⓑ multiply ionized carbon and oxygen and ⓒ singly ionized carbon, hydrogen and simple molecules. Existence of multiply ionized ions suggests the production of hot spot in the plasma. Images of X-ray and particle pinhole camera indicate that the size of pinched REB is less than ~ 0.5 mm in diameter, inside which micro-structure of size less than ~ 0.05 mm exists. X-ray spectrograph of the plasma indicates that multiply ionized metallic ions exist in the plasma.

Acknowledgment

This work was carried out under a collaborative research program in National Institute for Fusion Science, Nagoya, in FY 1990. The authors would like to express their sincere thanks to many persons concerned.

References

1) S.A.Goldstein and R.Lee: Phys. Rev. Lett. 35, 1079 (1975).
2) M.Sato: Jpn. J. Appl. Phys., 26, 927 (1987).
3) M.J.Rhee: Rev. Sci. Instrum., 55, 1290 (1982).
4) N.Okuda: Master Thesis (Nagaoka Univ. of Tech., 1991).
5) D.J.Johnson, E.J.T.Burns, A.V.Fransworth,Jr., R.J.Leeper, J.P.Quintenz, K.W.Bieg, P.L.Dreike, D.L.Fehl, J.R.Freeman, and F.C.Perry: J. Appl. Phys., 53, 4579 (1982).
6) J.Bailey, A.L.Carlson, G.Chandler, M.S.Derzon, R.J.Dukart, D. A.Hammel, D.J.Johnson, T.R.Lockner, J.Maenchen, E.J.McGuire, T.A.Mehlhorn, W.E.Nelson, L.E.Ruggles, W.A.Stygar, and D.F. Wenger: Laser and Particle Beams, 8, 555 (1990).
7) P.G.Burkhalter, G.Mehlman, D.A.Newman, and B.H.Ripin: Rev. Sci. Instrum., 61, 2741 (1990).

EXPERIMENTAL STUDY ON SPECTRUM OF MICROWAVE RADIATION FROM IREB–PLASMA INTERACTIONS

Ritoku ANDO, Masaki ISHIKAWA, Kiyofumi KITAWADA,
Masayuki YOSHIKAWA, Hiroshi MORITA, Keiichi KAMADA
and Masaru MASUZAKI

Department of Physics, Faculty of Science,
Kanazawa University, Kanazawa 920

Abstract

Spectra of high-power microwave radiation from interactions between an intense relativistic electron beam (IREB) and an unmagnetized plasma with relatively uniform axial density profile or with an axially increasing one were measured in the frequency range from 18 GHz to 40 GHz. They were compared with those obtained in our previous experiment, in which the plasma had an axially decaying density profile and the plasma density was lower than that in the present experiment. The results suggest importance of the ratio of the beam density to the plasma density on the microwave emission mechanisms.

1. INTRODUCTION

Recently researches on generation of high-power microwave radiation from interactions between an IREB and an unmagnetized or weakly magnetized plasma have been carried out experimentally by two groups with different results.[1,2] In our previous experiment (hereafter called as Ex. I) high-power microwave radiation with a broad and rather flat spectrum or with a spectrum increasing with frequency was observed when an IREB was injected into an axially decaying unmagnetized plasma using a 5-channel spectrometer covering a frequency range from 18 GHz to 40 GHz. The maximum plasma

frequency in the drift tube was nearly equal to or less than 18 GHz, the beam density being comparable to the plasma density.[3] This report describes results of our recent experiment in which the IREB was injected into an unmagnetized plasma which had a relatively uniform density profile in the axial direction or an axially increasing density profile. The plasma density was higher than that in Ex. I.

2. EXPERIMENTAL APPARATUS

The experimental device consisted of a beam generator, a vacuum drift chamber and a plasma gun section (Fig. 1). The beam generator used was a PULSERAD 110A, maximum ratings of which were 1.5 MeV in energy and 27 kA in current when operated with a conventional diode at the Marx charging voltage V_M = 50 kV, and its pulse duration was 30 ns. The diode consisted of a 3-mm-diam. tungsten rod cathode and a foilless carbon anode with 2-cm-diam. hole in the axis. In the experiment V_M was kept to be 50 kV. The drift chamber was of stainless steel and its inner diameter and length were 17 cm and 60 cm, respectively. To eliminate microwave reflection, the inside wall of the chamber was covered with microwave absorber (Eccosorb AN73). The base pressure was kept less than 5×10^{-5} torr.

In Ex. I two rail-type carbon plasma guns placed face to face in the plasma gun section were used to produce a plasma as shown in Fig. 1(a).[3] In the present experiment, a coil-type carbon plasma gun[4] was placed at the downstream end of the drift chamber as shown in Fig. 1(b) to produce a plasma relatively uniform in the axial direction or a plasma with an axially increasing density gradient. A 50-kV, 0.3 μF capacitor was connected to the gun. For each gun system the delay time between the firing times of the gun and of the IREB, τ, was variable. Figure 2 shows time evolution of the axial density profile of the plasma produced by the rail-type guns and that of the plasma produced by the coil-type gun, τ being taken as a parameter. The plasma density was measured by electrostatic double probes. The axial distance

Z was measured from the downstream surface of the anode plate (Fig. 1). Using the coil-type gun the axial density profile could be changed significantly by changing τ. When τ was 5 - 7 μs nearly uniform axial density profile was obtained with the plasma density changed from 3 x 10^{12} cm^{-3} to 2 x 10^{13} cm^{-3} on the axis at Z = 17 cm by changing the charging voltage of the capacitor V_g. When τ < 5 μs, axially increasing density profile was obtained. For longer τ diode shortening prevented the operation of the beam generator.

Figure 3 shows a schematic diagram of the 5-channel microwave spectrometer used, which covers a frequency range from 18 GHz to 40 GHz. Its detail is described in Ref. 3. Microwaves emitted radially were received by a Ka-band and a K-band horn-antenna set face to face at Z = 17 cm. The E-polarization was fixed parallel to the drift chamber axis. The signal received by the K-band horn was transmitted to two channels called as K-1 and K-2, the signal received by the Ka-band horn to three channels called as Ka-1, Ka-2 and Ka-3. A channel named Q-band was added to this spectrometer. It was used as a monitor for higher frequency emission (40 - 60 GHz). To reduce number of oscilloscope beams, K-1 output, K-2 output delayed 50 ns and Ka-1 output delayed 100 ns were added together, while Ka-2 output and Ka-3 output delayed 100 ns were added together. Both added signals were displayed on a Tektronix 7844 oscilloscope and recorded photographically.

3. EXPERIMENTAL RESULTS AND DISCUSSIONS

Examples of observed signals are shown in Fig. 4, (a) corresponding to the case of V_g = -20 kV and (b) to -45 kV, and the plasma densities on the axis at the horn position n_H's were about 2.5 x 10^{12} and 1.8 x 10^{13} cm^{-3} respectively. Spectra of emitted radiation were obtained using peak values of outputs of each channels. Figure 5 shows spectra for the case of relatively uniform axial density profiles, n_H (or V_g) being taken as a parameter. The axial density profiles are also shown in the figure. The plasma frequencies corre-

sponding to each n_H were 14 GHz, 21 GHz and 38 GHz respectively. The frequency range includes the plasma frequency corresponding to n_H in the case of V_g = -30 kV and the spectrum seems to have a peak near the plasma frequency. Also the second harmonic is included in the frequency range in the case of V_g = -20kV and it seems that there is a peak near it. For the case of V_g = -45 kV the plasma frequency is higher than 40 GHz and the spectrum is an increasing function of frequency. The total power in this frequency range increased with n_H as shown in Fig. 6.

In order to examine whether the axial density profile affects the spectrum or not, the density profile was changed by changing the delay time τ. Figure 7 shows two pairs of two spectra corresponding to τ = 3 μs and τ = 7 μs respectively; V_g = -30 kV for the case of Fig. 7(a) (the lower density case) and -45 kV for the case of Fig. 7(b) (the higher density case) respectively. In each case n_H for both delay times were nearly equal to each other. The density profiles are also shown in Fig. 7; n_H was 2.5 x 10^{12} cm^{-3} for the lower density case and was 1.8 x 10^{13} cm^{-3} for the higher density case. In the lower density case, both spectra have similar pattern with a peak near second harmonic of the plasma frequency at the horn position, although output levels are different. In the higher density case, both spectra have also similar pattern in which the outputs increase with frequency. These results seem to show that the spectral pattern observed was determined partly by the local plasma density at the horn position. Difference in the output level in the lower density case might be attributed to difference in the propagation mode of the IREB.

Now let's compare results of the present experiment with results of Ex. I. In Fig. 8 an example of the spectrum obtained at V_g = -45 kV is plotted as well as that obtained when the plasma density was highest in Ex. I . Although n_H's were different one order or more each other and axial density profiles were different (axially flat and exponentially decaying on the axis), spectrum patterns of radiation had

similar tendency, that is, microwave outputs increased with frequency. Perhaps this might be attributed to difference of the ratio of the beam density to the plasma density.[1] In Ex. I it was on order of one, while in the present experiment it was on order of 0.1 or less.

The total powers in the frequency range obtained in the present experiment and Ex. I are plotted as a function of n_H in Fig. 6. These data were obtained at V_M = 50 kV. The total power increased with the plasma density in each case. The maximum was 1.8 kW/cm^2 in Ex. I and 3.4 kW/cm^2 in the present experiment. As can be seen from the figure the plasma density is not the only factor which affects the radiation. As mentioned above we think that the ratio of the beam density to the plasma density may play an important role.

4. CONCLUDING REMARKS

Radiation spectra obtained in the present experiment were rather broad, but it seems that there were peaks near the local plasma frequency or its harmonics. On the other hand spectra obtained in Ex. I were broad and rather flat or increasing functions of frequency. However, when the beam density was lowered by attaching a masking plate to the anode plate in Ex. I, the emission spectrum became rather peaky as seen in Fig. 9, although this measurement was done axially. This fact also suggests importance of the ratio of the beam density to the plasma density concerning with radiation mechanisms.

We are now preparing an experiment in which the frequency range is widened to 10 GHz. Also more precise measurements of the plasma and the beam densities are being planned in order to investigate in detail the dependence of microwave emission on the ratio of the beam density to the plasma density.

References

1) K. G. Kato, G. Benford, and D. Tzach: Phys. Fluids 26, 3636 (1983).

2) M. S. Di Capua, J. F. Camacho, E. S. Fulkerson, and D. Meeker: IEEE Trans. Plasma Sci. 16, 217 (1988).
3) M. Masuzaki, R. Ando, A. Yoshimoto, M. Ishikawa, M. Yoshikawa, K. Kitawada, H. Morita, and K. Kamada: Proceedings of the 8th International Conference on High-Power Particle Beams, edited by B. N. Breizman and B. A. Knyazev (Institute of Nuclear Physics Novosibirsk, USSR, 1990) p.683.
4) C. W. Mendel, Jr., D. M. Zagar, G. S. Mills, S. Humphries, Jr. and S. A. Goldstein: Rev. Sci. Instrum. 51, 1641 (1980).

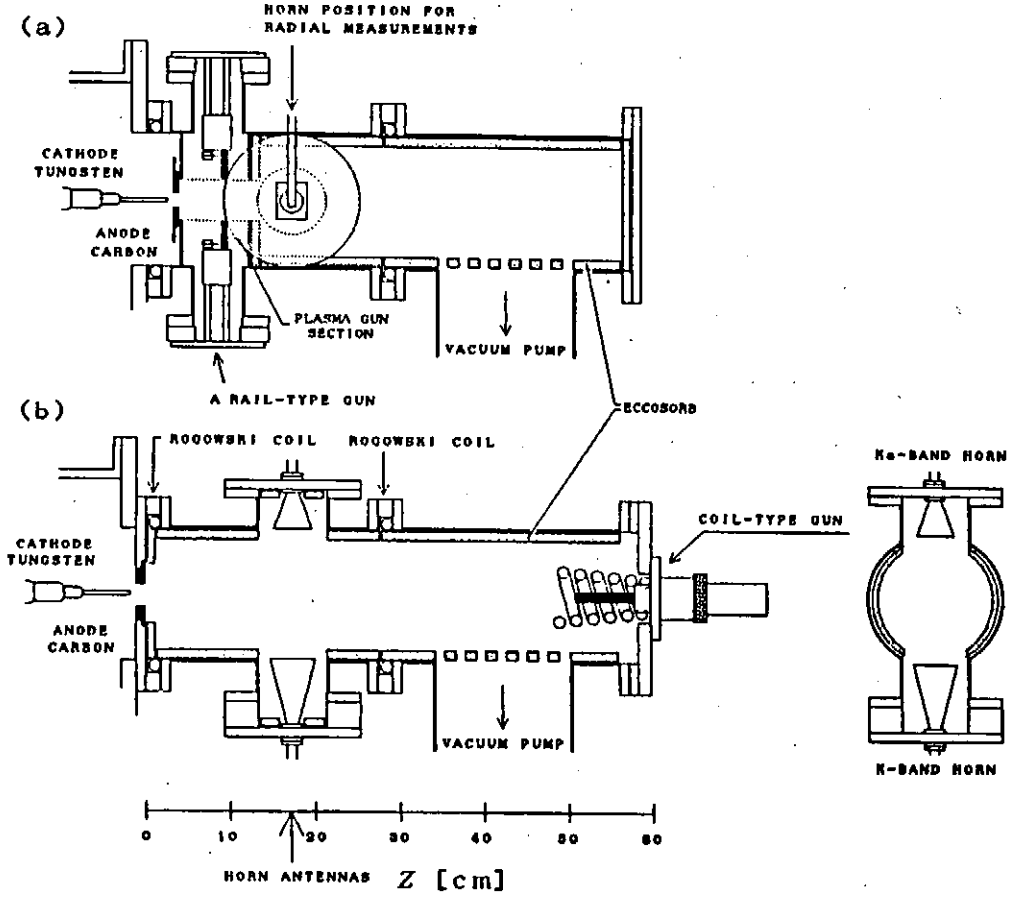

Fig. 1. Schematic diagrams of the experimental configuration: (a) Ex. I,. (b) the present experiment.

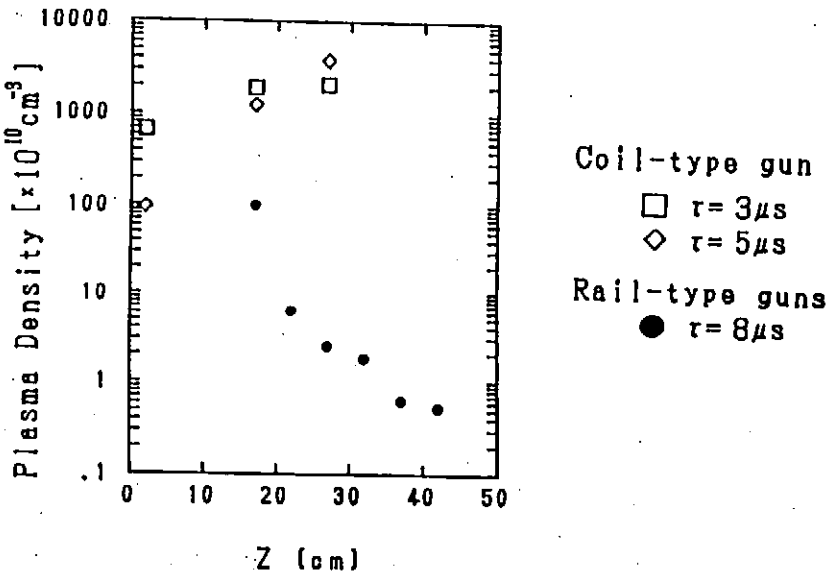

Fig. 2. Axial density profiles of plasmas in Ex. I and in the present experiment.

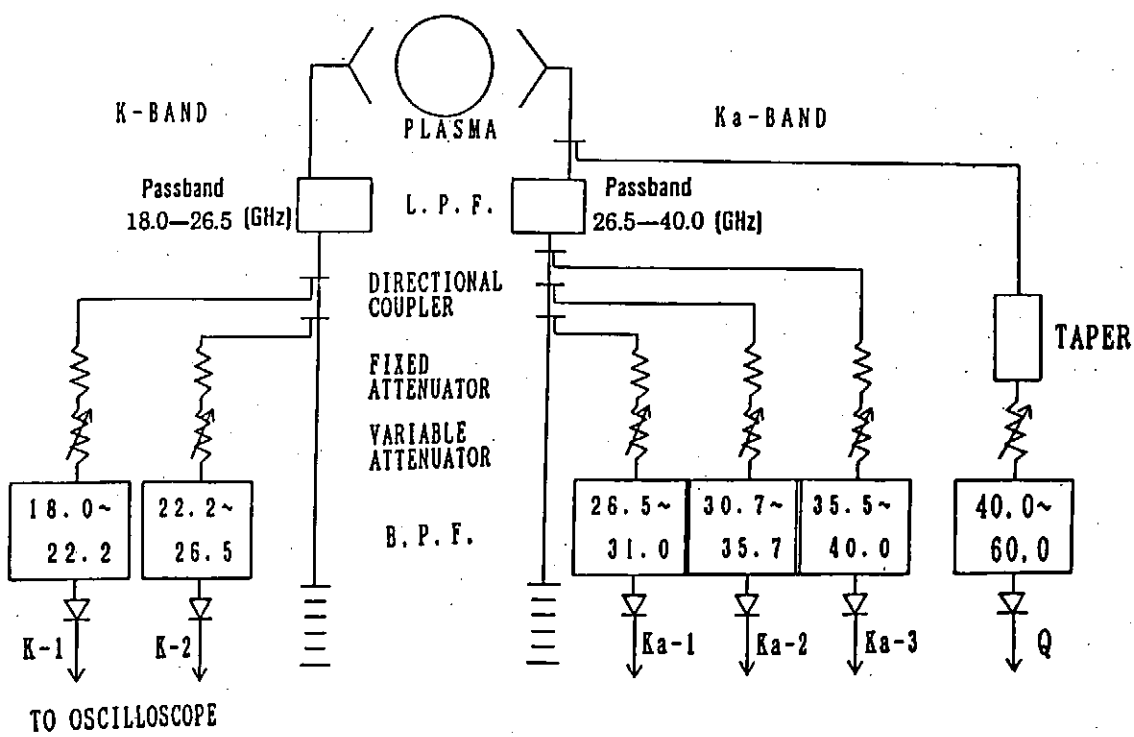

Fig. 3 A schematic diagram of the microwave spectrometer.

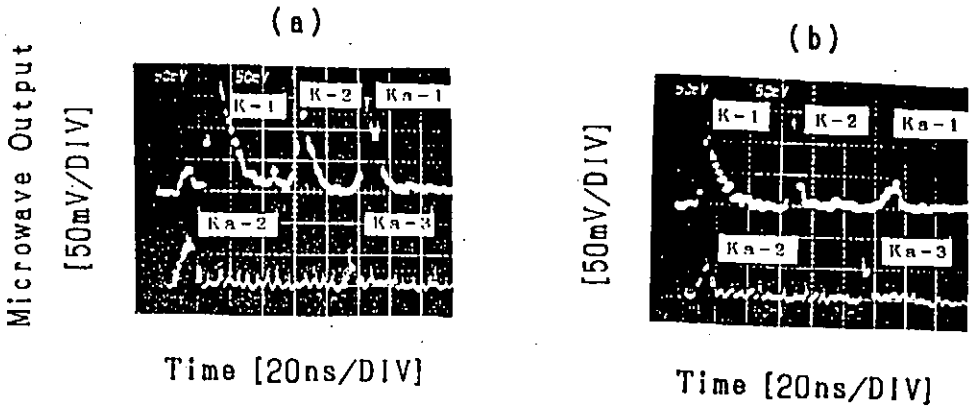

Fig. 4 Examples of microwave outputs from the IREB-plasma system. (a) V_g = -20 kV and (b) -45 kV.

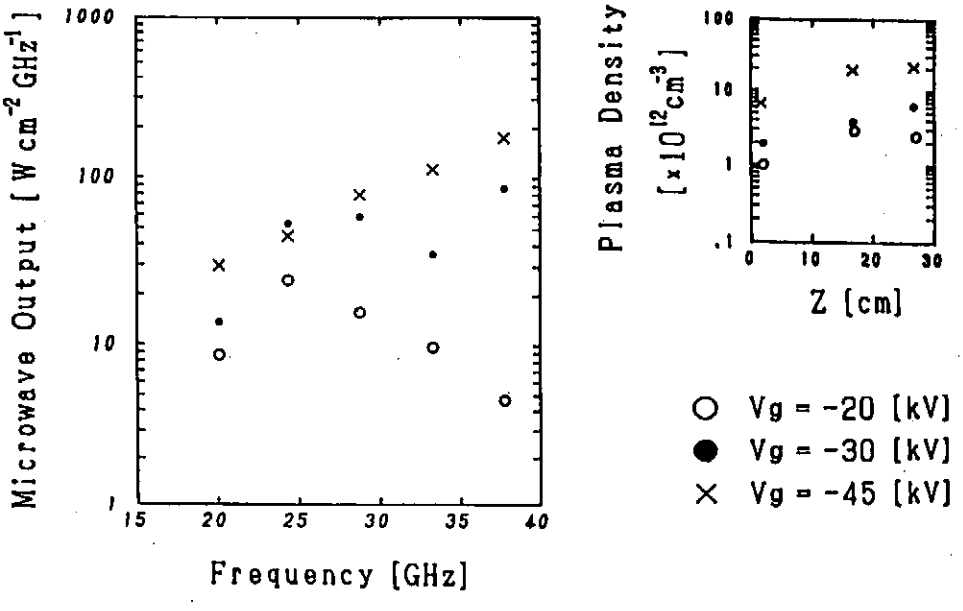

Fig. 5 Examples of observed spectra for the case of the axially uniform density profile. The density profiles are also shown.

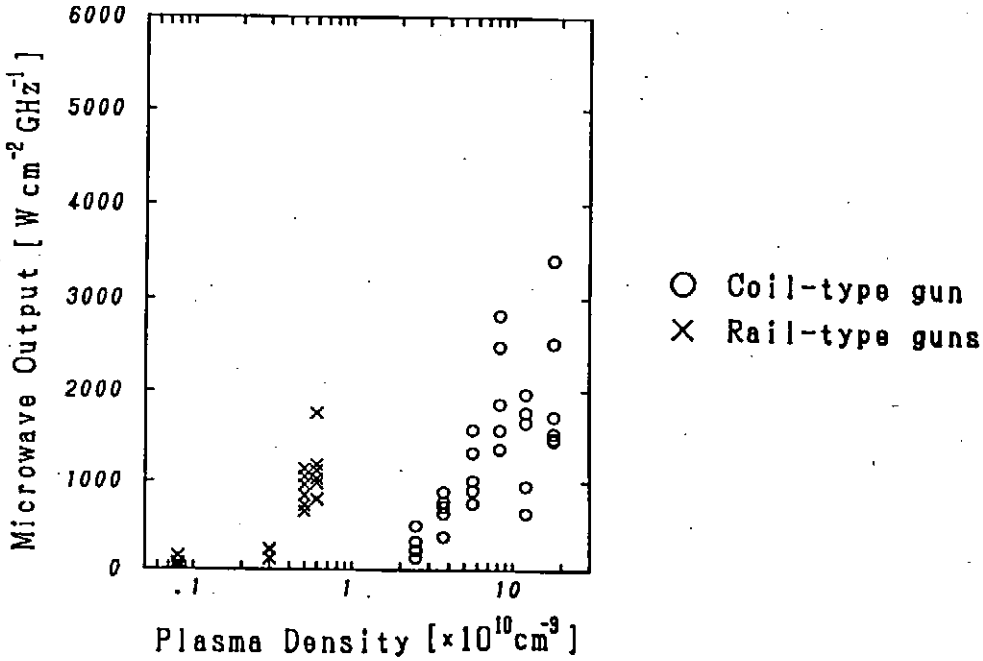

Fig. 6 Total powers of the observed microwaves versus n_H for Ex. I and for the present experiment.

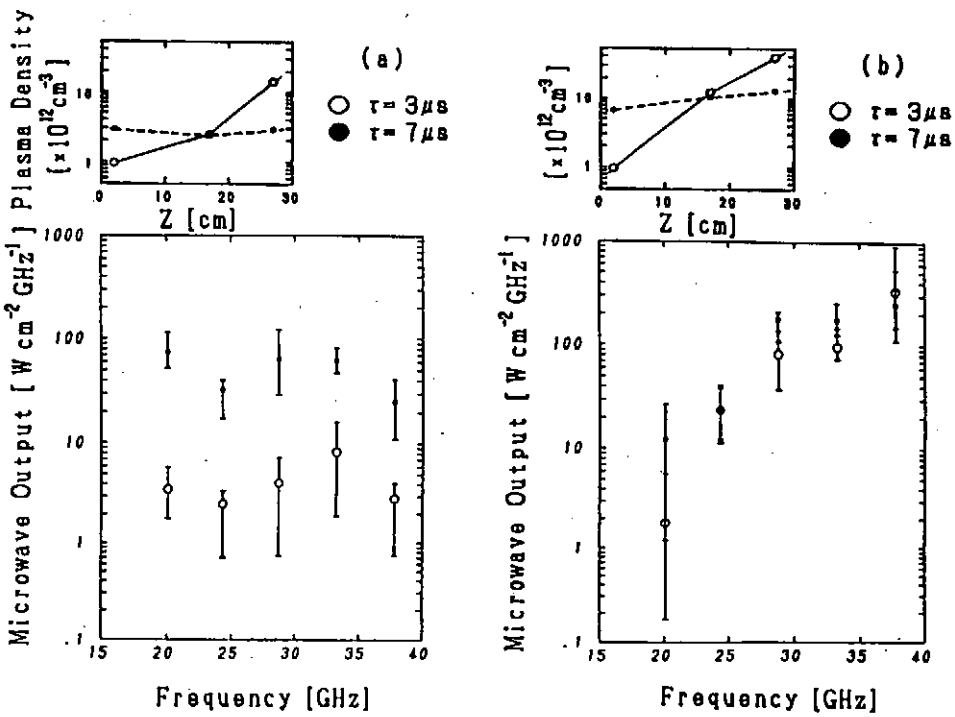

Fig. 7 Comparison of the spectrum obtained in the case of axially uniform density profile with that in the case of axially increasing density profile; (a) V_g = -30 kV, (b) V_g = -45 kV.

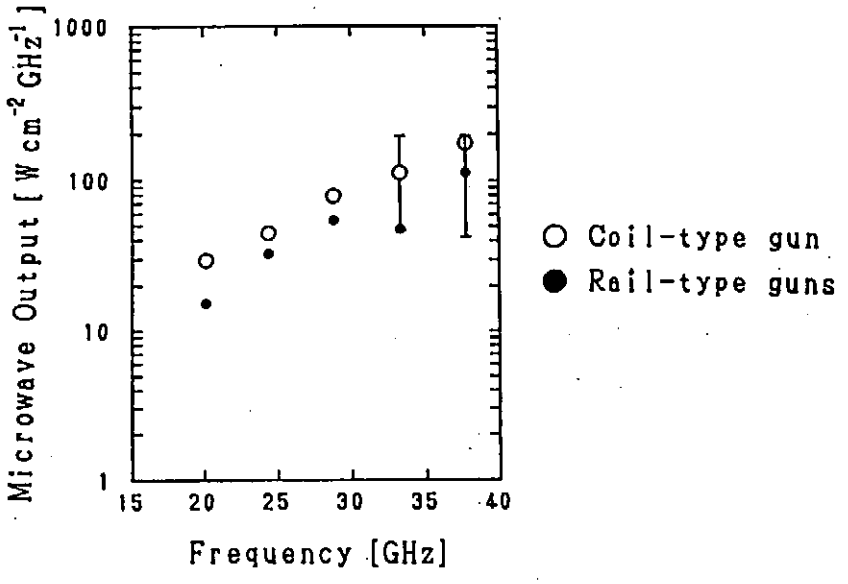

Fig. 8 Comparison of the spectrum obtained in Ex. I with that obtained in the present experiment, n_H being 6 x 10^{11} cm^{-3} and 2.5 x 10^{12} cm^{-3}, respectively.

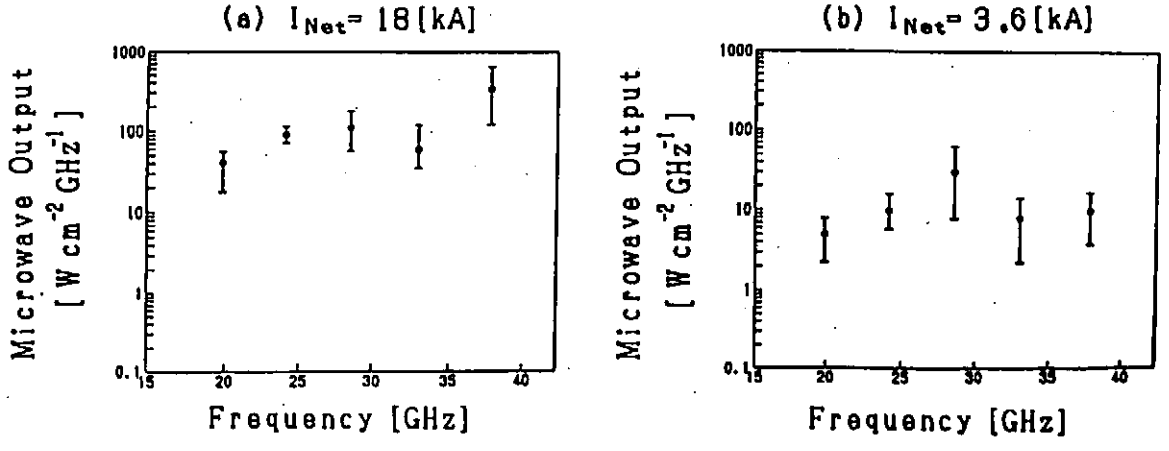

Fig. 9 Axially observed spectra with and without a masking plate in Ex. I.

Characteristics of Plasma Injection Type Pulsed Ion Diodes

Y.Saito, K.Horioka, T.Aoki, T.Suzuki and K.Kasuya

Department of Energy Sciences, The Graduate School
at Nagatsuta, Tokyo Institute of Technology,
Nagatsuta 4259, Midori-ku Yokohama, Japan 227

Abstract

We have investigated the characteristics of plasma injection diodes. A flashover source plasma is injected from 1cm behind the perforated anode surface. The diode is operated beyond the Child-Langmuir current level and the possibility of impedance control by means of flux of the injection plasma is investigated. We also performed 1-D PIC simulation to explain qualitative behavior of the diode.

I. Introduction

The diode which has flashover type plasma source has been mainly used to produce intense light ion beams for inertial confinement fusion (ICF).[1] However, this type of diode has undesirable characteristics that the diode impedance is high at the begining and it rapidly collapses at the end of the voltage pulse, which causes a beam debunching and impedance mismatch. The main cause of impedance falling is supposed to be insufficient production of source plasma at the begining and growth of the plasma during the voltage pulse. The flashover process is accompanied with a large amount emission of neutral particles, which degrade the characteristics of the diode.[2] Therefore, the development of new concept diodes is a highest priority now.[3,4,5] In order to improve the diode behavior, we have developed a plasma injection type diode and investigated the behavior of this diode over a wide range of the injection parameters.

To produce the source plasma, a flashboard driven by small

capacitors is activated early relative to the accelerating voltage pulse. Here, we mainly investigated the relationships of impedance behavior of the diode and the condition of injection plasma.

II. Experimental Set-up

A schematic diagram of typical experimental arrangement is shown in Fig.1. A Br-magnetically insulated diode had an effective area of $20cm^2$ and was driven with a 5Ohm-60nsec PFL(Pulse forming line). It was operated with geometical gap (d) of 8mm and the insulation field of B/Bc~1.1. The charging voltage of PFL was fixed at 500kV in this experiment. We used two types of configuration. One had a flashboard directly attached on the anode surface (Fig.2), and another one had a flashboard placed 1cm behind the anode surface (Fig.3). We call the former pre-ionized type and the latter plasma injection type. The flashboard was driven before the main pulse generation. Here, we define delay time as the time between flashboard activation and the main pulse.

A front-view photograph of the flashboard is shown in Fig.4(a). The flashboard which consists of four segmented series gaps was etched from a circuit board. It was observed that the

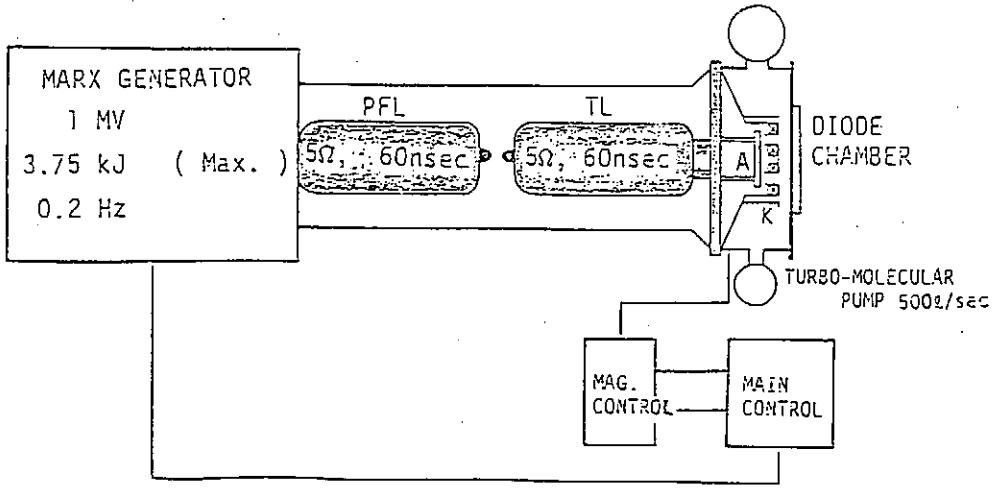

Fig.1 Schematic of Experimental Set-Up

brightness of discharge was uniform from the open shatter photograph shown in Fig.4(b). Plasma flux from the flashboard was measured with a biased ion collector placed at 1cm from the flashboard. It was observed that peak flux was about 300 A/cm^2 at

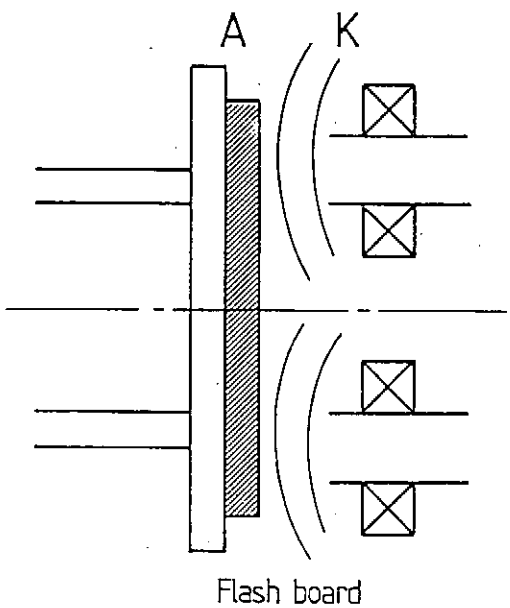

Fig.2 Schematic Diagram of Pre-ionized Type Diode

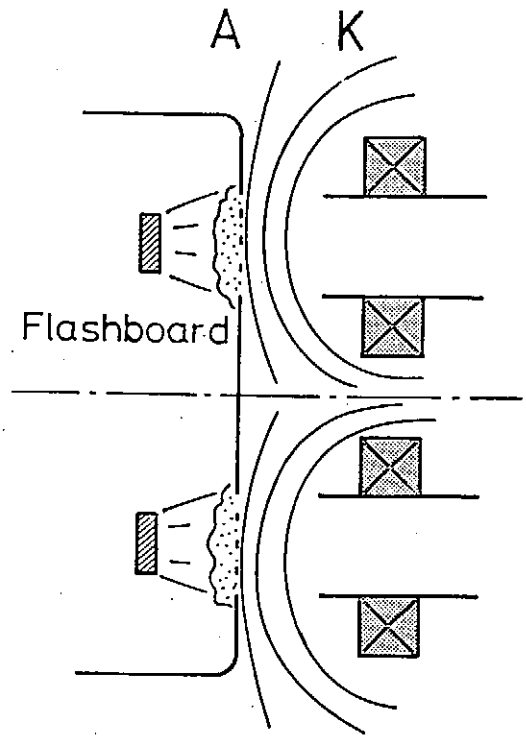

Fig.3 Schematic Diagram of Plasma Injection Type Diode

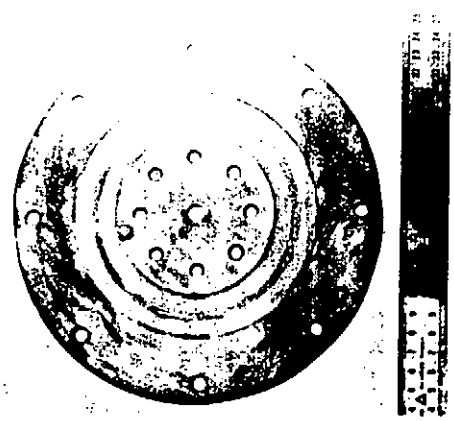

Fig.4 (a) A Front-View Photograph of Flashboard

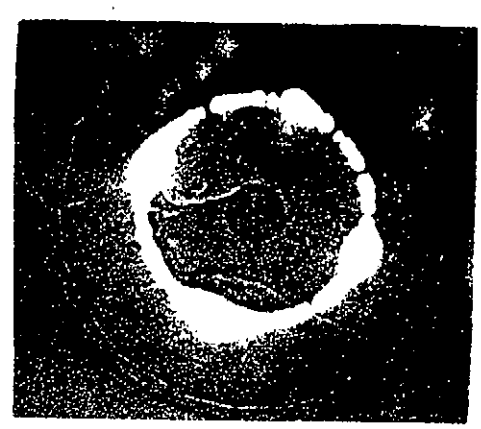

Fig.4 (b) Visible Light Emission from the Flashboard

200ns after the board activation. The average velocity of the flashover plasma was 5 cm/μs. From these results, we can roughly estimate the peak plasma density at this place to be about $4.0*10^{14}$ /cm^3. The flux of the injection plasma could be controled by the delay time.

III. Experimental Results

III-1 Pre-ionized Type Diode

Typical wave-forms of the diode voltage and current of the pre-ionized type diode are shown in Fig.5. With the delay time of 60ns, although the turn-on delay of the ion beam was decreased in comparison with that of convensional diodes, the diode impedance collapsed with time. When the delay time was increased more than 150ns, the diode voltage did not rise enough; the diode gap was almost closured. We think that not only the source plasma but also a large quantity of neutral gas which expands to A-K gap is produced by flashover process.

The overall impedance history of the pre-ionized diode was similar with convensional flashover ion diodes.

III-2 Plasma Injection Type Diode

The plasma injection type diode has a perforated Al board as an anode and a flashboard 1cm behind the anode. The plasma component of the flashover plasma is separated from neutral particles produced by the flashover process by the time of flight. The Al plate excludes the insulation field. Therefore, we can expect that only the plasma component is stagnated along the anode surface by the magnetic field in the A-K gap, which forms relatively high dense source plasma along the anode surface. Characteristics of the plasma injection diode were investigated as a function of the delay time. Typical wave-forms of the diode voltage, diode current and ion current are shown in Fig.6, with the delay time as a parameter. With the delay time longer than 250 ns, which corresponded to the time when the plasma flux from flashboard became maximum at the anode surface, the diode had a voltage hump. The diode voltage rose slowly at

the begining and rose rapidly at the end of the pulse. When the delay time was longer, the voltage hump at the end of the pulse became smaller.

Typical waveforms of ion current are shown in Fig.7, with distance from the anode surface as a parameter. At 75 cm from the anode, though the beam waveform was devided into the components of many ion species due to the time of flight, the pulse width of each ion species didn't expand ;i.e., the acceleration voltage was nearly maintained at a constant value.

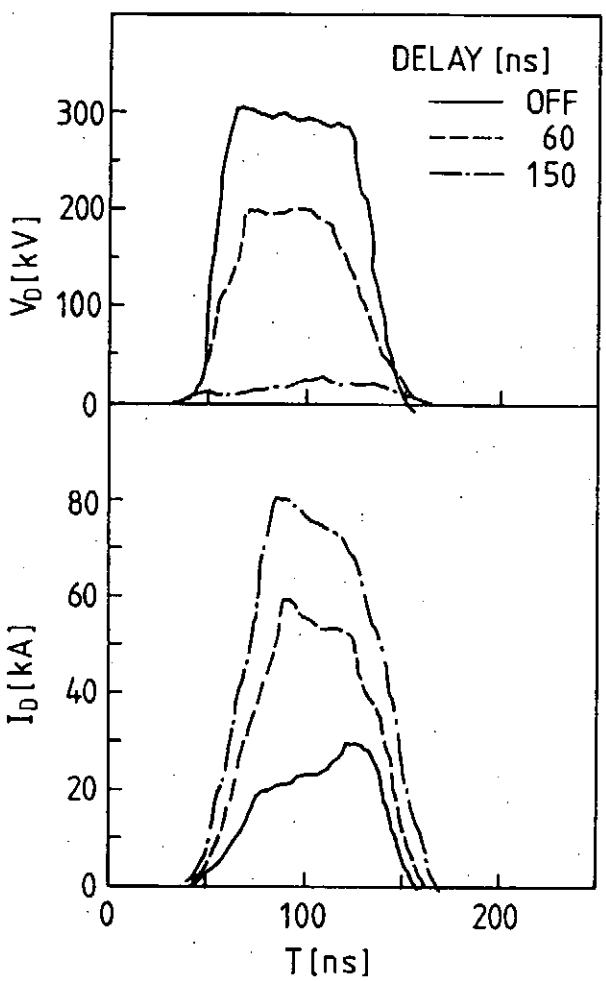

Fig.5 Typical Waveforms of Pre-ionized Diode

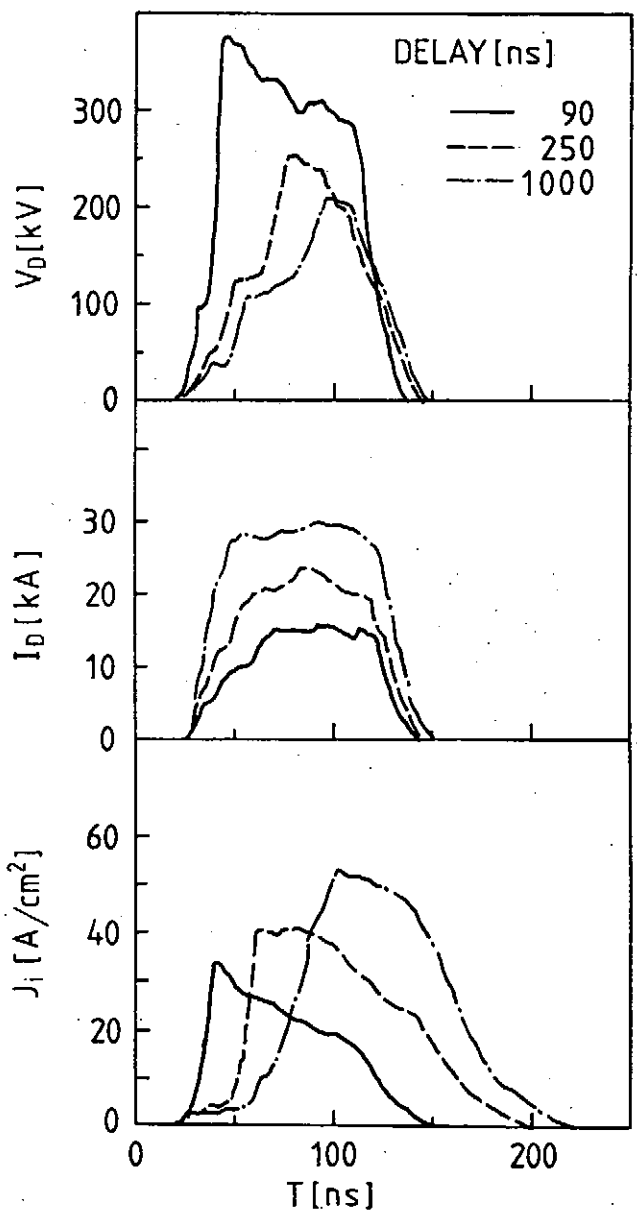

Fig.6 Typical Waveforms of Plasma Injection Diode

From these results, we can conclude that the diode impedance collapse can be avoided by this way and the diode behavior closely relates to the initial plasma distribution in the A-K gap. So we measured the plasma flux with magnetic field in the A-K gap. Typical results are shown in Fig.8. It was observed that the plasma sunk into the gap with time. If we assume one dimensional ideal model,i.e., perfect uniformity along the anode surface, it is impossible that the flashover plasma invade across the magnetic field of several kG. However experimental results showed that near one tenth of the plasma sunk into the A-K gap. It seems that the cause of the plasma invasion is local nonuniformity of the injection plasma, which induces plasma drift in the strong magnetic field. This phenomena may become important when much higher current density of beam is produced with this type of diode.

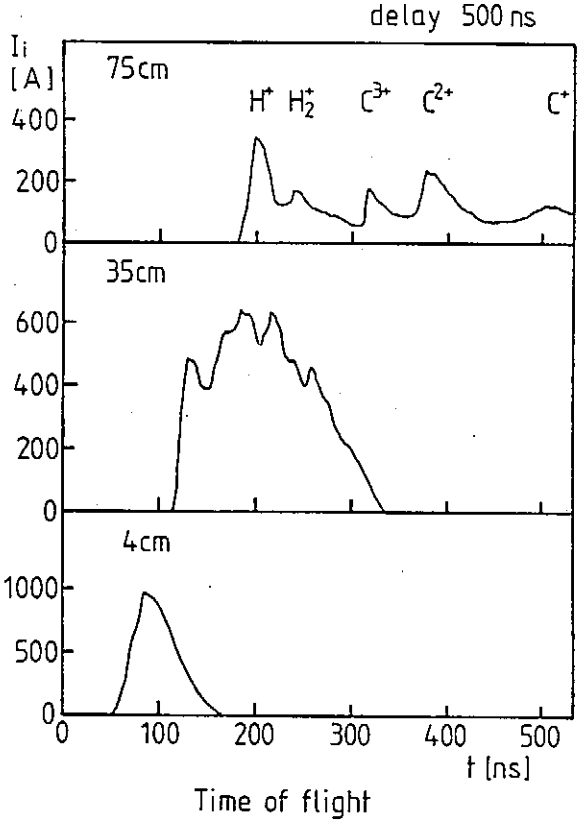

Fig.7 Time-of-Flight Waveforms of Ion Current

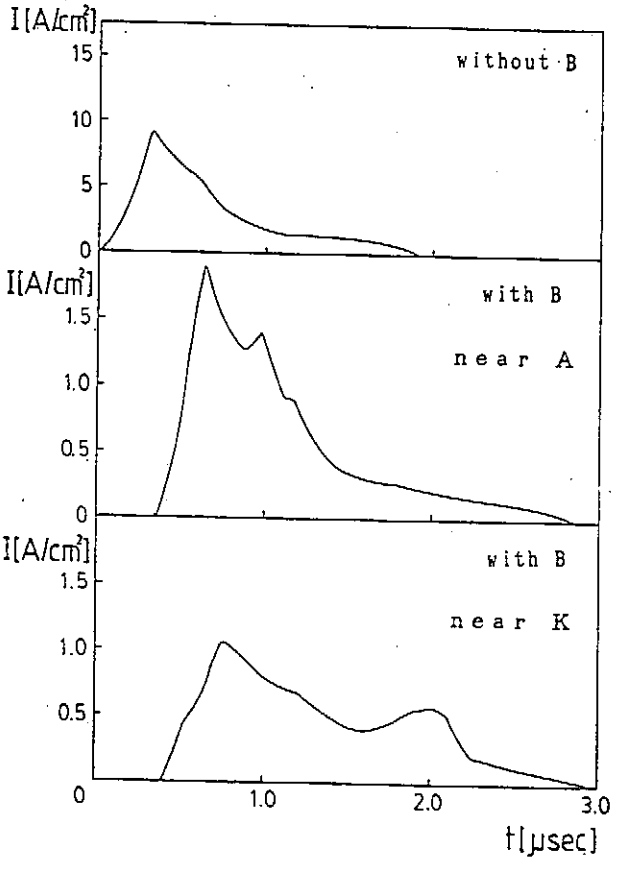

Fig.8 Plasma Flux with Insulation Magnetic Field

IV. 1-Dimensional-Simulation

In order to investigate qualitative behavior of the plasma injection diode, an one dimensional pareticle-in-cell code was used.[6] The 1D-particle code can treat diamagnetic effect of the electron motion and load effect of the diode section.

The pulse power was assumed to support the accerelation voltage for 5ns width, with 2.5ns rising and falling portion. The impedance of the pulse power and the inductance of the diode section was assumed to be 5Ohm and 10nH, respectively.

We performed numerical calculation for cases of space charge limited condition (Fig.9) and flux limited condition (Fig.10 and 11). The assumed waveform of the applied voltage is shown in those figures. As can be seen with Fig.9, for the former case, the diode impedance decreased with time due to the diamagnetic effect of the electron motion.

The time dependent calculation of potential distribution in the A-K gap indicated that the effective gap width was decreased by the diamagnetic effect of electron. The flashover passive ion source is considered to be approximately satisfied with such conditions.

On the other hand, diode impedance was increased for case of flux limited condition. In the latter case, the quantity of injected plasma was limited at experimentally obtained value.

When the injected plasma distributed in A-K gap as shown in the figure, the diode had a voltage hump as had been observed in the experiment of plasma injection diode.

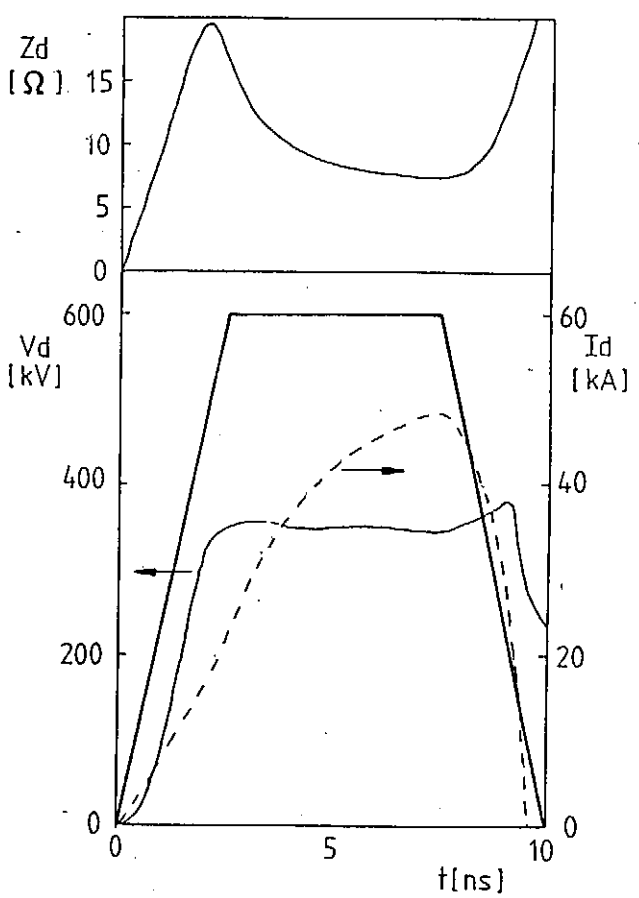

Fig.9 Typical Result for Space Charge Limited Condition

The effect of initial distribution of the injected plasma was investigated. When the injected plasma (same quantity with the calculation of Fig.10) linearly distributed in the A-K gap, the diode impedance increased with time.

From these results it is clear that the diode behavior is a function of both the quantity of the source plasma and the initial distribution of the plasma.

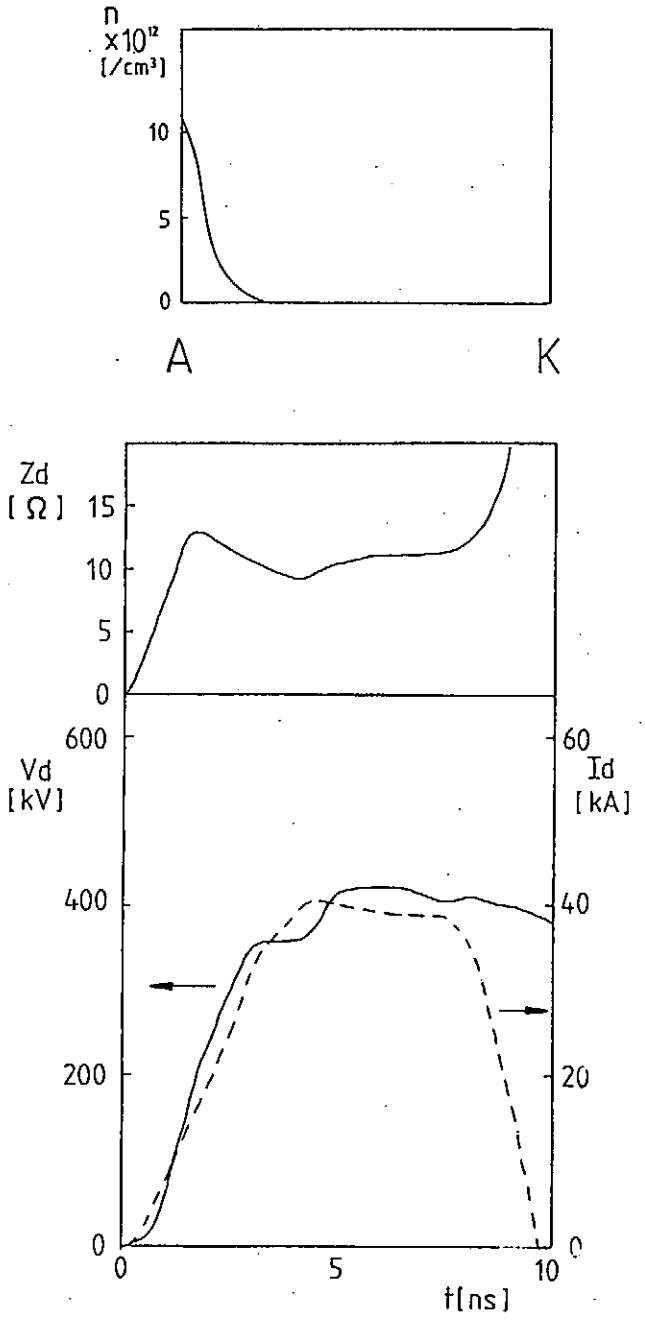

Fig.10 Typical Result for Flux Limited Condition

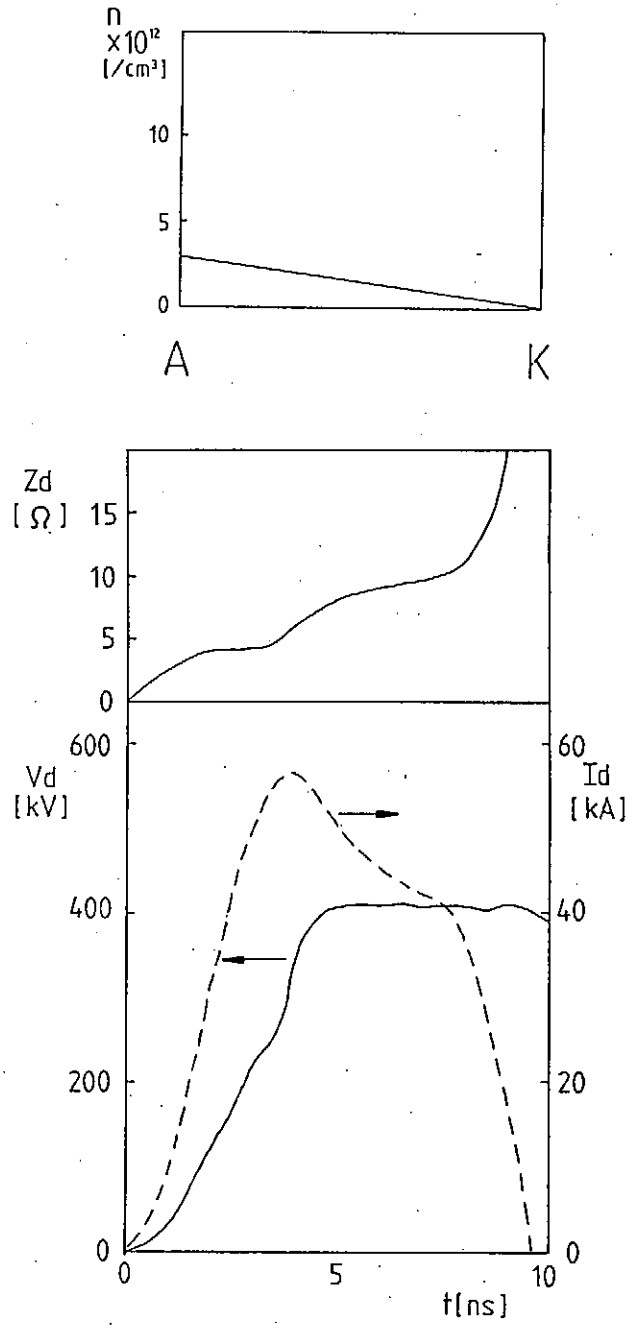

Fig.11 Typical Result for Flux Limited Condition with Linear Distribution of Injected Plasma

V. Conclusion

Generally, the plasma injection diode was successfully operated; high impedance was maintained through whole pulse at current level lower than the Child-Langmuir value. When the current was increased beyond the Child-Langmuir level, the rising impedance mode was appeared. It is shown that this configuration can improve impedance characteristrics of the diode.

The qualitative behavior of the diode operation could be explained well with a 1D-PIC simulaion. The diode behavior was determined both by the density of initial source plasma and distribution of the injected plasma in the gap.

To increase the operational range of the diode, a high flux capable of producing high current, uniform, neutral free and high purity including charge state purity plasma source must be developed. For the purpose, a new cryogenic flashboard which uses condensed materials as the plasma source, is under development now.

References

(1) D.L.Cook et. al., ; Proc. 7th Int. Conf. High Power Particle Beams, Ed. by W.Bauer & W Schmidt, 35 (1988)

(2) C.Litwin and Y.Maron ; Phys. Fluids, B1, 670 (1989)

(3) J.B.Greenly, M.Ueda, G.Rondeu and D.A.Hammer ; J. Appl. Phys., 63 (1988)

(4) S.Miyamoto, K.Imasaki, Y.Yasuda, K.Emura, N.Yugami, T.Akiba, H.Takabe and S.Nakai ; Proc. 7th Int. Conf. High Power Particle Beams, 47 (1988)

(5) K.Horioka, N.Tazima, Y.Saito and K.Kasuya ; Proc. Symp. Dev. Intense Pulsed Particle Beams & Its Applications, Res. Rep. NIFS, Ed. by K.Yatsui ; 21 (1990)

(6) T.Aoki and K.Niu ; ibid., 109 (1990)

Development of Intense Negative Ion Sources

K.Horioka, Yu.Quan and K.Kasuya

Department of Energy Sciences, The Graduate School at Nagatsuta, Tokyo Institute of Technology, Nagatsuta 4259, Midori-ku Yokohama, Japan 227

Abstract

The potentiality of surface flashover plasma is tested as an intense negative ion source of hydrogen. A coaxial magnetically insulated diode, whose cathode can be cooled by liquid nitrogen or liquid helium, is driven with a 5-Ohm/60nsec Blumlein line. Condensed materials on the cooled cathode are tested as the ion source and the experimental results confirm the source effect on the negative ion generation. The diode behavior under the operating condition of negative or positive voltage polarity is also discussed.

I. INTRODUCTION

A new concept is the highest priority for drivers of light ion beam (LIB) fusion. If the beam divergence is sufficiently small, high power beams of fast atoms obtained by stripping of negative ions probably eliminate many of present difficulties of the LIBs.

It was reported that magnetically insulated diode (MID) could produce multi-kiroampere range of H- beams.[1-4] A high H- concentration in the source plasma is essential for the high current operation. Generally, the source plasma has been produced by surface flashover of a hydrocarbon polymer (most popular dielectric material for making H- beams was Polyethelene). On the other hand, the surface flashover plasma produced from condensed material includes high density gas layers of molecular state.[5] It is considered that the presence of highly vibrationally excited H2 molecules in the plasma is

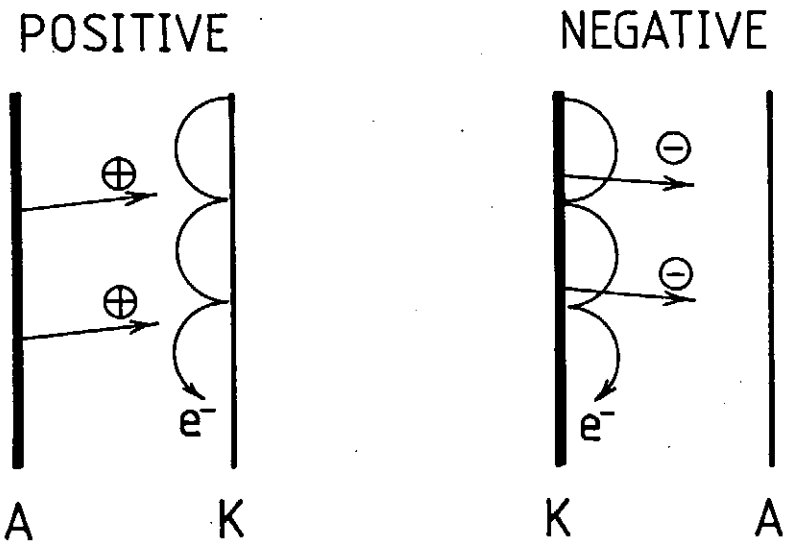

Fig.1 Schematic Diagram of Magnetically Insulated Diode with Positive or Negative Voltage Polarity

important for the production of the negative ions through the action of dissociative attachment process.[6] The high density gas layer of hydrogen molecules is expected to promote this process.

From this view point, intense beams of negative ions are produced from condensed dielectric materials on the cathode surface. The final aim of this work is to obtain intense H- or D- beams from solid H2 or D2 of condensed state. Advantages of using condensed hydrogen as the negative ion source are, firstly, we can expect emission of large number of hydrogen molecules during the surface flashover process, and secondary, we can increase H- abundance of the source plasma; there is no competitive negative ions such as C- or O-. The introduction of large density gradients in the cathode plasma is probably essential[7] for the efficient negative ion production and the dissociative attachment cross section is considered to be several orders of magnitude larger for hydrogen molecule which is in a high state of vibrational excitation.

The behavior of MID with negative polarity is also interesting from the point view of diode physics. A schematic diagram of MID with positive or negative voltage polarity is shown in Fig.1. Generally, the impedance of positive diode collapses with time, because of the bootstraping effect of ion enhancement and electron charge accumulation in the acceleration gap. On the contrary, in negative MID, the electron charge compete with that of negative ions, so it is expected that the

behavior of MID with negative poarity is quite different from that of positive polarity. Therefore, characteristics of the MID under the operating condition of negative or positive voltage polarity are also investigated.

II. EXPERIMENTAL SETUP

A magnetically insulated coaxial diode[3,4] was used for the experiments. A schematic diagram of the diode section is shown in Fig.2. The diode consisted of a center electrode made of a brass cylinder and an outer electrode made of a perforated stainless cylinder of 1mm thickness and 70mm inner diameter. The diameter of the center electrode is 40 or 58mm and it has grooves of 2mm width, separated 2mm and 2mm depth on the surface. The center electrode has a reservoir of coolant and transfer tubes of spiral shape to cool down the electrode with liquid N2 or He. In order to make thermal insulation, the diode is connected to a 5-Ohm/60nsec Blumlein line through prepulse switch. However the gap distance is kept very small not to degrade the prepulse effect[4] on the plasma formation.

Magnetic insulation of the diode gap is given by an axial field of 6.5kG or 5.2kG, which is created by a solenoidal coil with a pulse duration of 1.8ms. The same magnetic field is used for ion collector and the mass spectroscopy of the beams. The ion

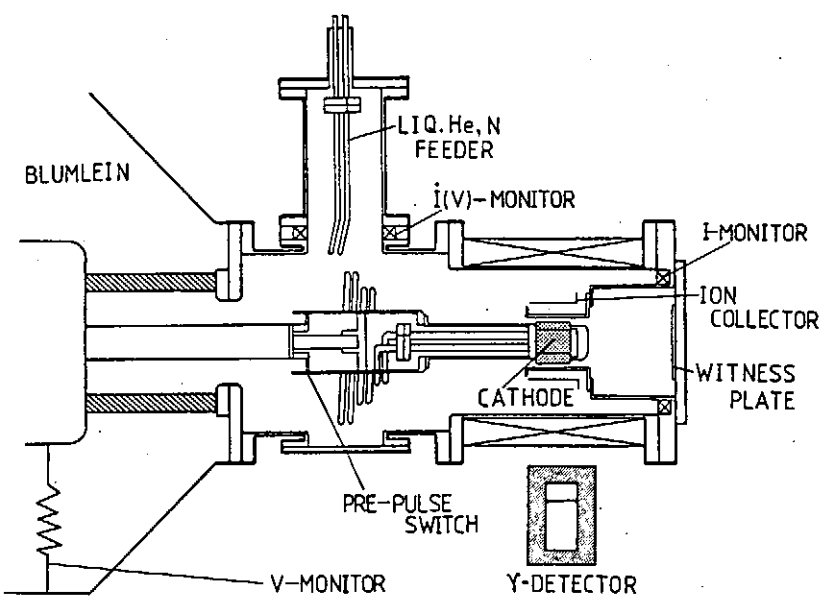

Fig.2 Schematic Diagram of Experimental Set-up

collector is made of a 0.1mm thick stainless cylinder of 100mm or 140mm diameter. The prepulse level of diode voltage is controlled by the value of charging inductance of the Blumlein. The diode volatge is measured with a $L\dot{I}$ voltage monitor placed at the spiral section and the diode current with a Rogowskii coil.

The cathode plasma was formed by surface flashover discharge of a dielectric material (Paraffin Wax or H2O ice) filled in the grooves of the electrode surface. Ion beams extracted from the coaxial diode were measured with the ion collector of coaxial shape.

III. EXPERIMENTAL RESULTS

III-1 Diode Electrical Characteristics

Typical waveforms of the Blumline output voltage are shown in Fig.3, for positive and negative polarity. The intermediate electrode of the Blumlein, which was connected to the ground outer electrode by 0.6μH inductor, was charged through 4.4μH charging inductor. As shown, typical prepulse of the system had about 100kV level of negative and positive parts with 300ns duration. The diode characteristics was tested as functions of the voltage polarity, anode-cathode geometrical gap d, and ion source materials.

At first, the diode electrical characteristics was investigated. Typical waveforms of the diode voltage VD, diode current ID and ion current Ii are shown in Fig.4, for bare (Brass) electrode of positive or negative polarity. As is clear from this figure, the diode gap impedance was maintained at very high value especially for positive polarity. When negative voltage pulse was applied on the gap, positive ion signal of 30A/cm^2 level was detected,

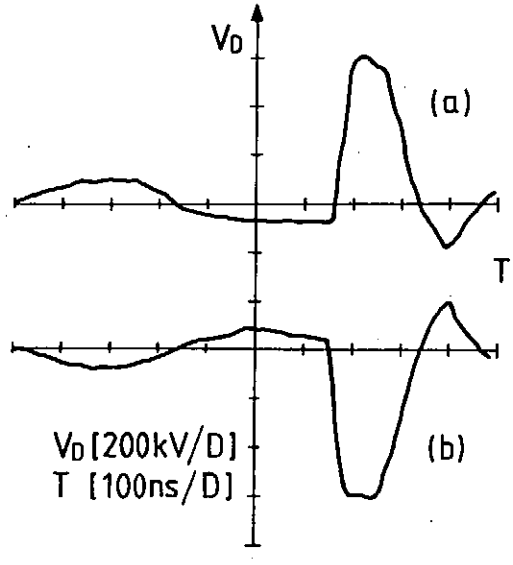

Fig.3 Typical Diode Voltage (d=6mm, B=6.5kG)

which was probably produced from metal contained center electrode plasma by the positive part of the pulse. For negative polarity, a small leakage electron current along the magnetic field, ie; through the surface of the center electrode, was detected on the back plate of the chamber, which was confirmed by the damage pattern of witness sheet (Nitto Radcolar film). From these results, it was supposed that the voltage pulse of negative polarity was much more effective than that of positive polarity for the source plasma formation.

III-2 Ion Beam Generation

The waveforms for wax filled electrode are shown in Fig.5, for positive(a) or negative(b) polarity. As shown here, the diode produced near 60A/cm^2 ion current density for positive voltage pulse, which is almost the Child-Langmuir value for H+ beams of (600keV, d=6mm). When the voltage polarity was reversed, ion current signal was never detected in the primary voltage pulse. In operating condition of wax ion source, the ion signal was detected only in the second positive voltage pulse. Fig.6 shows

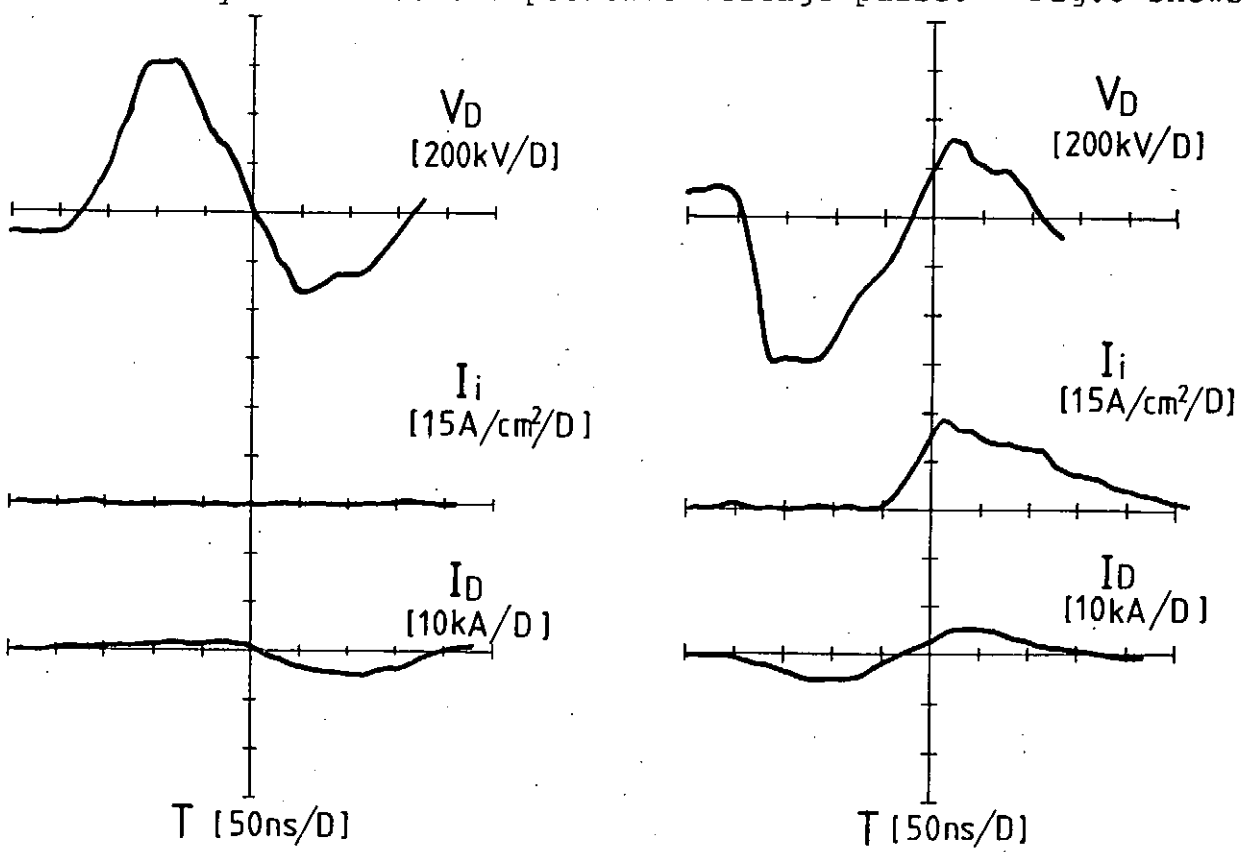

Fig.4 Waveforms of Diode Voltage VD, Current ID and Ion Current Ii (Bare (Brass) electrode, d=6mm, B=6.5kG)

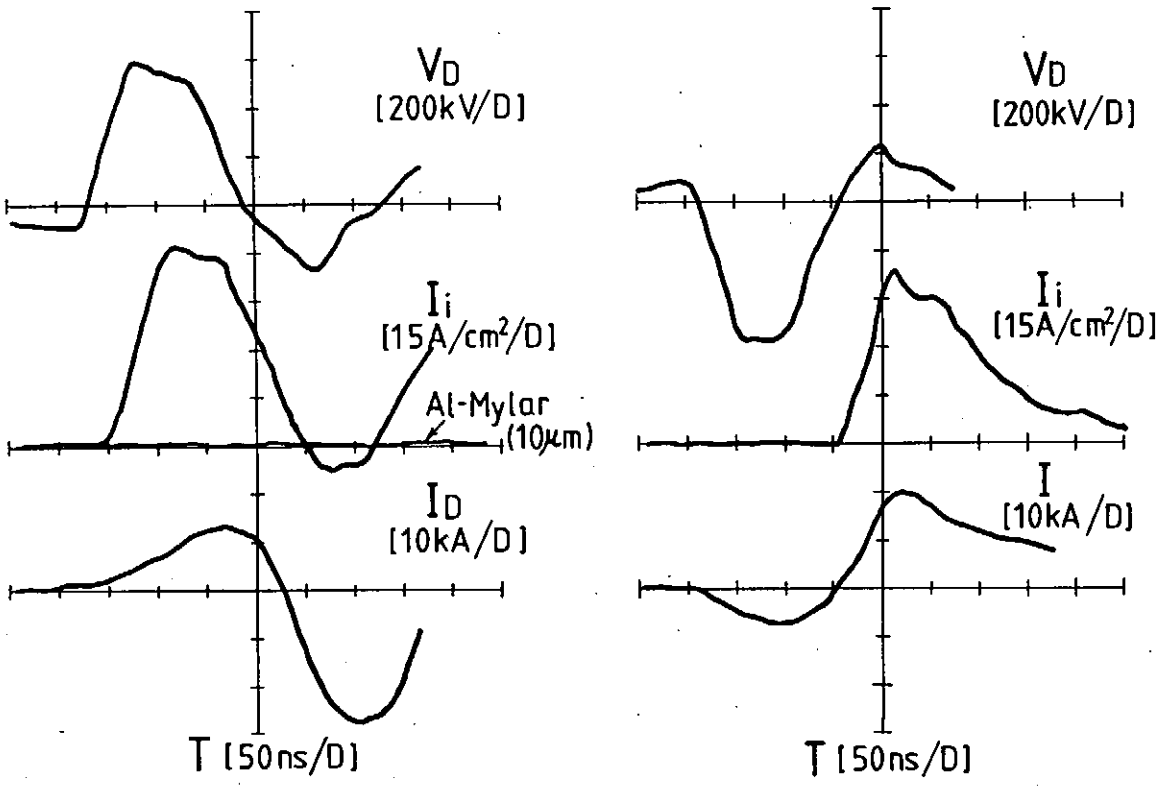

Fig.5 Waveforms of Diode Voltage, Current and Ion Current (Positive or Negative Polarity, For Wax Ion Source, d=6mm, B=6.5kG)

damage patterns of the Al-coated mylar sheet placed 10mm or 20mm from the surface of the center electrode. As has been reported in ref.(10), the extracted beam had large divergence, which made the precise mass spectroscopy impossible.

Next, the source material was converted to H2O ice under the liquid N2 cooling of the center electrode. Typical waveforms of diode voltage VD and ion current signal Ii are shown in Fig.7. The diode was operated at the same condition of the results shown in Fig.5, except source dielectric material. As shown with this figure, signals of negative ions of a few A/cm^2 level were detected with this operationg condition. The negative ion signal was confirmed by a filtered ion

(a)
10mm

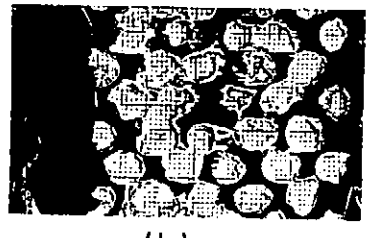

(b)
20mm

Fig.6 Beam Damage Pattern on Witness Sheeet (Al-Mylar)

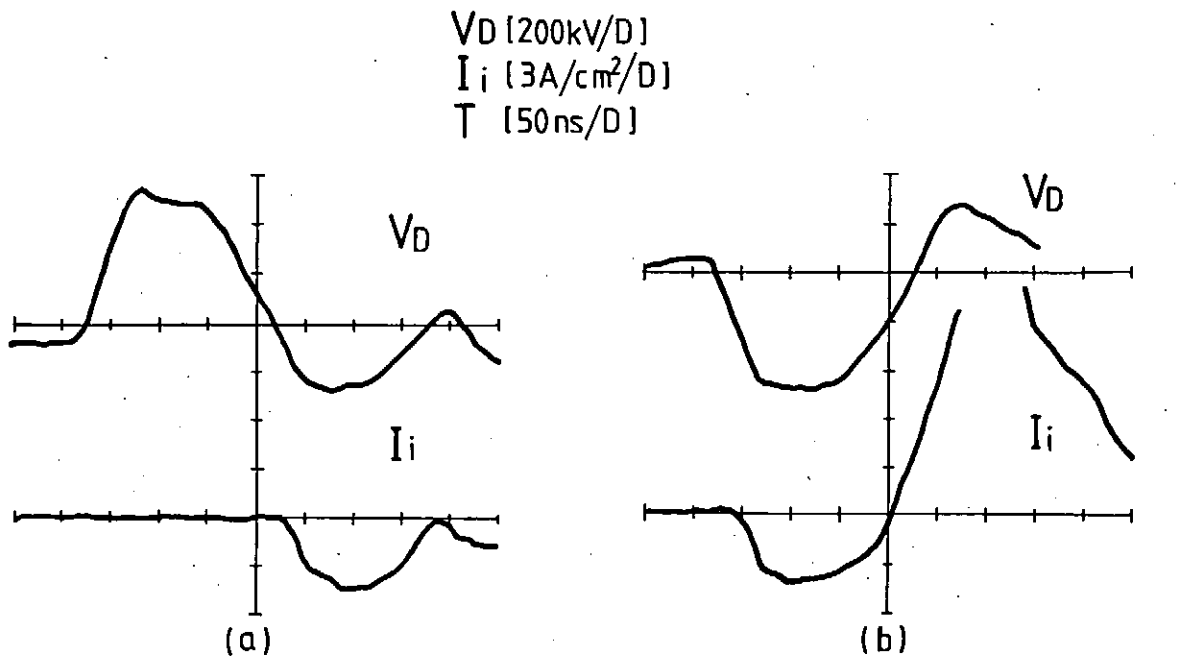

Fig.7 Waveforms of Diode Voltage VD, Current ID and Ion Current Ii (Negative Polarity, For H2O Ion Source, d=6mm, B=6.5kG)

collector. Although the reproducibility of the results was not good, as shown in Fig.7, a peculier characteristics was found in the ion current signal produced from condensed H2O ice. Probably, dense layer of neutrals produced by the evaporation of condensed H2O contributes the formation of H- ions in the source plasma.

When the insulation field was weakened from 6.5kG down to 5.2kG, although the reproducibility was poor, negative signal increased near to 15A/cm^2 (about 2kA total current). Typical waveforms of ion current are shown in Fig.8, with those of diode current.

IV. SUMMARY

A coaxial magnetically insulated diode was operated to test condensed dielectric materials as the ion source of negative hydrogen. When we used condensed material as the source, signals of negative ion of 3-4 A/cm^2 was assured. The negative ion signal could be attributed to the source effect. When we decreased insulation magnetic field down to 5.2kG, we could

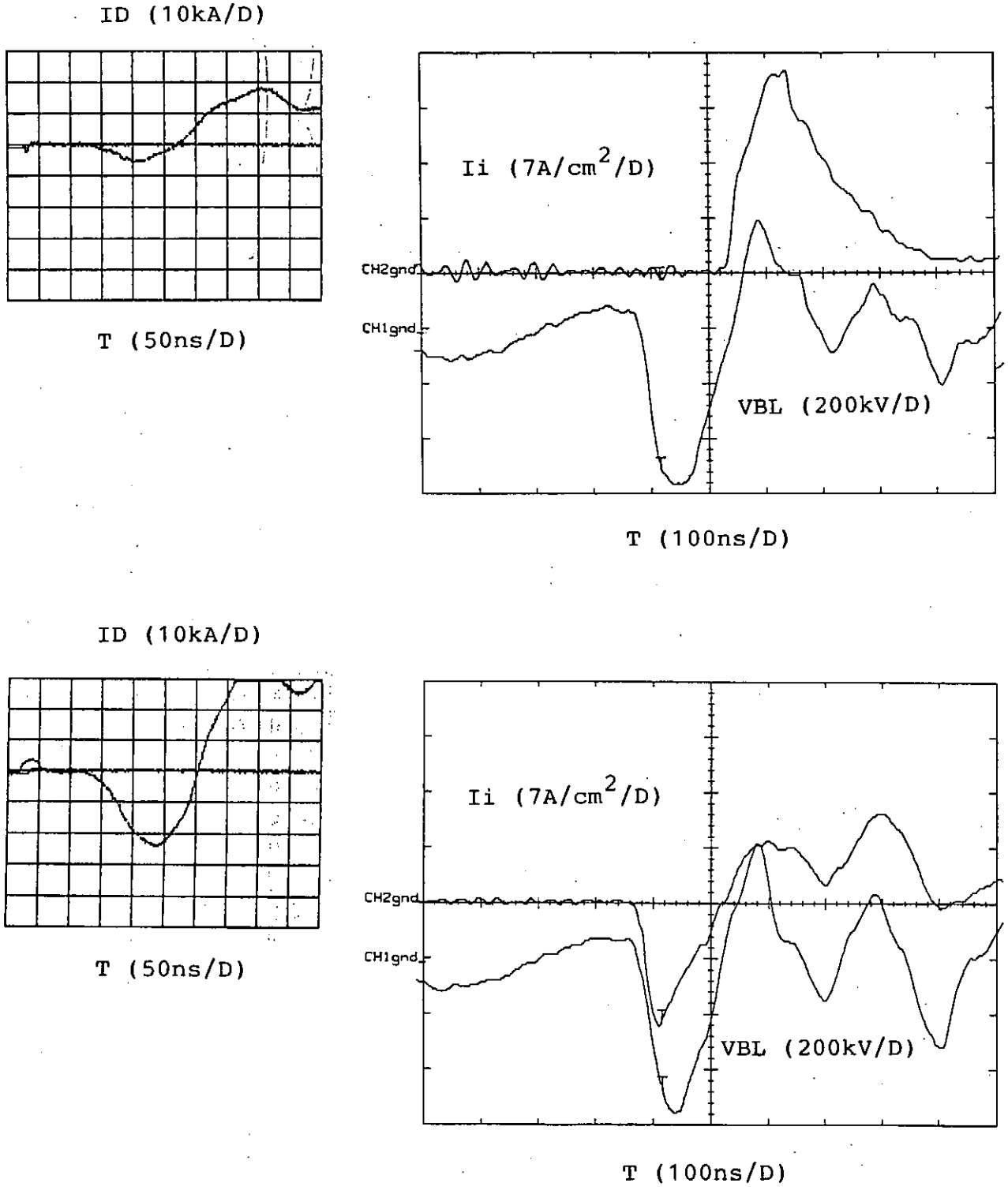

Fig.8 Waveforms of Ion Current Density Ii and Diode Current ID (d=6mm, B=5.2kG)

observe near 15A/cm^2 negative current. However reproducibility of the results was not good. As can be seen, the negative ion signal apparently is a function of the diode current. If we use solid hydrogen as the source material, H- density of the source plasma will be increased and we probably can expect more current of hydrogen, because of the above mentioned effect.

The surface current flowing through the cathode surface, ie; conditions close to the experiments in magnetically insulated vacuum transmission lines[8,9], are provably necessary as pointed out in ref.(4,11,12). In view of this problem, systematic investigations on the cathode plasma formation process are in progress now including the study of the effect of source mayterials, cathode surface current and also the operation under the liquid He cooling.

The authors would like to express our thanks to Mr.N.Matsuura for invaluable assistance of the experiment. This work was partly supported by Grant-in-Aid for Scientific Research from the Ministry of Education, Science and Culture in Japan.

REFERENCES

(1) A.A.Kolmensky, A.N.Lebedev, V.A.Papadichev, S.A.Pikuz, B.N.Yablov ; Proc. Int. Conf. High Power Particle Beams, Sanfrancisco, p.533-539 (1983)

(2) A.Fisher, H.Lindenbaum, and N.Rostoker ; Proc. Int. Conf. High Power Particle Beams, Kobe p.116-118 (1986)

(3) V.M.Bistritsky, S.N.Volkov, Ya.E. Krasik, V.M.Mativienko, and V.G.Tolmacheva ; Proc Int. Conf. High Power Particle Beams, Kobe, P.113-115 (1986)

(4) V.A.Papadichev, S.A.Pikuz and T.A.Shelkovenko ; Proc. 7th Int. Conf. High Power Particle Beams, Karlsruhe NP9 p.715-720 (1988)

(5) K.Horioka, H.Yoneda and K.Kasuya ; IEEE Trans. Plasma Sci., PS-17, p.793-797 (1989)

(6) M.Bacal ; Physica Scripta, T2/2, p.467-478 (1982)

(7) R.Prohaska, H.Lindenbaum, A.Fisher, G.Sheperd and N.Rostoker; Proc. APS Meeting (Anahaim) (1989)

(8) J.P.VanDevender, R.W.Stinnet and R.J.Anderson ; Appl. Phys. Lett., 38, No.4 p.229 (1981)
(9) R.W.Stinnet, M.A.Palmer, R.B.Spielman and R.Bengtson ; IEEE Trans. Plasma Sci., PS-11, No.3 p.216-219 (1983)
(10)H.Lindenbaum, A.Fisher and N.Rostoker ; Proc. 7th Int. Conf. High Power Particle Beams, Karlsluhe NP3 p.677-682 (1988)
(11)V.A.Papadichev, S.A.Pikuz and T.A.Shelkovenko ; Rev. Sci. Instr., 61 No.1 p.439-441 (1990)
(12)V.A.Papadichev, private communication

Production of Pulsed Beams of Negative Light-Heavy Ions

S. Shibata, A. Kitamura, Y. Furuyama and T. Nakajima

Department of Nuclear Engineering,
Kobe University of Mercantile Marine,
Fukaeminami-machi 5-1-1, Higashinada-ku, Kobe 658, Japan

Abstract

Preliminary results of experiments on production of pulsed F^- beamsare reported. Using an MID with a mesh-covered CF_2 cathode, a tace of F^- beam is observed only in the third phase of a diode voltage pulse train. To produce F^- ions before the diode voltage is applied, we examine use of auxiliary power sources to initiate the discharge on the cathode. Optical measurements are performed to find optimum conditions for preformation of F^- ions in the surface flashover plasma and an alternative arc discharge plasma.

1. Introduction

Beams of negative ions attract increasing attention in science and technology. In the field of controlled fusion research, intense neutral beam injector for heating, fuelling and sustaining magnetically confined plasmas require intense negative ion beams of hydrogen isotopes because of higher efficiency of conversion to the neutrals than positive ion beams. The goal is to obtain 100A beams of 1MeV D^- continuously. In connection with inertial confinement fusion (ICF) research, production of H^- beams have been investigated in several laboratories [1-3]. Most of them aim principally at their application to ICF drivers after stripping them to neutral H. They intend to take advantage of the insensitivity to the electric and magnetic field, which, if the driver beam were of light ions, could arise in the beam as a result of insufficient neutrality of the beam and/or instabilities in the beam plasma, and deteriorate transmission and focusing properties seriously. Successful extraction of H^- beams with current

density reaching 200A/cm^2 have been reported in ref. [1], where a magnetically insulated diode (MID) was driven by a pulsed power source having suitablly shaped prepulses.

On the other hand, beams of heavy ions have also been considered alternative candidates for the ICF driver [4,5]. The above problems of transmission and focusing are expected to be less severe for heavier ions, since the beam current necessary for compression of targets could be reduced by orders of magnitude in reward for increased particle energy, and since the larger inertia makes heavy ions less sensitive to electric and magnetic fields.

In our laboratory efforts have been directed toward development of pulsed beams of light-heavy ions for possible applications including those to the ICF driver and to material processing. The latter is one of the most promissing application of pulsed ion beams and attracts increasing interest [6-10]. Following successfull production of Na^+ beams [11], we try to produce pulsed beams of negative fluorine ions. In this paper preliminary results of the experiments are reported.

2. Operation of MID with negative polarity

A schematic of the experimental arrangement is shown in Fig.1. The cathode of the race-track-type MID was driven negatively by a 5kJ pulsed power machine ERIDATRON-II to extract negative ions through the slits of width 8mm with an interval of 14mm on the anode. The magnetic field of 4.8kG was applied parallel to the cathode surface to prevent extraction of electrons from the diode. This is 1.4 times as large as the critical field for insulation at the maximum diode voltage of 550kV applied to a 9.5mm diode gap. The downward motion of electrons due to ExB drift is expected to augment the surface flashover on the cathode. The cathode was made of 5mm-thick Teflon (CF_2) sheet either with copper pins distributed with a 2mm spacing to stimulate the flashover or covered with a copper mesh (61% transparency with 0.35mm diam. wires) in expectation of enhancing the negative ion formation.

The current of the extracted beam was measured with a magnetically insulated collector (MIC), which has a pair of permanent magnets producing 4kG as the electron repeller. The mass of ions of the extracted beam was analyzed with a Thomson parabola spectrometer (TPS).

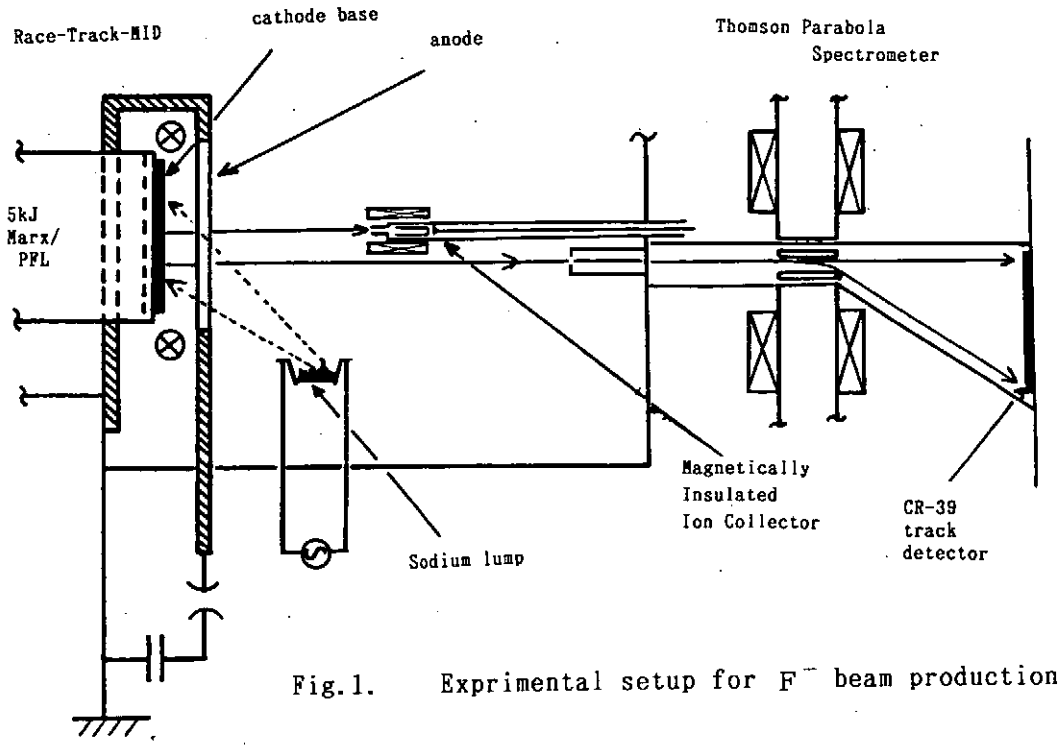

Fig.1. Exprimental setup for F^- beam production.

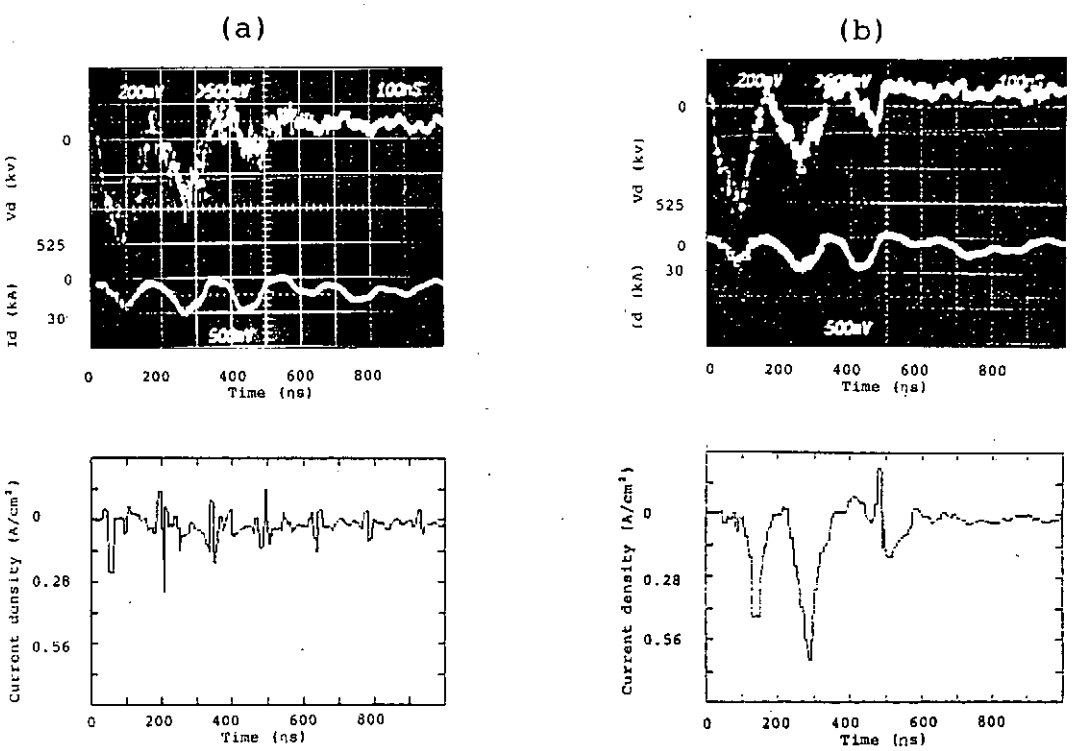

Fig.2. Typical waveforms of the diode voltage V_d, the diode current I_d and current j_i into the MIC located at 50mm from the cathode :
(a)cathode with copper pins ;
(b)mesh-covered cathode.

Typical waveforms of the diode voltage V_d, the diode current I_d and the curent j_i into the MIC located at 50mm from the cathode are shown in Fig.2-(a) and (b) for the cathode with pins and the mesh-covered cathode, respectively. Due to the high impedance of the diode, pulse trains with three prominent peaks are observed in V_d and j_i. Although a trivial trace is observed in the MIC signal in the case (a), three peaks are clearly observed corresponding to the three phases of the diode voltage in the case of the mesh-covered CF_2 (b). The third peak in the MIC signal corresponding to the third phase of the voltage pulse has a delay of about 50ns. To examine more precisely, a time-of-flight plot of the voltage waveform is compared with the measured waveform of j_i, which is shown in Fig.3. Here in the upper, the current which might be recorded when the beam of H or F was extracted from the diode under the space-charge-limited condition is expressed as the thinner line or the thicker line, respectively. A fair agreement of the appearance of the third peak with that of the calculated one

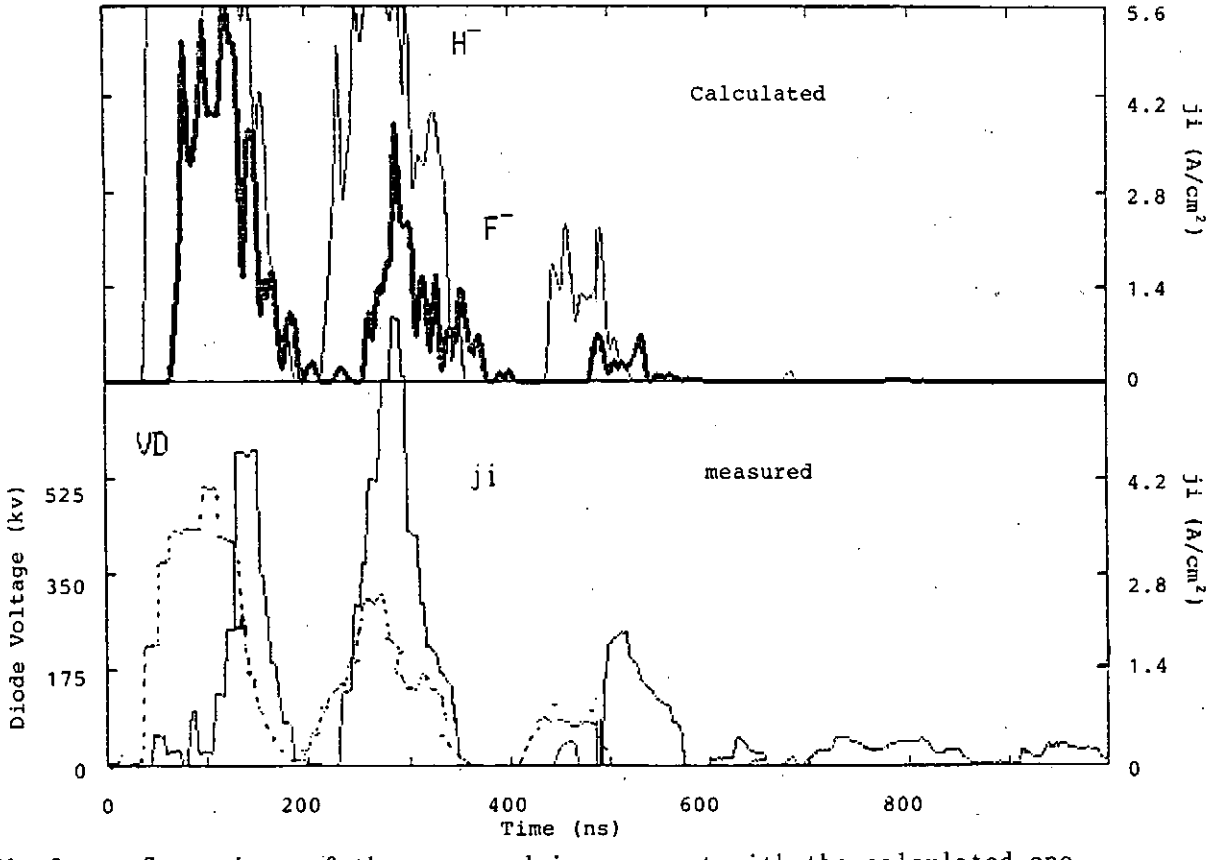

Fig.3. Comparison of the measured ion current with the calculated one. The dotted line shows the diode voltage.

suggest that the F^- ions are extracted during the third phase of the diode operation. The time spent during the first and the second phase is considered to be necessary for storing negative ions in the cathode plasma; the first and the second phase of the voltage pulse train act as the prepulse, which has been proved indispensable for H^- beam production [1]. Unfortunately, it was not possible to confirm the ion species with use of the TPS, since the beam energy of less than 100keV was too low to be recorded on the CR-39 track detector.

To find more suitable condition for production of negative ions, several modifications of the cathode configuration were examined: covering the CF_2 cathode surface with a vapor-deposited sodium film, spraying CF_2 powder onto a polyethylene cathode disk and coating polyethylene surface with KF. However, no observable effect was found.

3. Preliminary operation of MID with an auxiliary power source for flashover

It has been found necessary to produce and store negative ions in the cathode plasma before the high voltage pulse is applied. The next step we tried is to apply another voltage pulse to initiate the surface flashover prior to the main pulse. A pair of electrode strips for the surface flashover was attached on the cathode surface. A 10kV pulse with a ringing frequency of 40kHz from a capacitor bank of 4.8μF was transmitted to the electrodes through a coaxial cable, which is wound to form an inductance of 5μH and exihit 90ohms against the high voltage main pulse.

Typical waveforms when operated without and with the auxiliary pulse are shown in Fig.4-(a) and (b), respectively. In the latter case, where the diode voltage was applied with a delay of 2μs after triggering the auxiliary source, the second phase of the voltage pulse has disappeared. This indicates a decreased impedance of the diode as a result of faster production of the cathode plasma. Although a trace of neutrals was found on the CR-39 detector in the TPS, no indication of the negative ion beam was obtained in the MIC signal. It seems necessary to examine the process of negative ion formation in the flashover plasma, and find more suitable discharge condition.

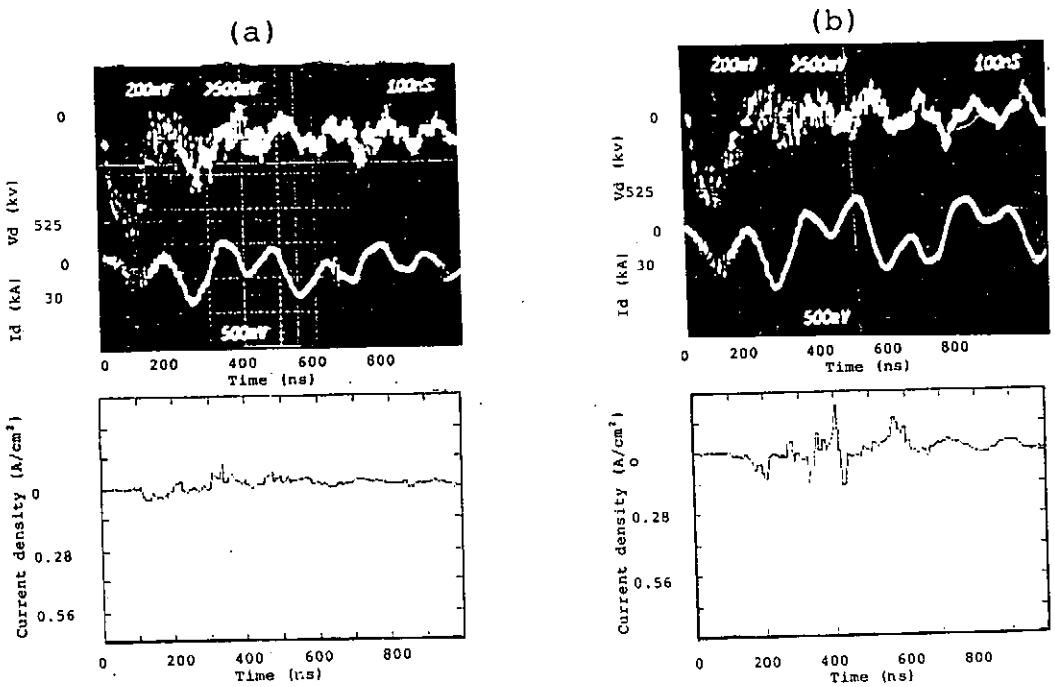

Fig.4. Typical waveforms of the diode voltage V_d, the diode current I_d and current j_i into the MIC (a) without the auxiliary pulse; (b) with the auxiliary pulse.

4. Investigation of evolution of F atoms in pulsed discharges

Optical method is suitable for diagnosing such a localized plasma with large gradient of density and temperature as the flashover discharge. Since negative ions of F are expected to be formed through recombination reactions, $F+e \rightarrow F^- + h\nu$, and/or $F+2e \rightarrow F^- + e$, we try to follow the behavior of F atoms to examine the process of F^- ion formation.

A schematic of the arrangement for the optical diagnastics of the pulsed discharge is shown in Fig.5. A capacitor bank of variable capacity C from 0.02μF to 112μF is used to produce 0.5-2 kA through the discharge between a pair of copper electrode strips embedded with a spacing of 10mm on the surface of a CF_2 disk. The emitted photons are focused by a lens onto the entrance slit of a 400mm grating monochrometer followed either by a camera or by a photomultiplier (PM).

Among several FI lines we could distinguish only two or three lines from background continuum with a marginal S/N ratio of 3. These include those of 623.96nm and 634.85nm. The time-dependent intensity

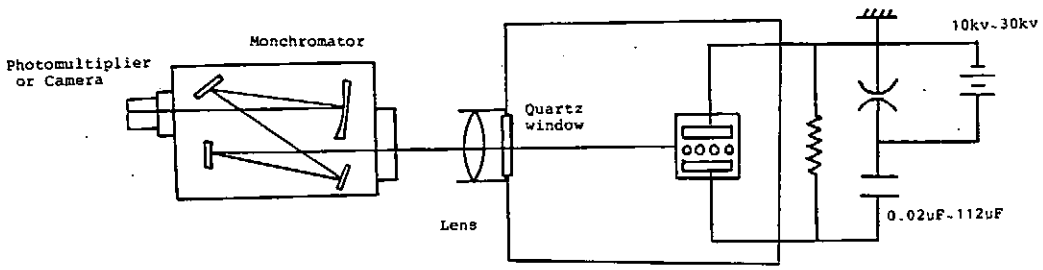

Fig. 5. Schematic of the arrangement for the optical diagnostics of the flashover.

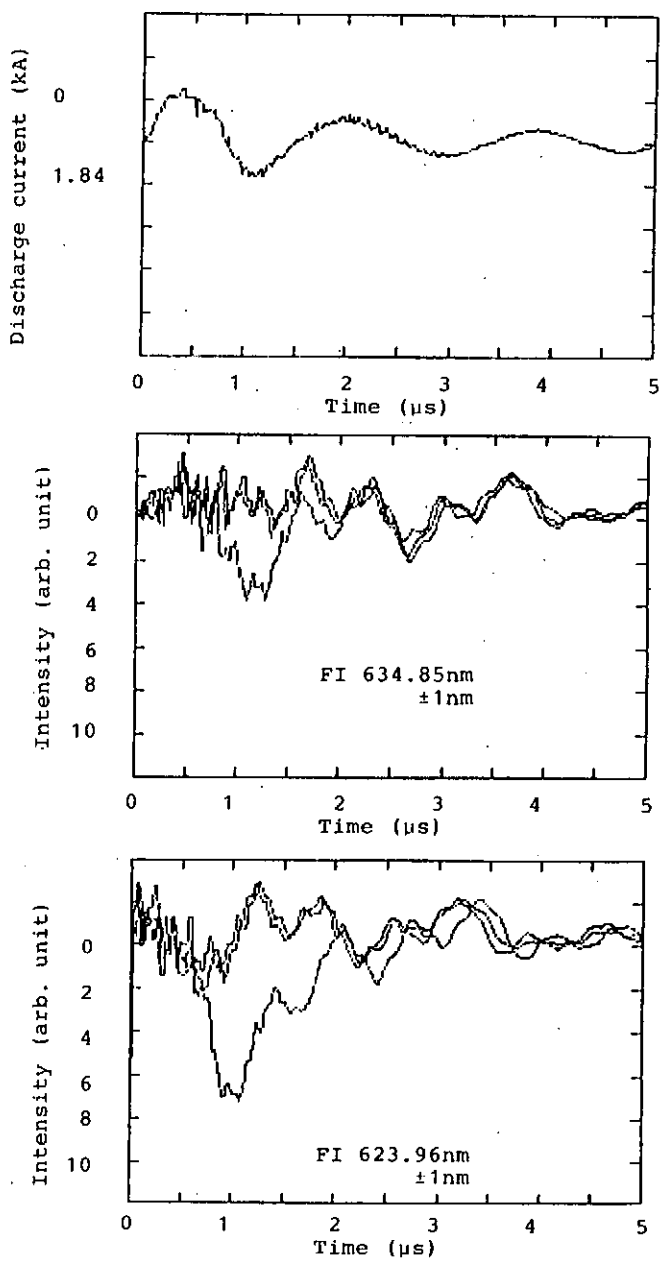

Fig. 6. Typical waveforms of the flashover discharge current and the time-dependent intensity of FI lins and the background signal recorded by the PM.

of these lines recorded by the PM are shown in Fig.6 for the case of C=0.57μF. We see in the figure that F atoms exist only in the early phase of the pulse. Dependence of the peak intensity of these lines on the discharge energy which was varied by changing the applied voltage are plotted in Fig.7 to show that there is an optimum discharge energy for the existence of atomic F.

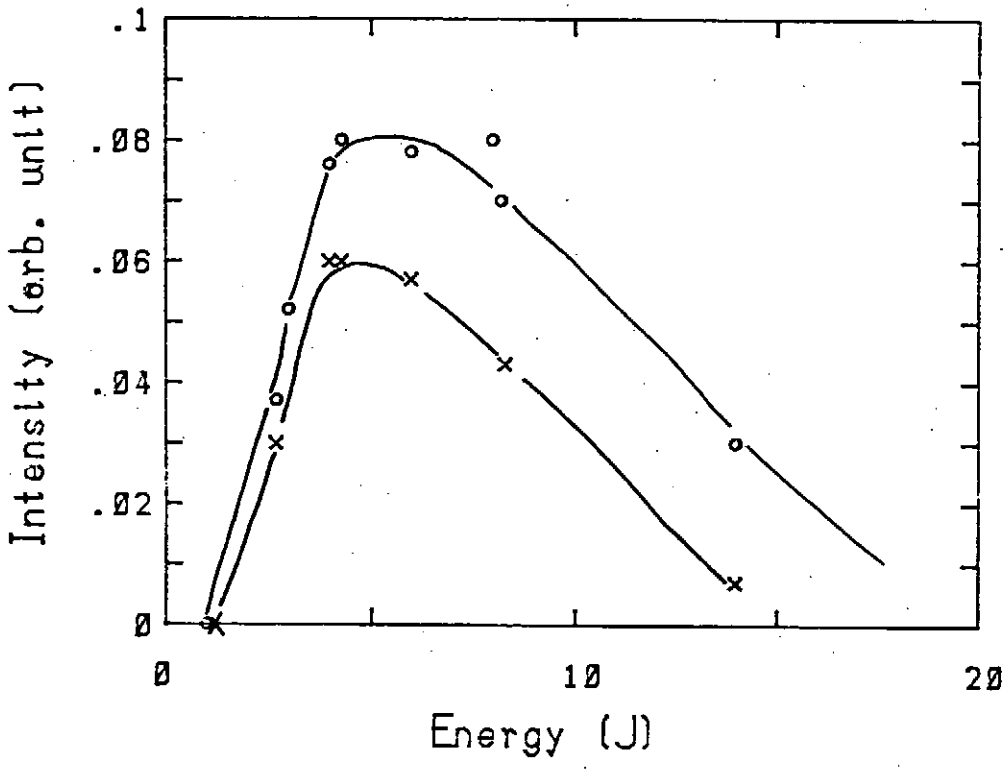

Fig.7. Dependence of the peak intensity of FI lines on the discharge enegy: (○) 623.96nm; (×) 634.85nm.

As an alternative for the F^- source an arc discharge is now under analysis with the same optical method. The discharge is driven between a pair of copper rods spaced by 8mm in a SF_6 gas of 70-400Pa. To show that the arc discharge seems to be more promissing for F^- production, only a preliminary result with C=112μF charged to 2.5kV is shown in Fig.8. We see in the figure that the S/N ratio is much better than in the case of the flashover discharge.

For both of the discharges, however, extended measurements on the spatial distribution of F atoms as well as detailed analysis of the time dependence are required to clarify the F^- formation process and to the optimum discharge condition for F^- extraction.

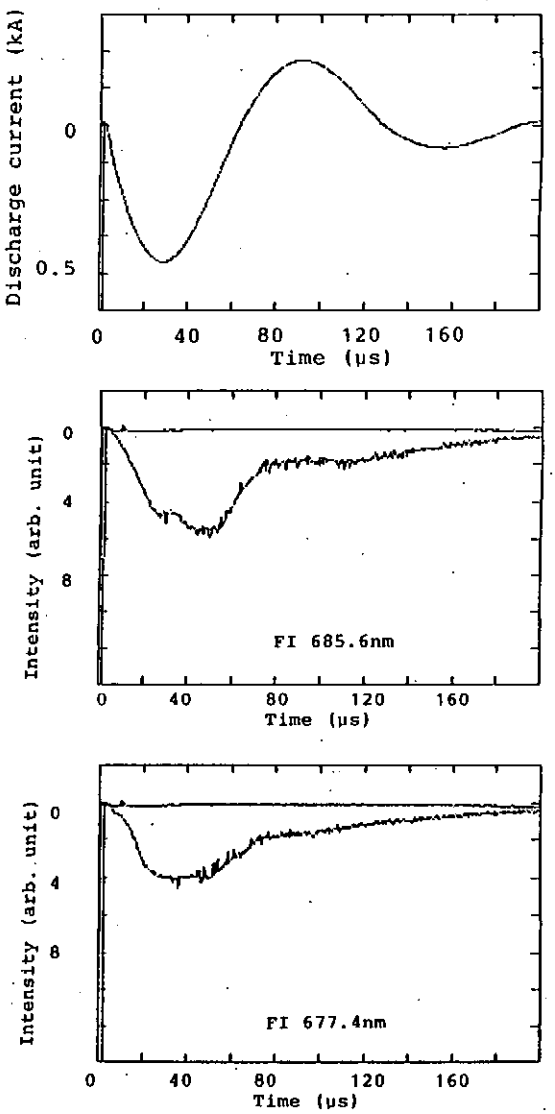

Fig.8. Typical waveforms of the arc dischage current and the time-depndent intensity of FI lins and the background signal recorded by the PM.

5. Concluding remarks

Extraction of F^- beams from a mesh-covered CF_2 cathode of an MID has been suggested by ion collector measurements. Since the emission was during the third phase of a main pulse train, the first and the second phase acting as a prepulse to form F^- ions, the energy of F^- ions was less than 100keV.

To produce F^- ions before the main pulse is applied, we examined the use of auxiliary power sources to initiate the discharge. Optical measurements of the discharges have suggested that an arc discharge is a promissing alternative to a conventional surface flashover for the preformation of F^-.

Thanks are due to K. Takahashi and Y. Minejima for their help in the measurements.

references

[1] V.A. Papadichev; Proc. 7th Int. Conf. High Power Particle Beams, Karlsruhe, F.R.G. (1988) 479, and references therein.

[2] H. Lidenbaum, A. Fisher, N. Rostoker; ibid. 677.

[3] K. Horioka and K. Kasuya; Proc. 8th Int. Conf. High Power Particle Beams, Novosibirsk, USSR, 1990 (to be published).

[4] S. Humphries, Jr., R.J.M. Anderson, J.R. Freeman, T.R. Lockner, J.W. Poukey and J.J. Ramirez; Nucl. Instrum. Meth. **187**(1981)289.

[5] I. Hofmann; Proc. 8th Int. Conf. High Power Particle Beams, Novosibirsk, USSR, 1990 (to be published).

[6] K. Yatsui; Proc. 7th Int. Conf. High Power Particle Beams, Karlsruhe, F.R.G. (1988)283: Laser & Paticle Beams **7**(1989)733.

[7] A.D. Pogrebnjak, G.E. Remnev and I.G. Romanov; Nucl. Instrum. Meth. **B43**(1989)41.

[8] O.I. Goncharov, I.F. Isakov, V.N. Kolodii, V.M. Matvienko, M.S. Opekunov, G.E. Remnev, Yu.P. Usov and A.N. Zakutayev; Proc. 8th Int. Conf. High Power Particle Beams, Novosibirsk, USSR, 1990 (to be published).

[9] Y. Nakagawa, T. Ariyoshi, M. Itami and Y. Fujii; Jpn. J. Appl. Phys. **27**(1988)L719.

[10] A. Kitamura, Y. Furuyama, S. Kamihata and T. Nakajima; Proc. 8th Int. Conf. High Power Particle Beams, Novosibirsk, USSR, 1990 (to be published).

[11] A. Kitamura, K. Mitsuhashi and S. Yano; Laser & rticle Beams **5**(1987)683.

PULSED POWER GENERATOR BY AN INDUCTIVE ENERGY STORAGE SYSTEM

Naoyuki SHIMOMURA,
Department of Electrical and Electronic Engineering,
Faculty of Engineering, Tokushima University
Tokushima 770
Masayoshi NAGATA,
Department of Electrical and Electronic Engineering,
Technical College, Tokushima University
Tokushima 770
Tsuyoshi FUKUZAWA, Hidenori AKIYAMA, and Sadao MAEDA
Department of Electrical Engineering and Computer Science,
Faculty of Engineering, Kumamoto University
Kumamoto 860

Abstract

A pulsed power generator using an inductive energy storage system has been constructed. The pulsed power generator, named ASO-I, is extremely compact and light in comparison with a conventional pulsed power generator which consists of a Marx bank and a water pulse forming line. The ASO-I has a two-staged opening switch, consisting of fuses in water and a plasma erosion opening switch, and can be operated hundreds of times a day at the output power of 300kV and 40kA. The plasma erosion opening switch is successfully operated as a second opening switch, and the rise time of the current through the short-circuit load decreases from 250nsec to about 10nsec.

§1 Introduction

Pulsed power technology is useful in a wide variety of

fields. Conventional pulsed power generators, which consist of a Marx bank and a water pulse forming line, are huge machines. Pulsed power generators with an inductive energy storage system can be extremely compact and light, and have been investigated. Opening switches[1)2)] to interrupt high currents rapidly are necessary to realize pulsed power generators using an the inductive energy storage system. A long conduction time and short opening time are achieved by using two-staged opening switches consisting of both fuses[3)-7)] and PEOS[7)-9)]. The pulsed power generator named PAWN[4)7)9)] at NRL is a pulsed power generator with a two-staged opening switch. The PAWN, which generates comparatively large output power, is operated only few times a day. The pulsed power generator named ASO-I[10)11)], which has been developed at Kumamoto University, generates comparatively small output power. However, the ASO-I is able to be operated hundreds of times a day.

In this paper, the characteristics of the pulsed power generator, ASO-I, which uses an inductive energy storage system with a two-staged opening switch are described.

§2 Pulsed Power Generator ASO-I

Figure 1 shows the schematic configuration and equivalent circuit of the pulsed power generator ASO-I. The ASO-I consists of capacitors as a primary energy source having 3.5μF, a main gap switch of field distortion type, an energy storage inductor, fuses in water, a spark gap, the PEOS, and the load. Two kinds of energy storage inductors, one of the coaxial configuration having 0.5μH and the coil with 4.0μH, are used. The fuses which are used as the first stage of the opening switch are thin copper wires in water. Several wires with

lengths between 4 and 26cm are set in the water. The PEOS, which has four plasma guns[1,2], is the second stage of the opening switch. Each plasma gun is driven by a 0.4μF capacitor that is charged to 25kV. The spark gap located between the fuses and the PEOS is used for pulse sharpening and prepulse suppression.

§3 Characteristics of ASO-I using Fuses as the Opening Switch

The characteristics of the ASO-I are described in the case using fuses as an opening switch. The PEOS is not used in these experiment.

A. Open-circuit Load

The open-circuit load was connected to the ASO-I. Figure 2 shows the typical waveforms of the voltage across wires, V_w, the current through the energy storage inductor, I_s, and the resistance of wires, R_w. The number, diameter, and length

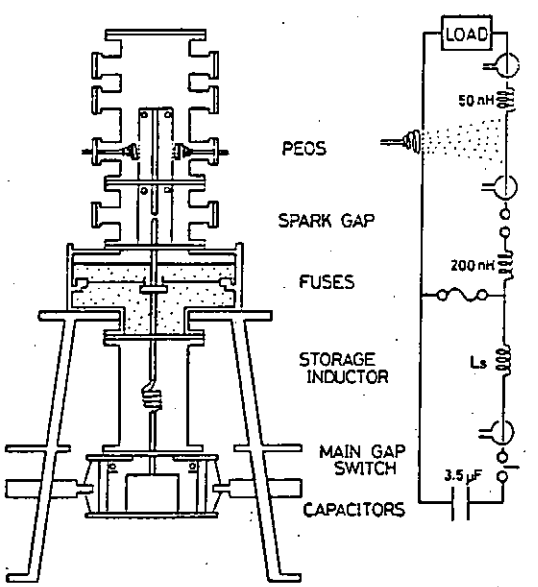

Fig.1 Pulsed power generator ASO-I.

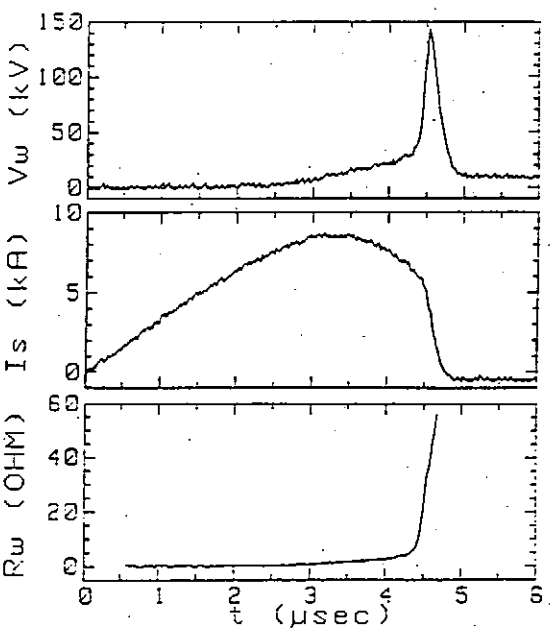

Fig.2 Typical waveforms of V_w, I_s, and R_w.

of wires are four, 0.1mm, and 17cm, respectively. The inductance of the energy storage inductor, L_S, is 4μH. The wires are vaporized by joule heating, and then a peak voltage, V_{WP}, of about 150kV was obtained across wires. The voltage multiplication factor ,which is the ratio of V_{WP} on the charging voltage of the capacitors, is about ten. Figure 3 shows the relation between V_{WP} and the length of the wires, l.

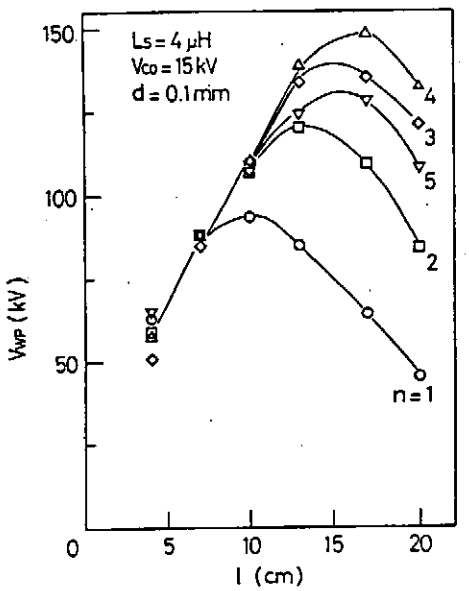

Fig.3 Relation between V_{WP} and l.

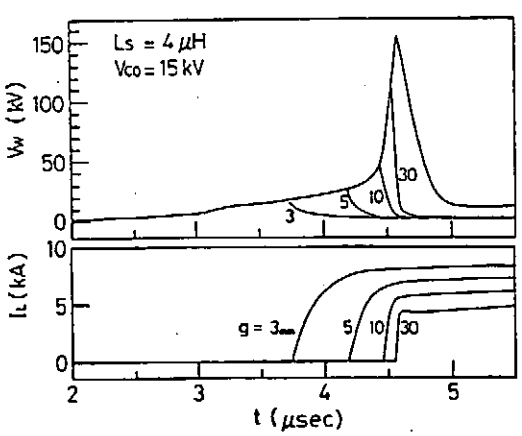

Fig.4 Waveforms of V_w and I_L.

The charging voltage of capacitors, V_{CO}, was 15kV. The diameter of the wires, d, was 0.1mm. The number of the wires, n, was changed from 1 to 5. The output voltage linearly increased with the length of the wires in the case of comparatively short length of wires. The output voltage for short wires was limited by the breakdown of vaporized copper wires and the breakdown voltage is in direct proportion to the length of the wires. The dielectric strength of the copper vapor is about 12kV/cm, and does not change with the number of wires.

B. Short-circuit Load

The short-circuit load was connected to ASO-I. The spark gap is located between the fuses

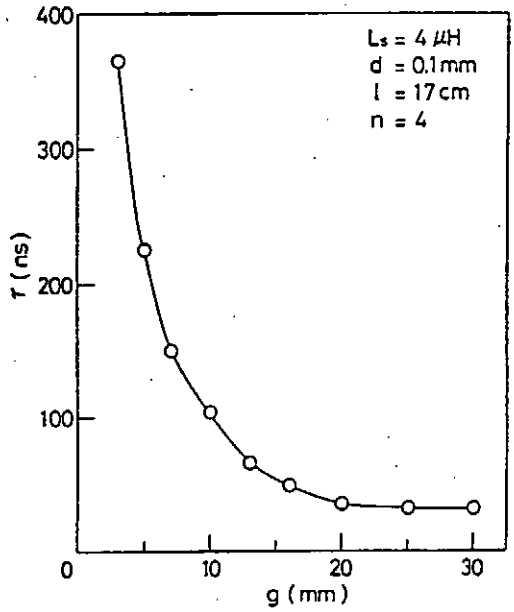

Fig.5 Dependence of τ on g.

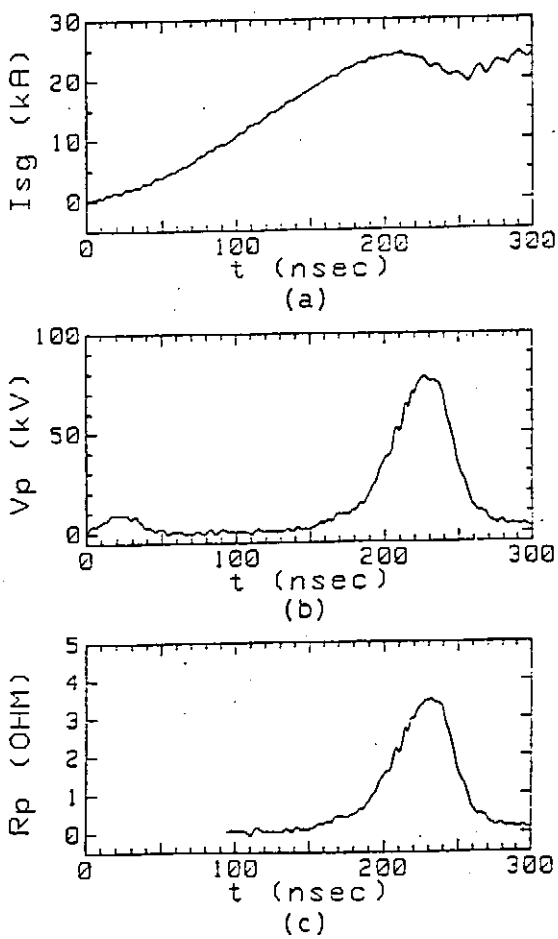

Fig.6 waveforms of Isg, V_P and R_P.

and the short-circuit load. Figure 4 shows the waveforms of V_w and the current, I_L, through the short-circuit load. The number, diameter, and length of wires are four, 0.1mm, and 17cm, respectively. The inductance of the energy storage inductor was 4μH. The breakdown voltage of the spark gap was determined by the gap separation, g. When the voltage reached the breakdown voltage of the spark gap, the spark gap fired, and V_w decreased. The load current simultaneously began to flow. The rise time of I_L decreased with the increase of g. Figure 5 shows the dependence of the rise time, τ, of I_L on g. The rise time decreases with the increase of g. The rise time of the load current was about 30nsec for g>20mm.

§4 Characteristics of ASO-I using Two-staged Opening Switches

The fuses and the PEOS were used as first and second stage, respectively, of the opening switch. The long conduction and

short opening times are achieved by making a two-staged opening switch. In experiments, the value of L_S was 0.5μH, and the charging voltage of capacitor is 25kV. The delay time from triggering the plasma guns to firing the spark gap is changed.

A. Open-circuit Load

The open-circuit load was first connected to the PEOS. Figure 6 shows the waveforms of the current, Isg (which is measured by the Rogowski coil placed between the spark gap and the PEOS), the voltage across PEOS, V_P, and the resistance of PEOS, R_P. After a conduction time of about 200nsec, the current interruption by the PEOS started. An induced voltage of about 80kV was produced across the PEOS due to the decrease of the current through the PEOS. The current then increased again. This phenomenon means that a restrike has occurred at the switch region of PEOS. The magnetic insulation of the PEOS is insufficient. Therefore, the voltage across the PEOS did not increase very much. The resistance of the PEOS is calculated from the ratio of the voltage to the current. The peak resistance is about 3.5Ω.

B. Short-circuit Load

The short-circuit load was connected to the PEOS next. To be exact, the load was not the short-circuit, but a damping resistor of 0.2Ω and the parasitic inductor. The resistor of 0.2Ω was connected to prevent a large voltage reversal on capacitors. Figure 7 shows the waveforms of the current, I_1 and I_2, which are measured by Rogowski coils placed between the spark gap and the PEOS and between the PEOS and the load, respectively. The delay time, T_{PG}, from triggering the plasma

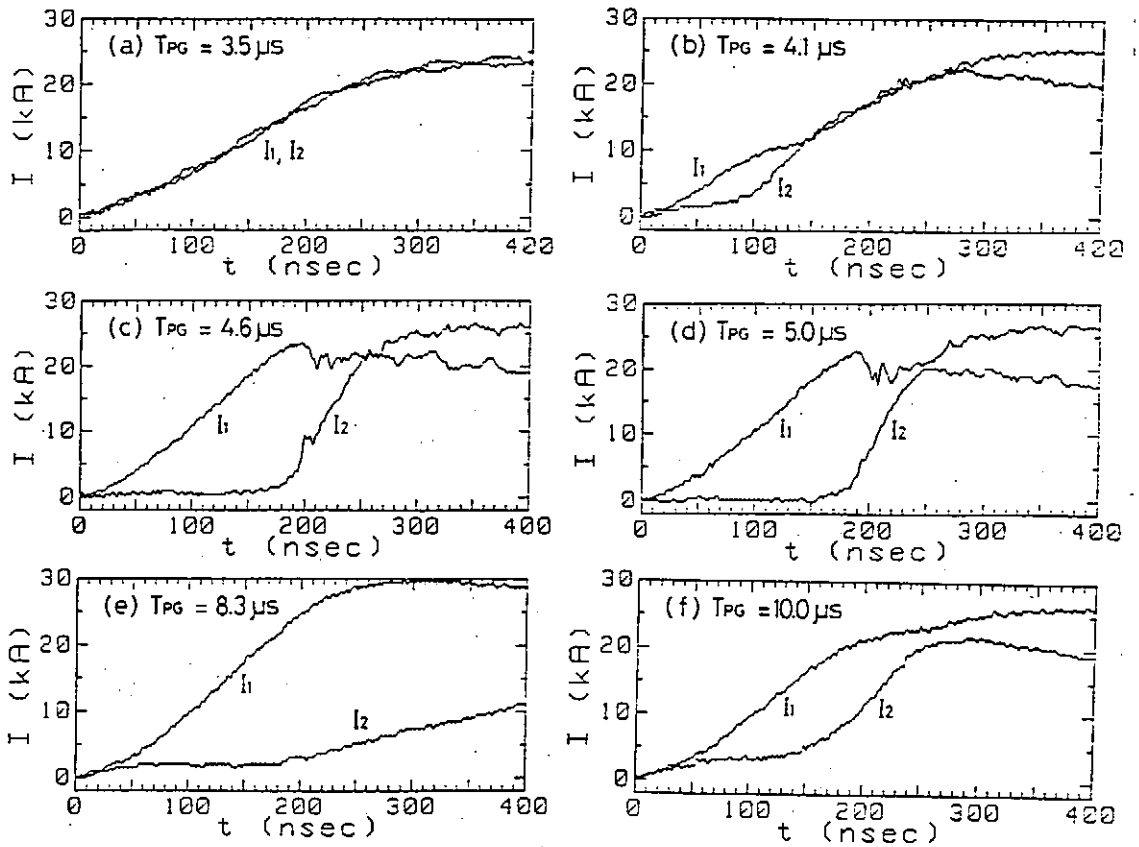

Fig.7 Waveforms of I_1 and I_2.

guns to firing the spark gap was varied. The waveforms in Fig.7(a) are the same as the waveforms obtained without the operation of plasma guns. Since the plasma produced by the plasma guns did not fill the region of the PEOS, I_2 corresponds with I_1. The value of T_{PG} was too small to operate the PEOS. In Fig.7(b), there is a little conduction time of the PEOS. In Fig.7(c) and (d), the sufficient conduction time and the rapid increase of I_2 were obtained. The plasma with proper parameters filled the switch region of PEOS, when the spark gap fires. In Fig.7(e), the delay time, T_{PG}, is so large that the plasma flowing into the switch region was too much. Therefore, the rapid increase of I_2 was not observed. In Fig.7(f), the increase of I_2 is observed again for the larger delay time.

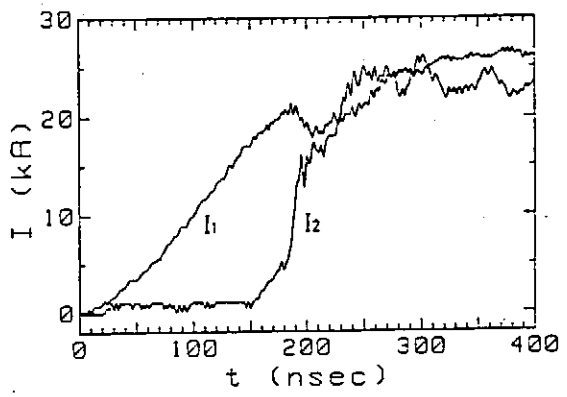

Fig.8 Waveforms of I_1 and I_2.

Figure 8 shows the waveforms of current without the damping resistor at the cost of the life time of the capacitors. A short opening time was observed. The decrease of load impedance by the removal of damping resistor causes the rapid increase of I_2.

§5 Conclusions

A compact and light pulsed power generator, ASO-I, which uses an inductive energy storage system, was constructed. The ASO-I has a two-staged opening switch, which consists of fuses in water and a PEOS, and is able to be operated hundreds of times a day.

Several parallel thin copper wires were used as the first stage of the opening switch. The output voltage linearly increased with the lengths of wires in the case of comparatively short length. The dielectric strength of the copper vapor is about 12kV/cm. The voltage multiplication factor is about ten. The PEOS by four plasma guns was used as the second opening switch. The current rise time was improved from 250ns to 10ns. The resistance of the PEOS was 3.5Ω for the open-circuit load. The two-staged opening switch was successfully operated.

The ASO-I is useful for basic studies of many applications in the pulsed power, and for investigations of opening switches themselves.

References

1) Karl H.Schoenbach, M.Kristiansen, and Gerhard Schaefer: PROCEEDINS OF THE IEEE, 72, 1019 (1984).

2) A.Guenther, M.Kristiansen and T.Martin: ADVANCES IN PULSED POWER TECHNOLOGY Vol 1 ,PLENUM PRESS (1987).

3) J.N.Dimarco and L.C.Burkhardt: J.Appl.Phys., 41, 3894 (1970).

4) G.Cooperstein, et al.: Proceedings of the 6th International Conf.on High-Power Particle Beams, 843, (1986).

5) H.Akiyama, K.Fujita and S.Maeda : Laser and Particle Beams, 5, 487 (1987).

6) N.Shimomura, H.Akiyama and S.Maeda: Trans. of the Institute of Electrical Engineers of Japan, 109-A, 323 (1989).

7) R.J.Commisso, et al. : Proceedings of the 7th IEEE Pulsed Power Conf., 272 (1989).

8) C.W.Mendel,Jr. and S.A.Goldstein : J.Appl.Phys., 48, 1004 (1977).

9) B.V.Weber, et al.:IEEE Trans. Plasma Sci.,PS-15, 635(1987).

10) H.Akiyama, N.Shimomura, H.Machiki and S.Maeda: Proceedings of the 7th IEEE Pulsed Power Conf., 692(1989).

11) H.Akiyama, K.Fujita, T.Majima and S.Maeda:Jpn.J.Appl.Phys., 26, L1743 (1987).

12) C.W.Mendel, D.M.Zager, G.S.Mills, S.Humphries and S.A.Goldstein : Rev.Sci.instrum., 51, 1641 (1980).

Generation of Relativistic Electron Beams by Pulsed Power Generator Using an Inductive Storage System

Kouichi NAGANO, Sunao KATSUKI, Hidenori AKIYAMA, Sadao MAEDA

Kumamoto University

Abstract

The pulsed power generator using an inductive energy storage system is extremely light and compact. Here, a light and compact pulsed power generator, which is named ASO- I , is used to generate relativistic electron beams. A thin copper fuse is used as an opening switch,which is necessary in the inductive storage pulsed power generator. The relativistic electron beams are successfully generated by the inductive storage pulsed power generator.

§ 1. Introduction

The pulsed power technologies have made remarkable development. As the applications of pulsed power technologies, there are many fields, for example, microwave sources, free electron lasers, soft X-ray sources, neutron sources and mass drivers. The relativistic electron beams are necessary for several those fields.

The conventional pulsed power generators, which consist of a Marx bank and a water pulse forming line, are too large. A development of compact pulsed power generator has been desired to study many applications of relativistic electron beams. The pulsed power generator using an inductive energy storage system is very attractive in size, weight and cost[1-8]. However, opening switches to interrupt the high current in very short time

are necessary. We use the fuse as the opening switch.

In this paper, it is studied that the relativistic electron beams could be generated by the inductive storage pulsed power generator, in which the fuses in water are used as an opening switch.

§ 2. Experimental apparatus

Figure 1 shows the schematic configuration of the experimental apparatus of the pulsed power generator, ASO- I , which was constructed in Kumamoto University. After the five capacitors, which are 0.7 μ F, 20nH and the nominal voltage of 50kV each, were charged till 20kV, the triggered switch of field distortion type is fired. The current flows through the capacitors, the inductor(11.5 μ H) consisting of the coaxial configuration, and three parallel copper fuses of 0.1mm diameter and 20cm length. When the energy stored in the capacitors is transferred to the inductor, the fuses vaporize. Then the induced voltage, Ldi/dt, is produced and transmitted to the electron beam diode. The water is selected as the ambient material of fuses.

The pulsed power is transmitted to the electron beam diode through the spark gap. The spark gap is used to achieve the prepulse suppression and rise time sharpening. The gap separation is about 3mm. The graphite cathode and the stainless mesh anode are used as electrodes of the electron beam diode. The diode is placed in the vacuum chamber. The electrons are extracted from the plasma produced on the cathode surface, and accelerated by the pulsed power. The diode current and voltage are measured by the Rogowski coil and the resistive voltage divider respectively. The electron beams are measured by the Faraday cup.

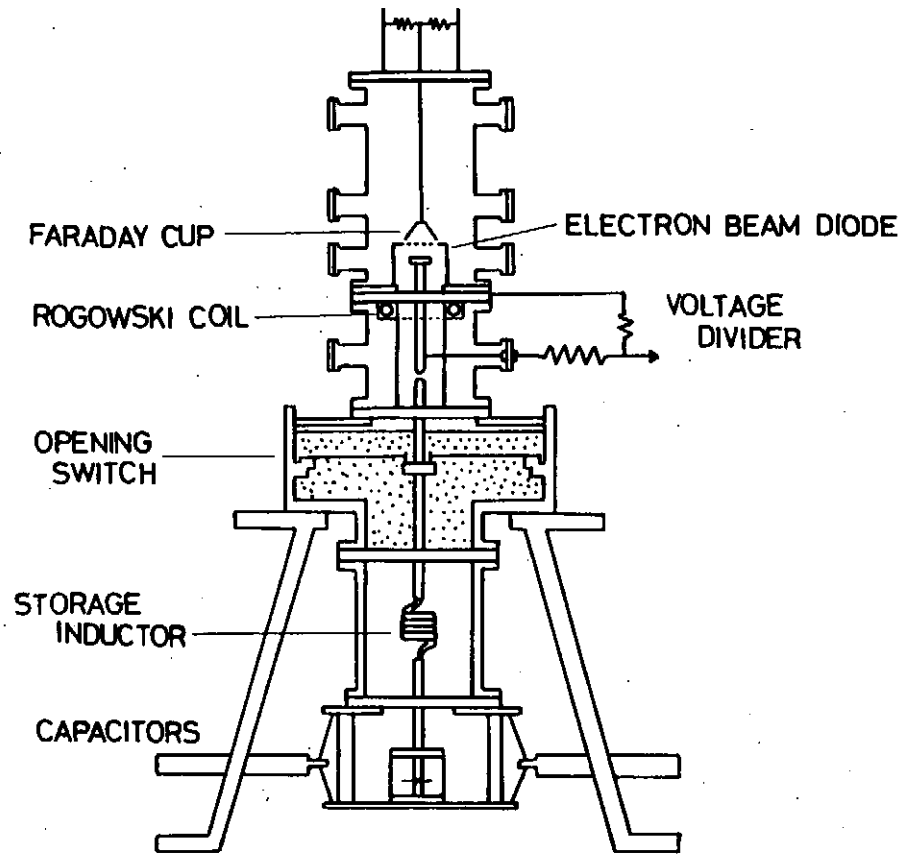

Fig.1. Schematic configuration of the experimental apparatus.

§ 3. Experimental Results and Discussions

Figure 2 shows the dependence of the output voltage, V_{wp}, on fuse length, l. The fuse diameter, d, is 0.1mm, and the charging voltage of capacitors, V_o, is 20kV. The number of parallel copper wires, n, is changed

from 1 to 5. The output voltage linearly increases with the fuse length for comparatively short fuses, because the dielectric strength of fuses just after the fuse vaporization is proportional to the fuse length. The optimal fuse parameters, l=20cm, n=3 in d=0.1mm. In this case, the output voltage is about 173kV.

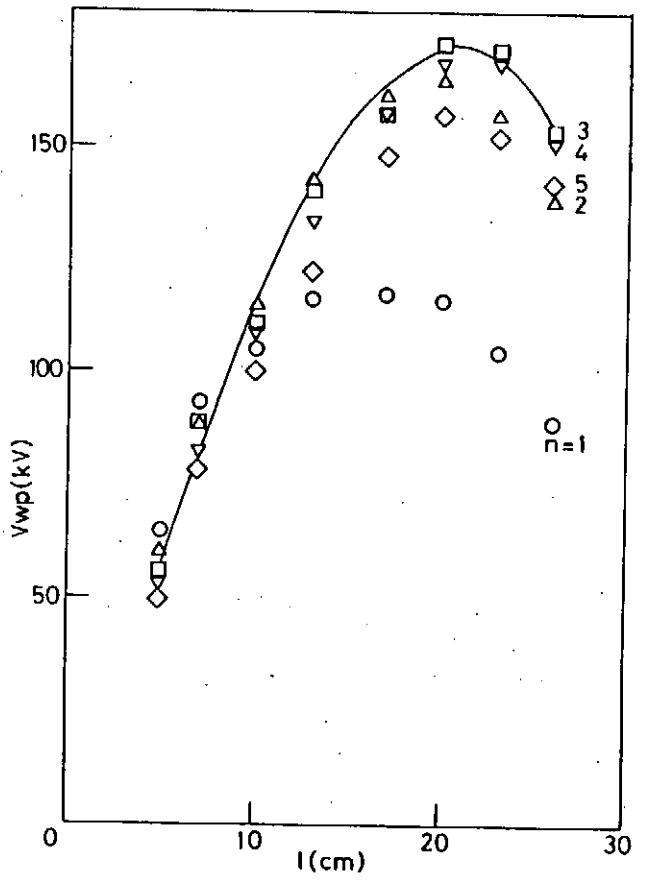

Fig.2. Dependence of output voltage on fuse length.

Figure 3 shows the typical waveforms of the diode voltage, V_d, the diode current, I_d, and the electron beam current, EB. The separation between anode and cathode is 7.5mm. The diameter of cathode is 50mm. The waveform of V_d, especially in the rise part, is able to be changed by the separation of the spark gap, which is placed between the fuse and the electron beam diode. The maximum diode voltage of about 60kV is smaller than the output voltage of 173kV for the open-circuit load, as shown in Fig 2. The maximum diode current increases with the decrease of the inductance of the energy storage inductor. The electron beam current rises with the diode current. Considering the transparency of the stainless mesh cathode, the most of the electron beam seem to be the diode current.

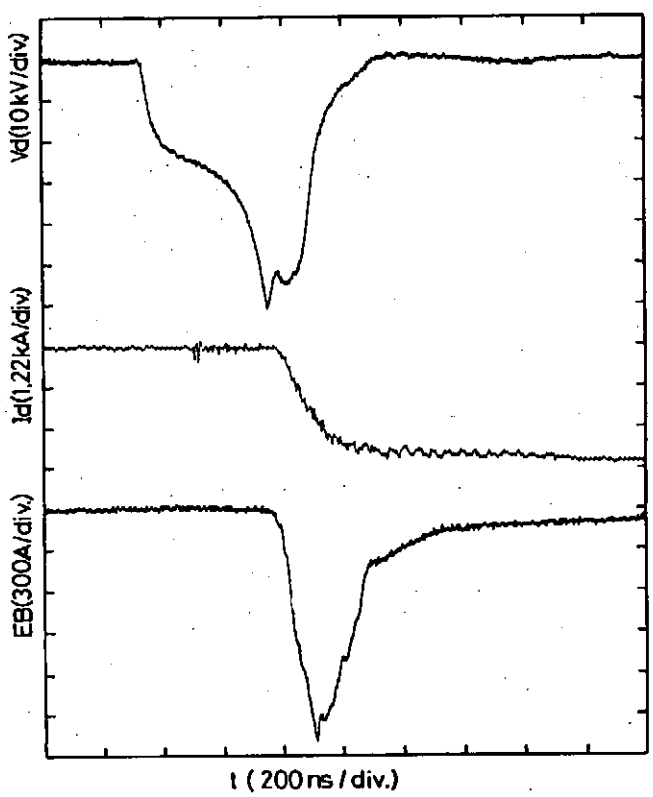

Fig.3. Typical waveforms of the diode voltage, V_d, the diode current, I_d, and the electron beam current, EB.

Fig 4 shows the diode voltage and the electron beam current for the different electrode separations at diode. The diameter of cathode is 50mm, and the distance between the anode and Faraday cup is 4cm. The time till peak value of EB increases with the gap separation. In the case of d=7.5mm, the diode voltage is large at the peak value of EB.

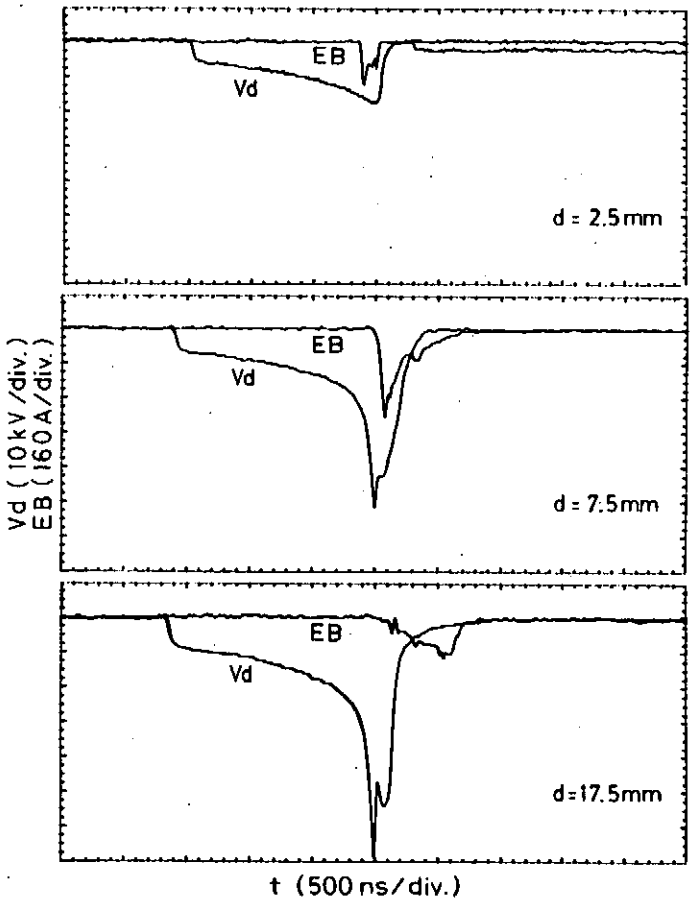

Fig.4. The diode voltage and the electron beam current at various A-K gap.

The peak current of EB and the diode voltage at the peak current are summarized in Figs.5 and 6. V_{eb} is the diode voltage at the peak current of EB. The electron beam current is limited by the space charge[7]. According to Child and Langmuir, the current density is decided by the diode voltage and the gap length. The electron beam current becomes peak value at the A-K gap is 7.5mm, because the diode voltage is large.

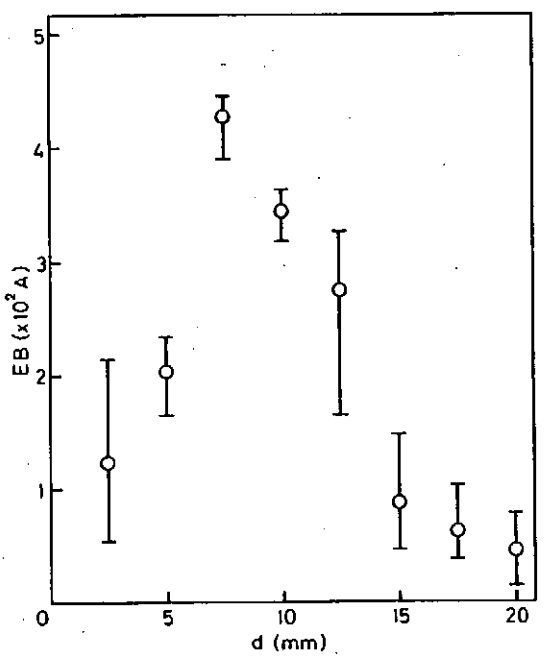

Fig.5. Dependence of electron beam current on gap length.

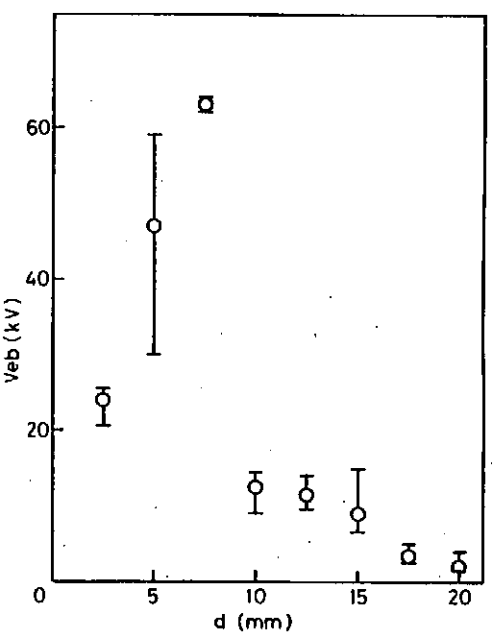

Fig.6. dependence of diode voltage on gap length.

§ 4. Summary

It is demonstrated that the inductive storage pulsed power generator, ASO- Ⅰ, is able to produce the relativistic electron beams. The peak values of the electron beam current and the diode voltage depend on the gap length between anode and cathode.

Further high power electron beam will be obtained by the pulsed power generator, ASO- Ⅱ, which is under construction.

References

1) D.D.Hinshelwood,J.R.Boller,R.J.Commisso,G.Cooperstein, R.A.Meger,J.M.Neri,P.F.Ottinger and B.V.Weber:Appl.Phys.Lett. 49(1986)1635.

2) H.Akiyama,K.Fujita and S.Maeda:Laser Part.Beams 5(1987)487.

3) H.Akiyama,T.Majima,K.Fujita and S.Maeda:Jpn.J.Appl.Phys.26 (1987)L1743.

4) N.Shimomura,H.Akiyama and S.Maeda:Trans.Inst.Electri.Engi. Japan A109(1989)323.

5) H.Akiyama,N.Shimomura,H.Machiki and S.Maeda:Pulsed.Power.Conf 7(1989)692

6) S.Katsuki,H.Akiyama and S.Maeda:Natio.Inst.Fusio.Sci Nagoya,Japan 5(1990)89.

7) I.Langmuir:Phys.Rev.3(1931)238.

INTENSE BEAMS OF HIGHLY-IONIZED METALLIC IONS GENERATED IN THE "POINT PINCH DIODE"

T. Tazima
National Institute for Fusion Science, Nagoya 464-01, Japan
M. Sato
Himeji Institute of Technology, Himeji, Hyogo 671-22, Japan

Abstract. Although the input energy to diodes was about 1 kJ, the "Point Pinch Diode" could produce an intense flux of ion beams up to 90 kA/cm^2. Significant fraction of metallic ion beams of anode materials was also detected and when heavier metallic anodes were employed, highly-ionized metallic ions were generated.

§1 Introduction

The "Point Pinch Diode" consists of a concentric elliptic(or spherical) inner cathode and outer anode,or a flat anode facing to a (semi-)spherical cathode[1,2]. When the pulse power is effectively fed to the diode, emitted electrons from the cathode tightly pinch at a point on the anode surface, producing a high-density plasma with a spot shape. The major energy flux from the spot plasma is an intense ion beam[1]. This paper describes experiments on currents of the ion beam and those species in the cases of various anode materials such as Al, Cu, Mo, W, Pb.

§2. Experimental setup

A pulse power generator LIMAY-I was used to obtained the data presented here. The characteristics of the LIMAY-I are as follows. The maximum stored energy of a Marx generator is 13.1 kJ at an output voltage of 1.6 MV. The characteristic impedance of the pulse line is 3 Ω. A normal self-magnetically insulated transmission line(MITL) of 1 m length, is connected at the end of the LIMAY-I. Figure 1 shows this experimental setup at the end of the MITL. Experiments were performed in the case of a flat anode facing to a semi-spherical mesh cathode or to a spherical cathode. .

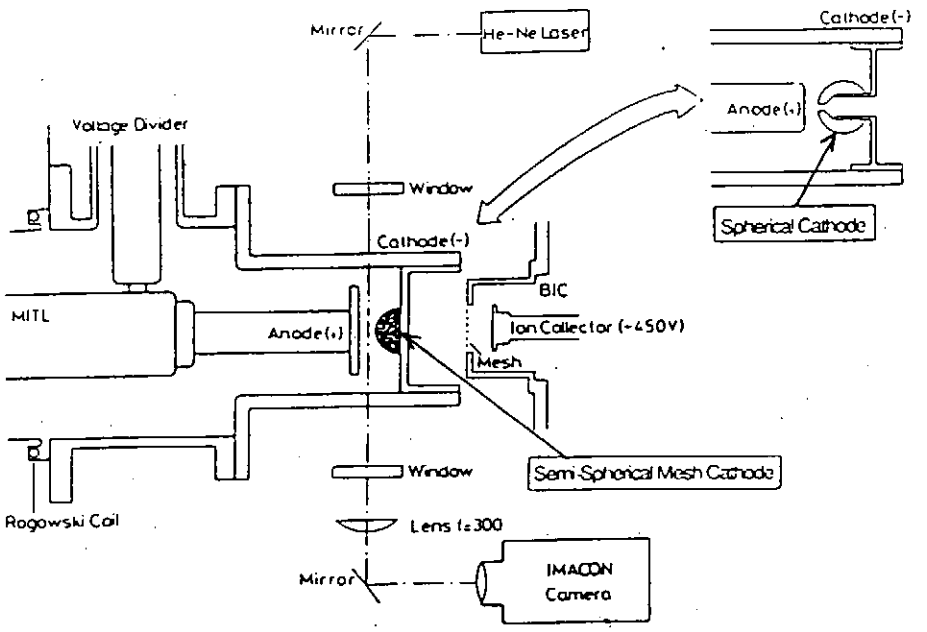

Fig.1 Schematic drawing of the experimental setup

The diode voltage was obtained by subtracting the inductive component from the signal measured with a resistive voltage divider. The diode current was measured with a Rogowski coil. The total current of the ion beam was estimated with a biased ion collector (BIC). The distances from the anode surface to the BIC is 30 and 230 mm. A brass mesh of 22% transparency was located in front of a charge collector. The biased voltage of the BIC is -450 V. A Thomson-parabola ion spectrometer was used for analyzing the species and those energies of ion beams. Ion beams that passed through a cathode hole and a collimator were deflected by magnetic and electric fields. Two pinholes (0.5 and 0.2 mm in respective diameter) were located at the entrance and the exit of the collimator. The maximum magnetic and electric fields were 0.55 T and 5 kV/cm, respectively. Finally, the deflected ions were detected with the film CR-39.

§3. The ion beam current

Figure 2 shows the dependence of the total currents of the ion beam on an anode-cathode (A-K) gap length. No difference was observed on the

peak value of the ion beam among various anode materials. In these experiments we employed the semi-spherical mesh cathode and the maximum diode voltage was 260 kV.

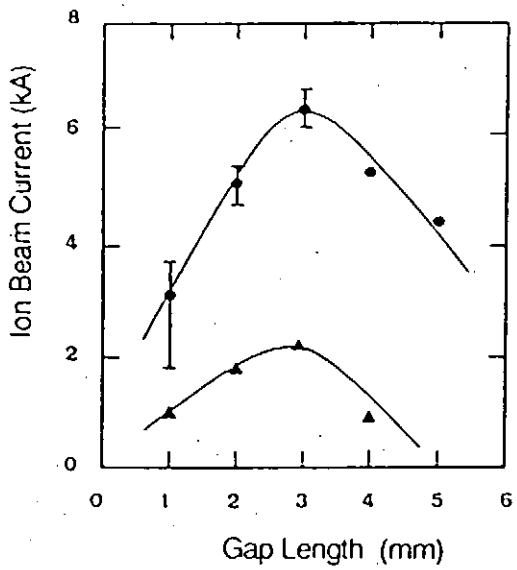

Fig.2 Dependence of the current density of the ion beam at 30 mm ● and at 230 mm ▲ on the A-K gap length.

The dependence of the beam current on the A-K gap can be explained as follows.The peak current of the ion beam is always observed near the phase of shorting of the diode voltage, i.e., just before the A-K gap is closed by plasma expansion. In other words, the main part of the ion beam is generated when the effective A-K gap length becomes very short. In the case that the initial A-K gap is small, the diode current is small at the shorting phase, so that the beam current should be small. On the other hand, since the induced diode voltage decreases before the shorting phase in the case of the long A-K gap, the beam current should also be small.

Differencies of the beam currents between those at 30 mm and 230 mm imply that the most major component is hydrogen, and this result was supported by the measurement with the Thomson-parabola ion spectrometer as described in the previous paper[2].

The maximum current of the ion beam was 6.5 kA and this value corresponds to a current density of 90 kA/cm^2 on the assumption that the

ion beam was extracted uniformly from the plasma surface and this plasma radius at the shorting phase was 3 mm as observed by the framing pictures of radiation emitted from the plasma with a high-speed camera IMACON 790. This current density is extremely large for the small input energy of about 1 kJ to the diode.

§4 Ion species of the beam current

We carried out the experiments employing a stainless-steel sphere cathode of 12.7 mm diameter . The ion beam generated from the anode plasma was extracted outside through the hole of 2 mm diameter at the center of the spherical cathode . A brass rod of 10 mm diameter was connected to the normal MITL. At the end of this brass rod, an anode plate of various materials such as Al, Cu, Mo, W, Pb was attached. The A-K gap length ranged from 2.8 to 3.2 mm. The maximum diode voltage was 340 kV.

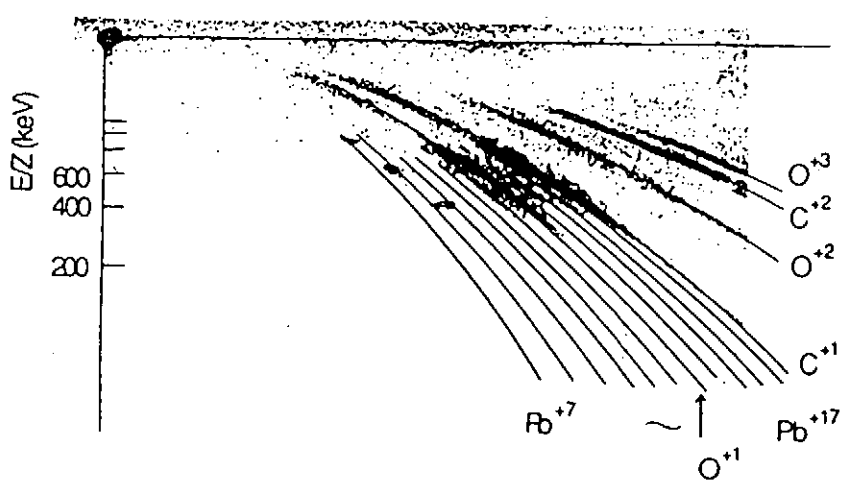

Fig.3 Typical traces on the film CR-39 in the Thomson-parabola ion spectrometer.

Figure 3 shows typical traces on the film CR-39 in the Thomson-parabola ion spectrometer where the respective magnetic and the electric fields were 0.5 T and 5 kV/cm. In this shot, the Pb anode was used, and the A-K gap length was 3.1mm. The spot at the top of the axis shown in

Fig. 3 is a trace of neutral particles. Major components of the ion beam were hydrogen, carbon, and oxygen, the origins of which were gases adsorbed on the anode, such as water vapor and oil mist[2]. In the carbon and oxygen components, components were found which have two- to four-times higher energies than the diode voltage. These high-energy ions can be produced through charge exchange process in the diode or in the pinhole of the Thomson-parabola ion spectrometer. Heavy metallic ions such as Pb^{+7}-Pb^{+17} were also detected.

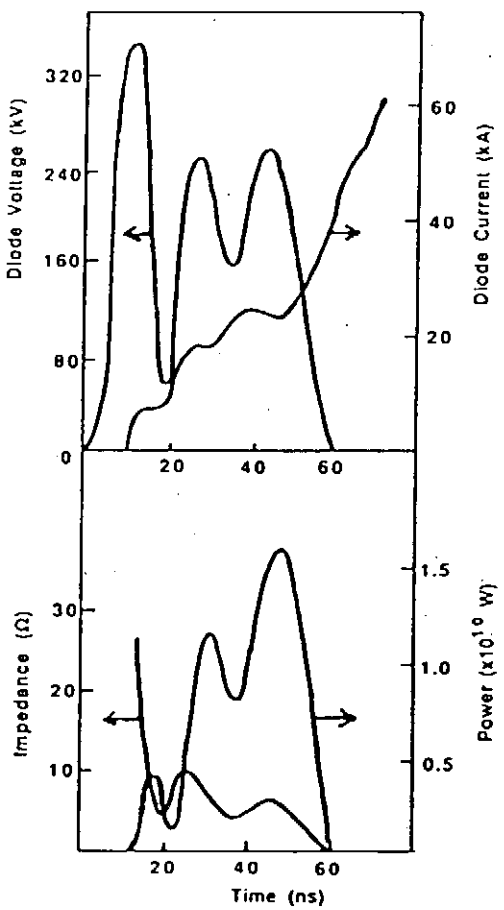

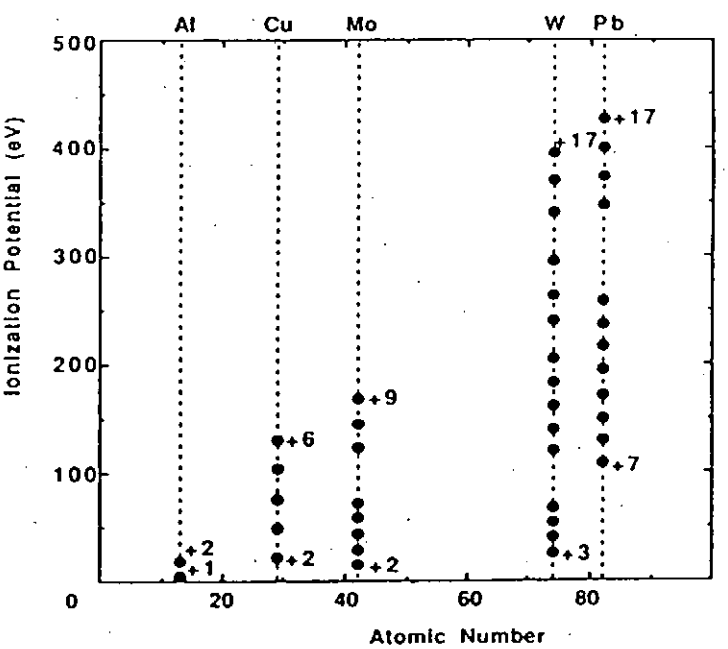

Fig.4(left) The wave forms of the diode voltage, the diode current, the diode impedance the input power to the diode.

Fig.5(right) Highly-ionized metallic ions observed in the ion beam in the cases of various anode materials.

The wave forms of the diode voltage and current of this case are shown in Fig. 4. The diode voltage reached a peak value at 10 ns. The pulse

width was 60 ns. The diode current started to rise 10 ns after the diode voltage rised. The energy put into the diode was 770 J in this shot.

As shown in Fig.5, the heavier metal as anode material was employed, the more highly-ionized metallic ions were observed. Since the stopping lengths in heavy metals are short, the temperatures of the anode plasma in the heavy metal case might be higher than that in the light metal case. In order to confirm this result, measurements of the density and the temperature of the anode plasma are needed and these are under going.

§5 Conclusions

In the "Point Pinch Diode", electrons emitted from the cathode tightly pinch at a point on the anode surface by strong self-magnetic fields which is formed at the early phase because the current density at the center of the diode becomes soon large due to the shortest gap length at the center. Therefore the input energy per unit volume at the anode surface was extremely large, i.e. the order of MJ/cc, so that the metallic anode plasma of high density and temperature colud be produced.

When the initial gap length of the order of mm is employed, the effective gap length becomes short during the pulse because of plasma expansion in the diode. Therefore the current density of the ion beam could become extremely large, for example, up to 90 kA/cm^2 even in the case of about 1 kJ input energy to the diode.

Major components of the ion beam were hydrogen, carbon, and oxygen, the origins of which were gases adsorbed on the anode surface. Significant fraction of the metallic ion beams of anode materials was also detected and when heavier metallic anodes were employed, highly-ionized metallic ions were observed.

References

[1] T. Tazima, M. Sato and H. Yonezu: Jpn. J. Appl. Phys. 25 (1986) L697.

[2] M. Sato: Jpn. J. Appl. Phys. 26 (1987) 927.

Recent Issues of NIFS-PROC Series

NIFS-PROC-1 *U.S.-Japan Workshop on Comparison of Theoretical and Experimental Transport in Toroidal Systems Oct. 23-27, 1989* ; Mar. 1990

NIFS-PROC-2 *Structures in Confined Plasmas –Proceedings of Workshop of US-Japan Joint Institute for Fusion Theory Program–* ; Mar. 1990

NIFS-PROC-3 *Proceedings of the First International Toki Conference on Plasma Physics and Controlled Nuclear Fusion –Next Generation Experiments in Helical Systems– Dec. 4-7, 1989* ; Mar. 1990

NIFS-PROC-4 *Plasma Spectroscopy and Atomic Processes –Proceedings of the Workshop at Data & Planning Center in NIFS–*; Sep. 1990

NIFS-PROC-5 *Symposium on Development of Intensed Pulsed Particle Beams and Its Applications*; Oct. 1990

NIFS-PROC-6 *Proceedings of the Second International TOKI Conference on Plasma Physics and Controlled Nuclear Fusion , Nonlinear Phenomena in Fusion Plasmas -Theory and Computer Simulation-;* Apr. 1991

NIFS-PROC-7 *Proceedings of Workshop on Emissions from Heavy Current Carrying High Density Plasma and Diagnostics;* May 1991